A Shallow Water Vertical Line Array Experiment
Technical Report under Contract N00039-88-C-0043
TD No. 01A021, Acoustic Support for Shallow Water Distributed Systems (Part 2)
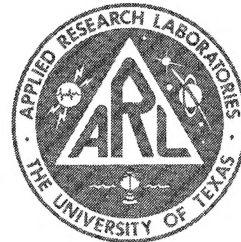
Karl C. Focke
Stephen K. Mitchell

Applied Research Laboratories
The University of Texas at Austin
P. O. Box 8029   Austin, TX 78713-8029

15 November 1994

Technical Report

19960311 219

DTIC QUALITY INSPECTED 1

UNCLASSIFIED

REPORT DOCUMENTATION PAGE

Form Approved
OMB No. 0704-0188

1. AGENCY USE ONLY (Leave blank)	2. REPORT DATE	3. REPORT TYPE AND DATES COVERED
	15 Nov 94	technical

4. TITLE AND SUBTITLE

A Shallow Water Vertical Line Array Experiment, Technical Report under Contract N00039-88-C-0043, TD No. 01A021, Acoustic Support for Shallow Water Distributed Systems (Part 2)

5. FUNDING NUMBERS

N00039-88-C-0043
TD No. 01A021

6. AUTHOR(S)

Focke, Karl C.   Mitchell, Stephen K.

7. PERFORMING ORGANIZATION NAMES(S) AND ADDRESS(ES)

Applied Research Laboratories
The University of Texas at Austin
P.O. Box 8029
Austin, TX 78713-8029

8. PERFORMING ORGANIZATION REPORT NUMBER

ARL-TR-94-20

9. SPONSORING/MONITORING AGENCY NAME(S) AND ADDRESS(ES)

Naval Research Laboratory
Department of the Navy
Washington, DC 20375-5000

Space and Naval Warfare Systems Command
Department of the Navy
Arlington, VA 22245-5200

10. SPONSORING/MONITORING AGENCY REPORT NUMBER

11. SUPPLEMENTARY NOTES

12a. DISTRIBUTION/AVAILABILITY STATEMENT

Approved for public release; distribution is unlimited.

12b. DISTRIBUTION CODE

13. ABSTRACT (Maximum 200 words)

Data were collected in a shallow water region off the coast at Corpus Christi, Texas. Data analysis included the vertical directionality of both the signal and noise fields. A slight bathymetric slope in the exercise area was found to have significant influence in the vertical directionality of the noise field.

14. SUBJECT TERMS

acoustic propagation
ambient noise
noise gain
shallow water
signal gain
vertical directionality

15. NUMBER OF PAGES

103

16. PRICE CODE

17. SECURITY CLASSIFICATION OF REPORT	18. SECURITY CLASSIFICATION OF THIS PAGE	19. SECURITY CLASSIFICATION OF ABSTRACT	20. LIMITATION OF ABSTRACT
UNCLASSIFIED	UNCLASSIFIED	UNCLASSIFIED	SAR

This page intentionally left blank.

TABLE OF CONTENTS

This page intentionally left blank.

LIST OF FIGURES

LIST OF TABLES

This page intentionally left blank.

1. BACKGROUND

Shallow water presents underwater acoustic surveillance with a difficult task. Many shallow water regions of interest are near harbors, shipping lanes, or fishing fleets, and the resultant high shipping densities contribute to high acoustic noise levels. Also contributing to high noise levels in these areas is the inherent close proximity of the receiver elements to the source of wind and wave noise: the sea surface. In addition to the high noise levels, shallow water is frequently characterized by a high degree of lateral variability. Variability in the bottom depth and composition and in the sound speed in the water column translates into variability in the acoustic propagation. An acoustic description obtained for one shallow water area cannot easily be extended to cover a large area or applied to another region. Acoustic surveillance in shallow water therefore must deal with a highly variable environment and high noise levels, such that each new area of interest can present a new and unique environment.

A practical surveillance system in shallow water would provide sufficient gain to overcome the high noise levels and would be sufficiently robust to provide coverage over an extended area. In deep water, these system characteristics can be achieved by taking advantage of the vertical noise directionality. In the frequency regime below 150 Hz, measurements of the noise directionality in the deep ocean show a persistent anisotropy in the vertical [1,2]. Distant shipping noise, which arrives near horizontal, dominates the noise, and the resultant noise field has a consistent bias towards the horizontal. Similarly, modeling studies of the vertical noise field indicate that a persistent anisotropy may also exist in shallow water [3,4]; in these cases the bias is away from the horizontal at frequencies above 150 Hz. System performance studies have shown that noise anisotropy of this form could be exploited for acoustic surveillance in shallow water.

Estimates of the vertical noise field can be calculated with a noise model developed by Kuperman and Ingenito [5]. In this model, referred to in this report as the K&I model, noise is generated by a uniformly distributed infinite noise sheet located near the sea surface. The radiation pattern at each point on the noise sheet is omnidirectional, and the radiated noise from each point propagates via normal modes. The modeled noise characteristics are therefore described by a weighted sum of the normal modes.

The K&I model has been used by its authors and others [3,6] to describe the spatial coherence of the noise field and, based on the coherence, vertical beam noise. The

resultant beam noise estimates nominally peak near ±30° with a reduced level near horizontal. Performance studies have found that modeled narrow horizontal beams can look between the noise peaks and achieve array gains in excess of 10 log(N).

In a related effort, ARL:UT has been investigating the directionality of noise recorded on a 13-element vertical line array (VLA). Results from that effort are promising. At frequencies above 200 Hz, the directionality peaks near ±30° with an intervening noise notch on the horizontal.

This report presents the results from a shallow water experiment designed to investigate the characteristics of noise directionality in a shallow water region. The remainder of this section presents details of the experiment, including the geoacoustic environment and the prevailing conditions during the experiment. Section 2 presents results from the propagation measurements conducted during the experiment. Section 2 also covers propagation loss and signal gain as measured by the VLA. Section 3 presents results from the ambient noise measurements. Ambient noise percentiles, time series, and vertical directionality are included in this final section.

1.1 SHALLOW WATER MEASUREMENTS

In April 1989, ARL:UT conducted an acoustic measurement exercise in the Gulf of Mexico in shallow water off the Texas coast. Acoustic data were received on a 25-element vertical array and radio telemetered to the RV Longhorn for recording. The recordings included an ambient noise event and four propagation events. During the propagation events, the RV Longhorn towed an acoustic projector and broadcast cw tones, broadband signals, and hyperbolic FM signals. For more detail about the exercise, see the exercise plan in Appendix A.

The exercise was conducted in shallow water off the Texas coast, approximately 75 nmi southwest of Corpus Christi, Texas (Fig. 1.1). The position of the array was 26°56' N, 96°27' W. The water depth at the array was 186 m.

Ancillary data were collected during the exercise to provide a description of the exercise area at the time of the measurements. Ancillary data included the source logs and environmental descriptors. Source logs included projector tracks, source levels, and source depth. Environmental descriptors included a sound speed profile, temperature

2
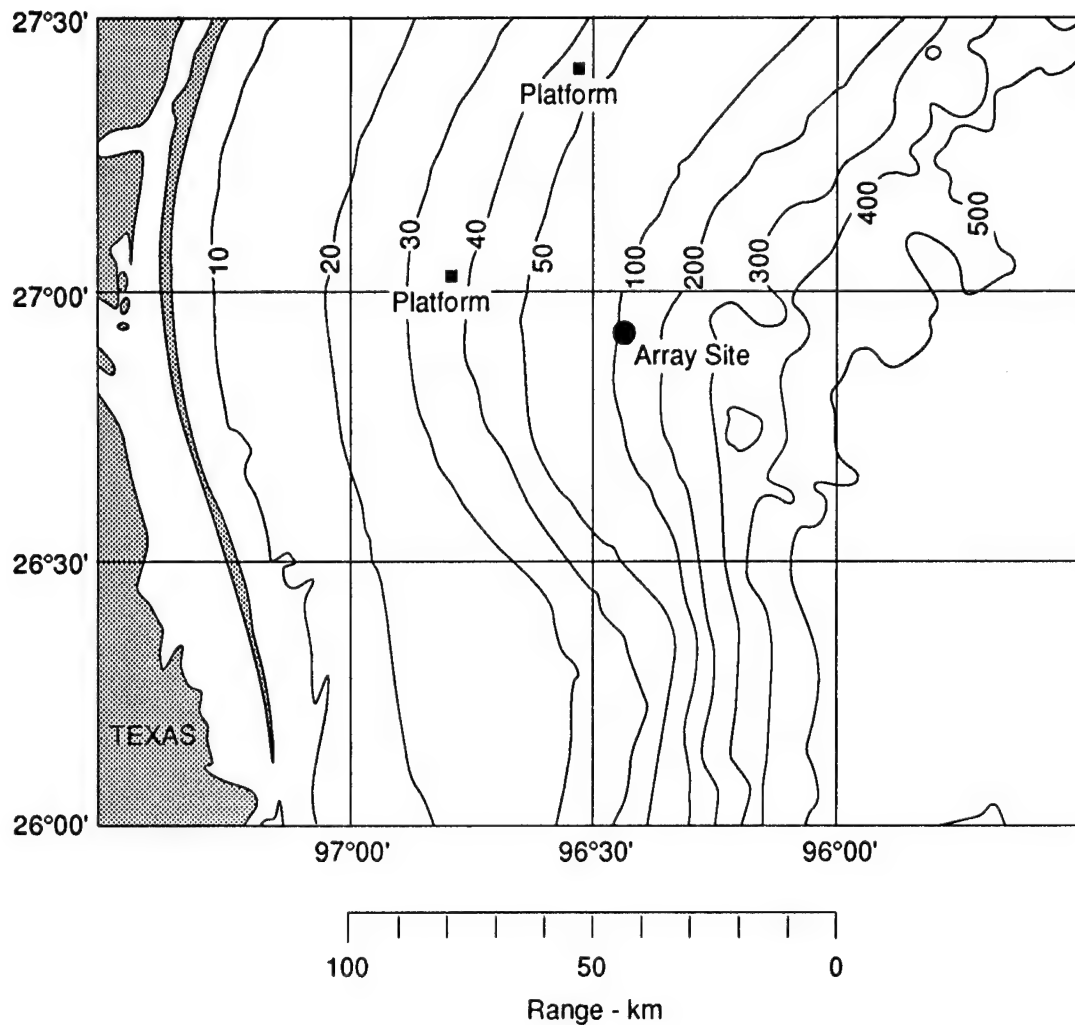
Figure 1.1
Shallow water exercise area.

profiles (AXBT AN/SSQ-36s), bottom grab samples, bathymetry, wind speed and direction, and radar contacts for shipping surveillance.

1.2   SOUND SPEED PROFILES

The sound speed profile at the array site was measured to a depth of 90 m, approximately half of the water column. The AXBTs, converted to sound speed, were used to extend the profile to the sea floor and provided measurements at other locations and times. With one exception, the AXBTs were within ±0.2°C of each other, and they indicated an isothermal layer depth of 38 m ±2.5 m. The exception was in the northernmost measurement. This AXBT differed from the others between the depths of 40 and 75 m where the isothermal layer extended to a depth of 55 m, 17 m deeper than seen in the other measurements. A single smoothed profile was generated from the measurements excluding the northernmost. The smoothed profile was compared with other synoptic profiles from the area [7,8]. The measured surface temperatures were between the synoptic values for April and May with the thermocline deeper than seen in the synoptic data for May (Fig 1.2).

The smoothed temperature profile was converted to sound speed using a salinity of 36 °/₀₀ and compared with the measured sound speed profile, SVP (Fig. 1.3). The two profiles differ by 1.7 m/s at the surface but are within ±0.5 m/s below 10 m. Based on this agreement, the converted profile was used to extend the SVP to the bottom (Table 1.1).

Table 1.1
Average sound speed profile in the exercise area.

Depth (m)	Sound Speed (m/s)	Depth (m)	Sound Speed (m/s)
0	1533.11	10	1533.41
20	1533.14	30	1532.64
35	1531.97	40	1531.73
50	1530.48	75	1524.70
100	1520.78	122	1517.53
125	1516.99	150	1513.33
175	1509.90	186	1509.34
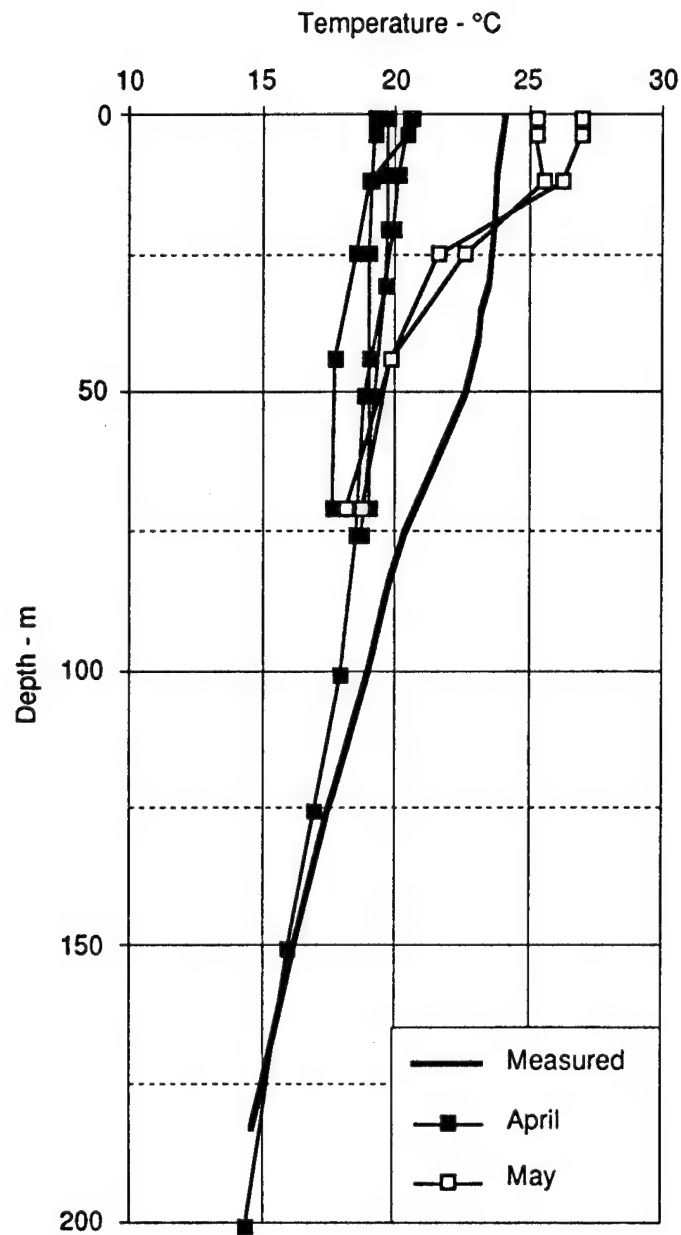
Figure 1.2
Synoptic temperature profiles in the shallow water exercise area.
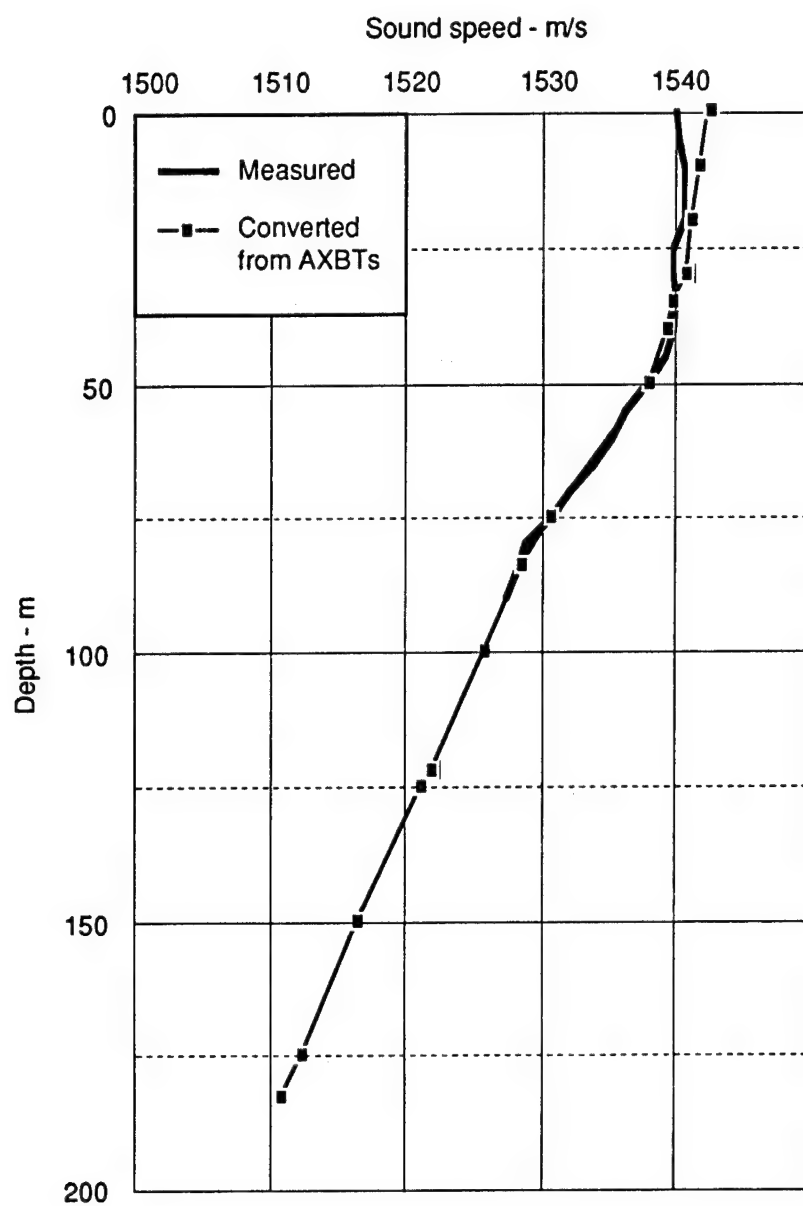
**Figure 1.3
Sound speed profile in the shallow water exercise area.**

6

1.3   OCEAN BOTTOM

The ocean bottom description includes both the bathymetry and the sediment composition. The bathymetry divides the exercise area into two provinces identified by a slight change in the bottom slope. The bottom toward shore is smooth (no outcrops or surface waves) with a slope of 0.3° (70 m depth change in 13 km). On the Gulf side of the array, the bottom is again smooth but with a slope of 1.1° (250 m change in 13 km).

The bottom composition in the exercise area was based on grain size analysis of a bottom grab sample (see Appendix B). The material in the grab sample was identified as "benthic foram-bearing detrital silty-clay." Approximately 90% of the material has grain sizes less than 4 ϕ. These results agree with those obtained at the PROJECT GEMINI Corpus Christi, Texas, site, 27°30' N, 97°00' W [9] and by the U.S. Geological Survey [10]. The geoacoustic description of the GEMINI site had 17.5 m of silty clay overlying 82.5 m of fine sand. Seismic profiling data indicate that this silty clay layer increases to a thickness of 40 m at the measurement array site [11]. The geoacoustic model developed for the GEMINI site was modified by increasing the thickness of the silty clay layer to 40 m, eliminating the discontinuity in sound speed at the water-sediment interface, and replacing the sand layer with a sedimentary rock substrate. The geoacoustic parameters for this area are given in Table 1.2.

Table 1.2
Geoacoustic model for the
exercise area.

Layer	Depth	V_c	Density	α_c	V_s	α_s
Water	0.0⁻	1509.3	1.024	0.0		
Sediment / Silty Clay	0.0⁺	1509.3	1.56	0.030		
	10.0	1513.5	1.57	0.046		
	20.0	1526.5	1.59	0.061		
	30.0	1539.5	1.60	0.073		
	40.0	1552.5	1.62	0.085		
Sedimentary Rock	40.0+	3000.0	2.50	0.03	1700.0	3.0

1.4   WIND CONDITIONS

The wind conditions were monitored and recorded once an hour. The recordings were collected relative to the ship and later corrected for the ship heading and speed. Figure 1.4 presents the corrected wind speed and direction during the exercise. Throughout this period the wind was consistently out of the southeast (135°) with wind speeds of 20 kt. The wind speeds did decrease to 15 kt between 1100 and 1600 on 26 April and to 10 kt between 0300 and 1200 on 27 April.

1.5   RADAR CONTACTS

Radar contacts were logged to identify times when ships were in the area. During the recording period, only three radar contacts were logged as possible ship contacts. At 0240, 26 April a possible ship contact was recorded 10 nmi from the array along a bearing of 28°T. At 2250, 26 April a possible sailboat was reported 3.5 nmi from the array along a bearing of 216°T. The last radar contact at 0045, 27 April was confirmed to be a sailboat. This boat was 4.3 nmi from the array along a bearing of 276°T.

There are several shipping lanes in the Texas coastal waters outside of the exercise radar coverage [12]. Figure 1.5 presents a chart of the shipping lanes surrounding the exercise area. Estimates of the amount of traffic in each of the lanes are also presented. A majority of the shipping is to the north and east of the array site.

1.6   ACOUSTIC EVENTS

The measurement exercise covered five acoustic events. These events were an ambient noise event, a cw propagation event, two broadband propagation events, and a hyperbolic FM-sweep propagation event. During the propagation events, the RV Longhorn towed the NOSC mobile acoustic towed source (MATS) out to the prevailing maximum range of the radio frequency (rf) telemetry link. The rf telemetry range was limited by strong radio interference (RFI). The most probable cause of the RFI is land based radio stations, although at the frequencies used the propagation is normally limited to line-of-sight. Often rf ducting occurs over the Gulf of Mexico, which would account for the RFI seen 50 nmi from land during the exercise. The received rf signal was monitored throughout the exercise, and ranges to the array were limited to maintain proper signal-to-noise ratios (SNRs).

8
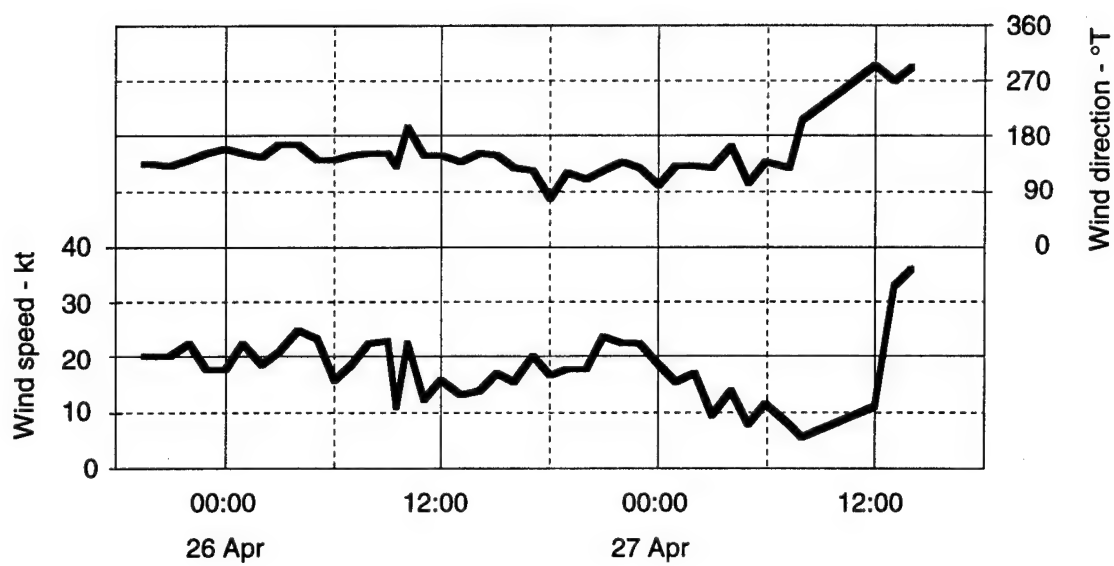
Figure 1.4
Wind conditions during the shallow water exercise.

9
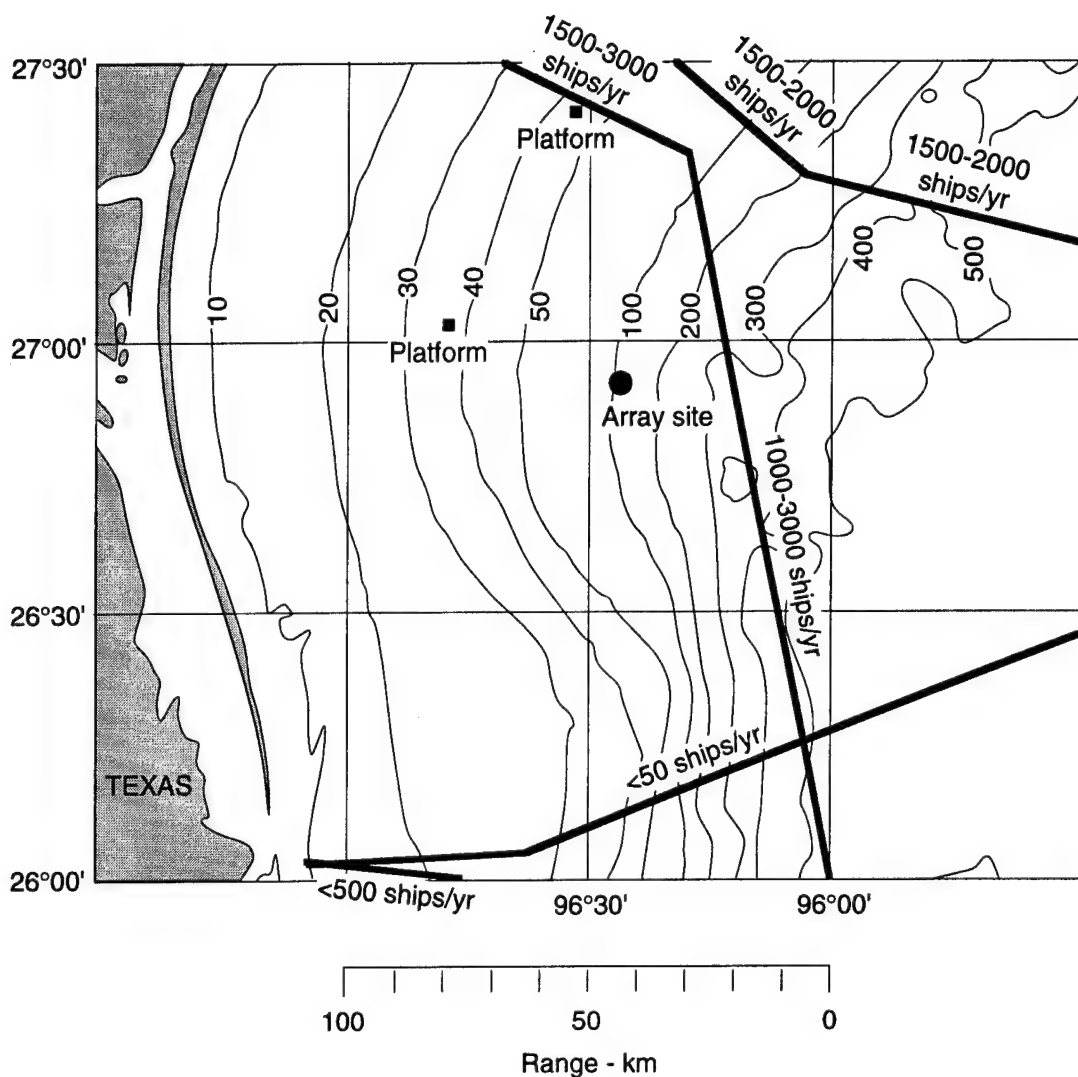
Figure 1.5
Shipping lanes in the vicinity of the experiment.
Numbers are approximate number of ships per year
transiting shipping lanes (Ref. 12).

10

Logs of the ship position, source spectra, source level, and source depth were collected during these events. Projected source spectra were collected every 0.5 to 1.0 h with scheduled changes in the source levels noted separately. Source depth was recorded every 10 minutes. The source depth was nominally 35 m, but variations occurred because of changes in course and speed (Fig. 1.6).

Ship positions were collected every 5 to 10 min. Figures 1.7-1.10 present ship tracks during the analyzed acoustic events.
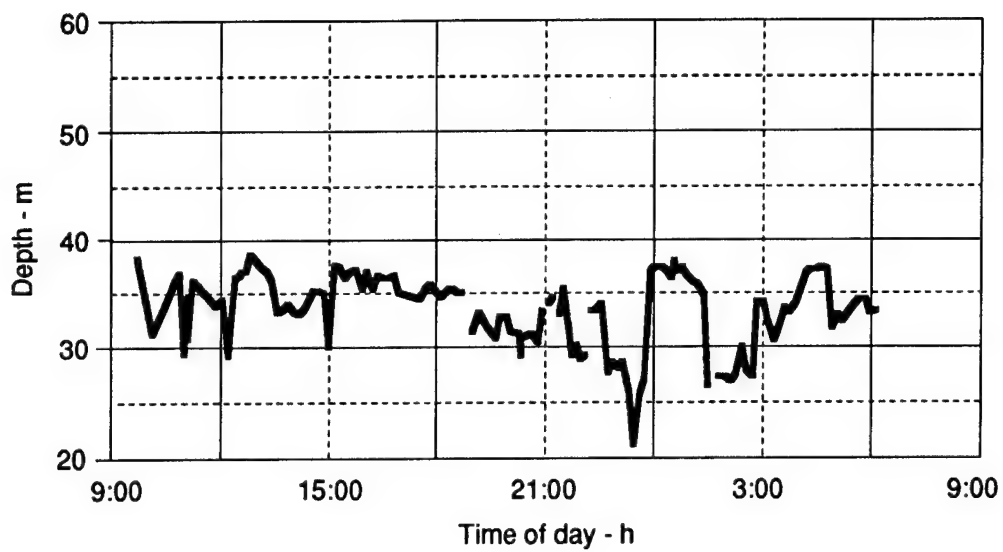
Figure 1.6
Measured source depth during projector operations.

Figure 1.7
Ship track during the ambient noise event.
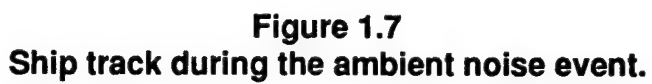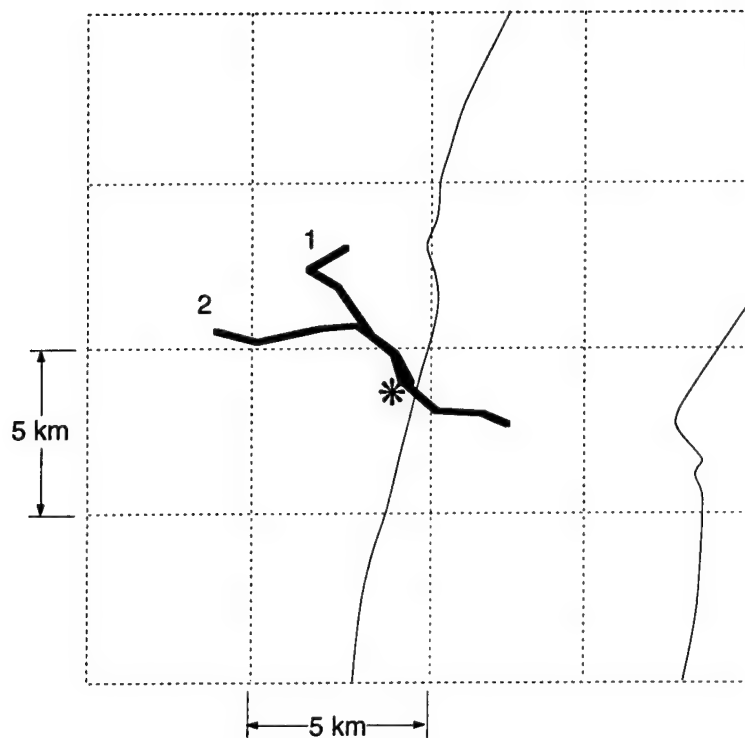
Figure 1.8
Ship tracks during the cw propagation events.
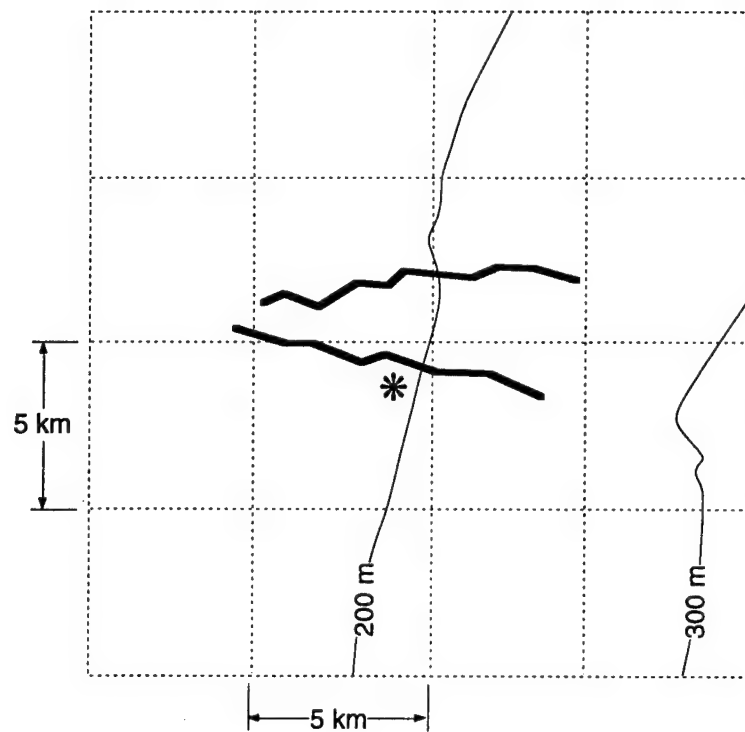
Figure 1.9
Ship tracks during the broadband events.
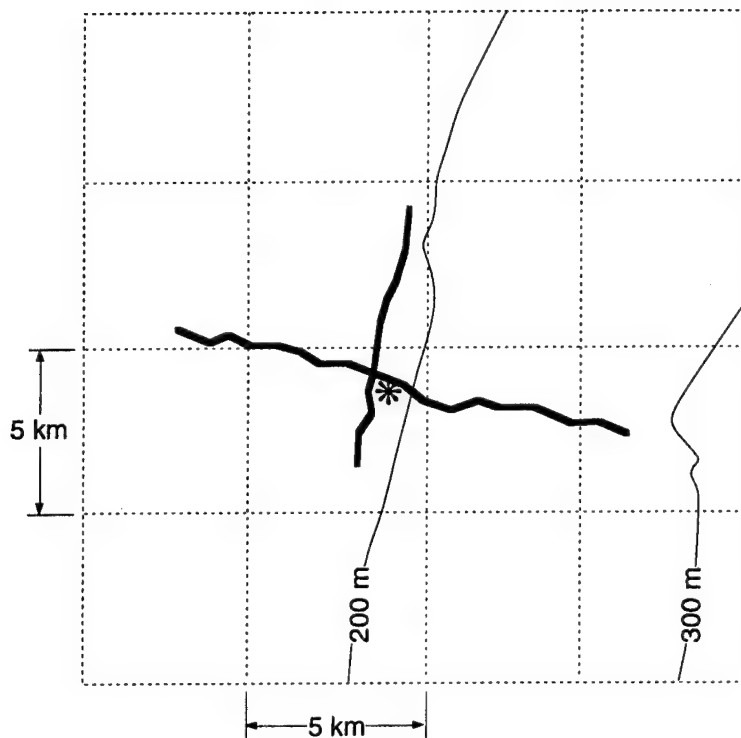
Figure 1.10
Ship tracks during the HFM events.

2. ACOUSTIC PROPAGATION

2.1 TRANSMISSION LOSS MEASUREMENTS

The cw projector events were conducted to support propagation analysis. Two time periods were selected for detailed propagation analysis. The selection was based on several factors. The selected tracks were to be radial to the array site, they should provide the maximum and minimum possible ranges and, if possible, one track should be parallel to the bathymetric contours and the other perpendicular. Bow tie source tracks were scheduled to provide cw runs perpendicular and parallel to the bathymetric contours. However, the prevailing weather conditions resulted in modifications to the tracks, and tracks parallel to the bathymetric contours did not occur.

The two time periods selected for data processing were 1230–1315 and 1615–1715 on 26 April. The ship tracks during these periods are presented in Fig. 1.8 and, for convenience, they will be referred to as Track 1 and Track 2, respectively. Although Track 1 was scheduled to be parallel to the bathymetric contours, as noted above, wind conditions altered the track to that shown in Fig. 1.8. The source to receiver range for these two tracks varied from 0.3 to 3.0 nmi, and therefore the analysis focused on short range issues.

Source depth was measured throughout the projector events (Fig. 1.6). For Track 1 the source was at an average depth of 37.0 m ($\sigma = 4.5$ m), and a median depth of 35 m. Along Track 2, the average source depth was 34.8 m ($\sigma = 1.2$ m) and the median depth was 34.5 m.

The projected acoustic signal during these events consisted of nine cw lines at frequencies of 57-905 Hz at one half octave spacing. The nominal source level for frequencies less than 900 Hz was 160 dB//1 μPa. The exact frequencies and the source levels measured during the exercise are given in Table 2.1. Note that at 0943 and again at 1123, the 905 Hz level was decreased by approximately 10 dB. At this frequency, the projector is very inefficient and requires excessive power to maintain high signal output. The decreased output levels at 905 Hz allowed the other frequencies to obtain output at levels of 160 dB.

17

Figure 2.1 presents a typical comparison of transmission loss (TL) for the two source tracks. Both source tracks cross over the receiver, resulting in two curves at short range. The two data sets exhibit similar losses at ranges less than 2 nmi. At ranges greater than 2 nmi, differences become apparent, with Track 1 exhibiting more loss. Comparisons at other frequencies and receiver depths consistently show similar differences, with Track 1 exhibiting higher losses beyond 2.2 nmi. Taking these results into account, and the higher variations in source depth along Track 1 and the slightly longer ranges for Track 2, the detailed data analysis in this section focused on the Track 2 data set.

Table 2.1
Source levels during cw events.

Frequency (Hz)	Spectrum level at indicated times (dB//1 µPa)				
	0930 0943	0943 1123	1123 1303	1303 1510	1510 1840
57	154.0	161.0	153.2	160.4	160.4
80	153.8	161.6	152.8	161.2	161.2
113	156.6	165.0	155.0	165.2	165.5
160	156.8	164.4	154.8	165.0	164.9
226	153.2	162.6	152.4	163.4	161.9
320	154.0	163.0	153.4	163.2	163.2
452	155.0	163.6	153.4	163.4	163.2
640	154.4	163.0	152.6	163.6	162.4
905	154.2	151.0	131.0	140.6	140.7

Figures 2.2–2.5 present examples of Track 2 TL at 80, 160, 320, and 640 Hz for hydrophone 1 at 88 m depth. Losses out to 3 nmi are low for frequencies below 100 Hz, increasing from 55 dB at less than 0.5 nmi to 66 dB at 2.5 nmi. As frequency increases, TL increases; at 640 Hz, TL has increased to 65 dB at 0.5 nmi and 85 dB at 2.5 nmi. An optimum frequency of propagation was not observed at frequencies above 100 Hz, as is often reported in the literature [13]. Similar results were seen at other receiver depths. A slight depth dependence was observed: TL increased 1–3 dB for receivers within 30 m of the sea floor.
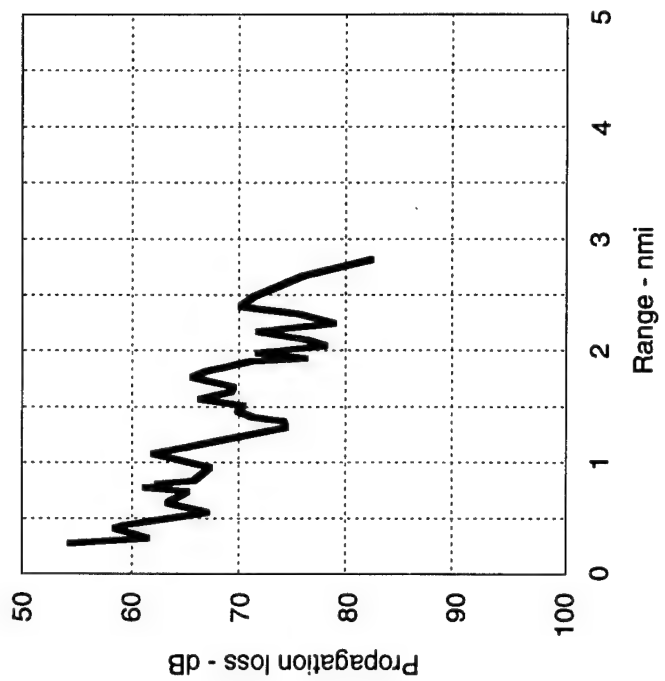
Figure 2.1
Transmission loss to the 88 m receiver, 226 Hz.

(a) Track 1

(b) Track 2
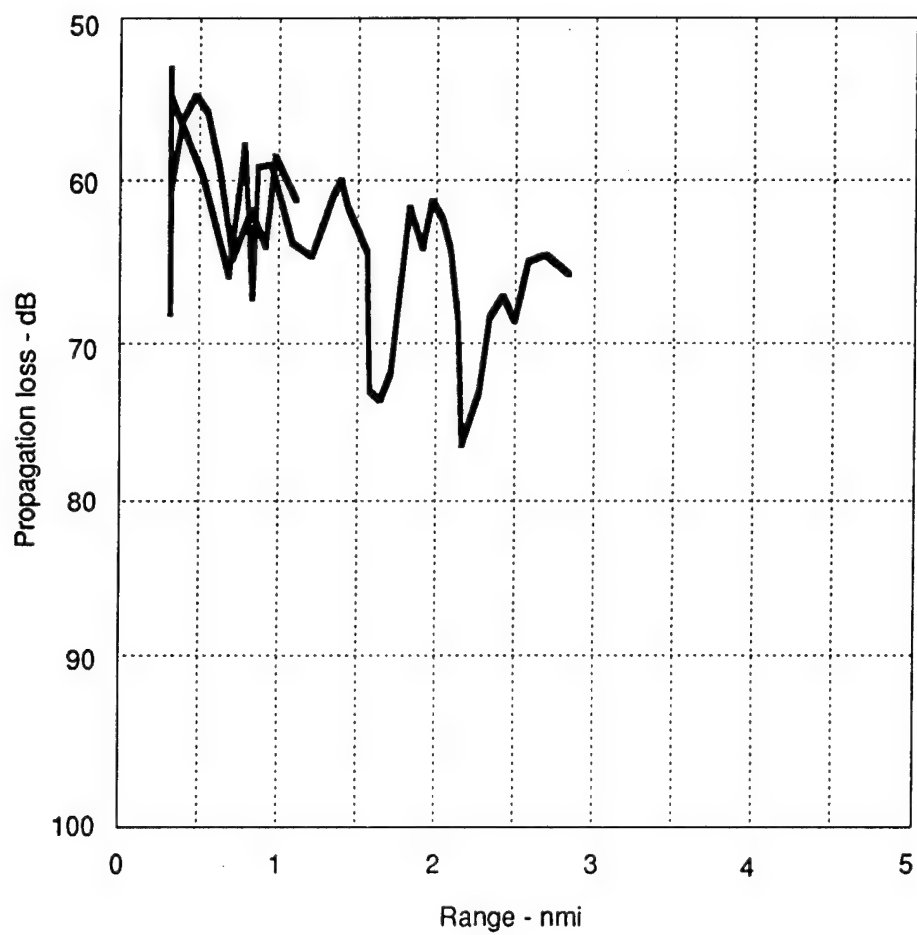
Figure 2.2
Transmission loss to the 88 m receiver, 80 Hz.

20
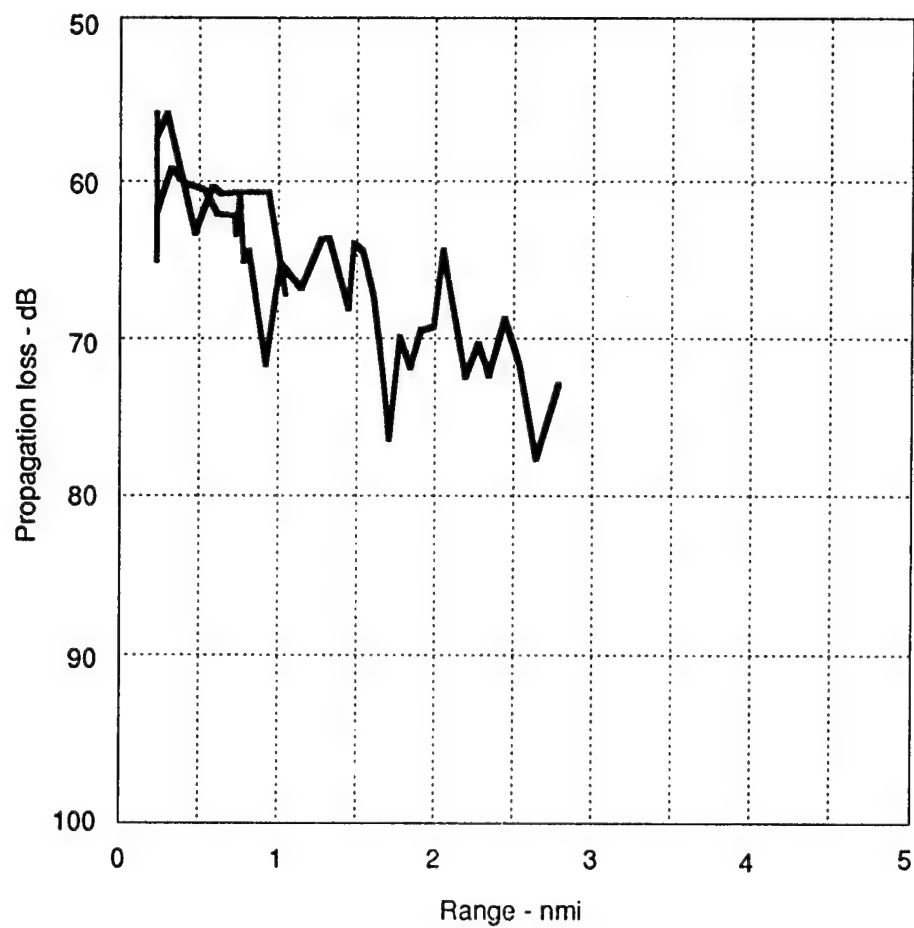
Figure 2.3
Transmission loss to the 88 m receiver, 160 Hz.
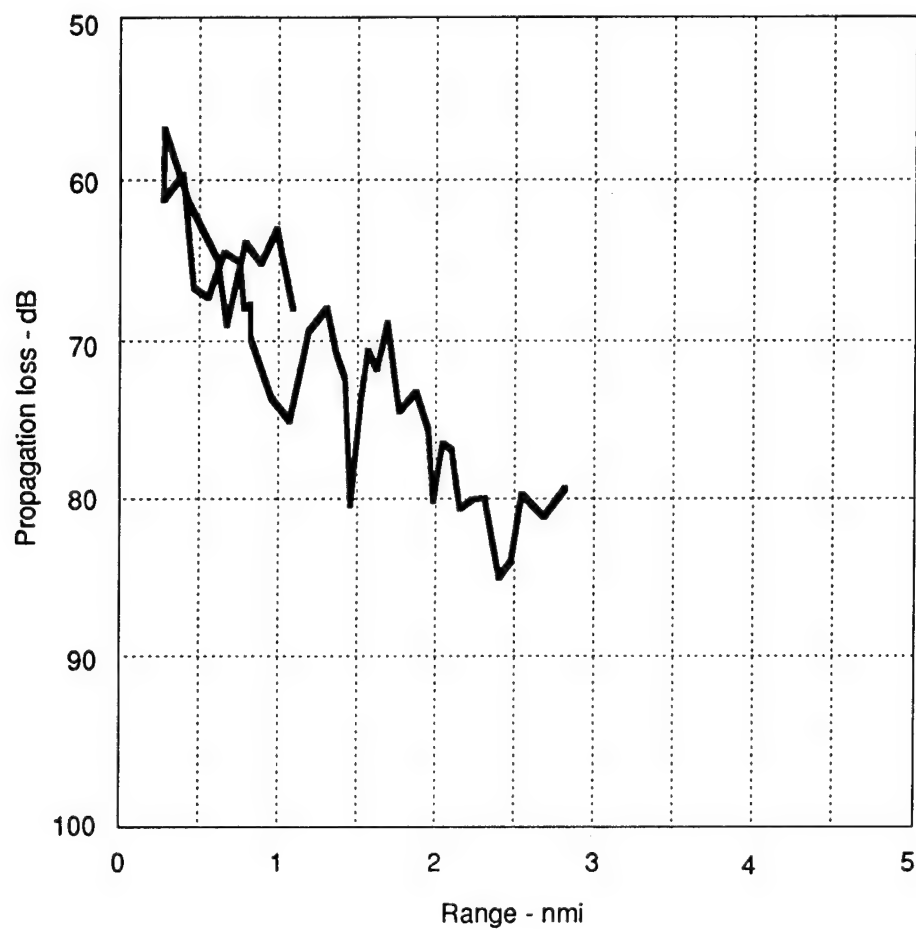
Figure 2.4
Transmission loss to the 88 m receiver, 320 Hz.
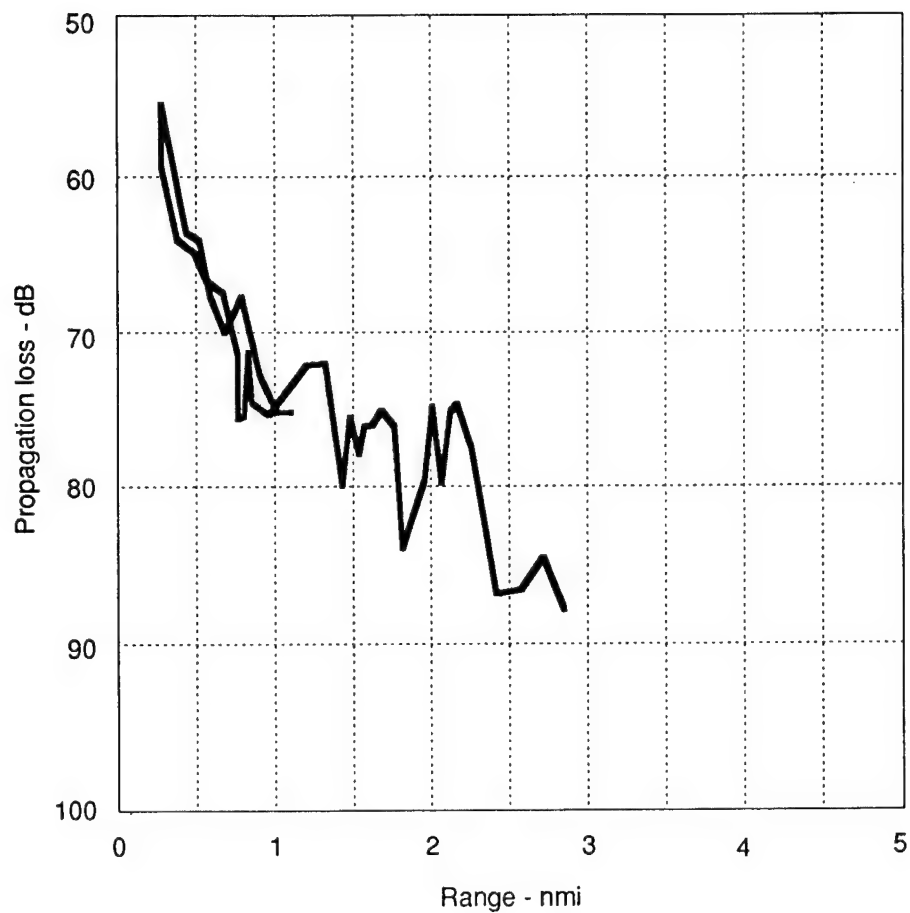
Figure 2.5
Transmission loss to the 88 m receiver, 640 Hz.

To explore the optimum frequency issue, each measured TL curve was fit with a curve of the form

$$TL = c + 10 \log(r) + \alpha r \quad ,$$

where the range r is in meters, and constant TL offset c and the attenuation α were the adjusted parameters. Average values for c and α were then computed for each frequency (Table 2.2). These curves were then used to generate contour plots of TL versus range and frequency (Fig. 2.6). Based on Fig. 2.6, an optimum frequency of propagation in the 50–1000 Hz frequency band may exist between 50 and 80 Hz.

Table 2.2
Estimated bulk attenuation
for the exercise area.

Frequency (Hz)	c (dB)	α (dB/m)
57	59.4	1.08×10^{-3}
80	60.6	5.78×10^{-4}
113	61.2	1.23×10^{-3}
160	62.2	1.06×10^{-3}
226	61.5	1.93×10^{-3}
320	64.4	2.19×10^{-3}
452	63.3	2.97×10^{-3}
640	66.0	2.92×10^{-3}
905	64.4	3.55×10^{-3}

In summary, TL measurements along the two source tracks exhibited similar characteristics and levels out to a range of 2 nmi, with Track 1 experiencing higher losses beyond 2.2 nmi. TL data exhibited an increase in loss with increasing frequency with the lowest losses occurring between 50 and 80 Hz. As frequency increased from 57 to 905 Hz, the nominal values of TL increased from 57 to 65 dB at 0.5 nmi, and from 67 to 85 dB at 2.5 nmi. The depth dependence of TL exhibited in the data was small, with TL 1–3 dB higher in the bottom 30 m of the water column.
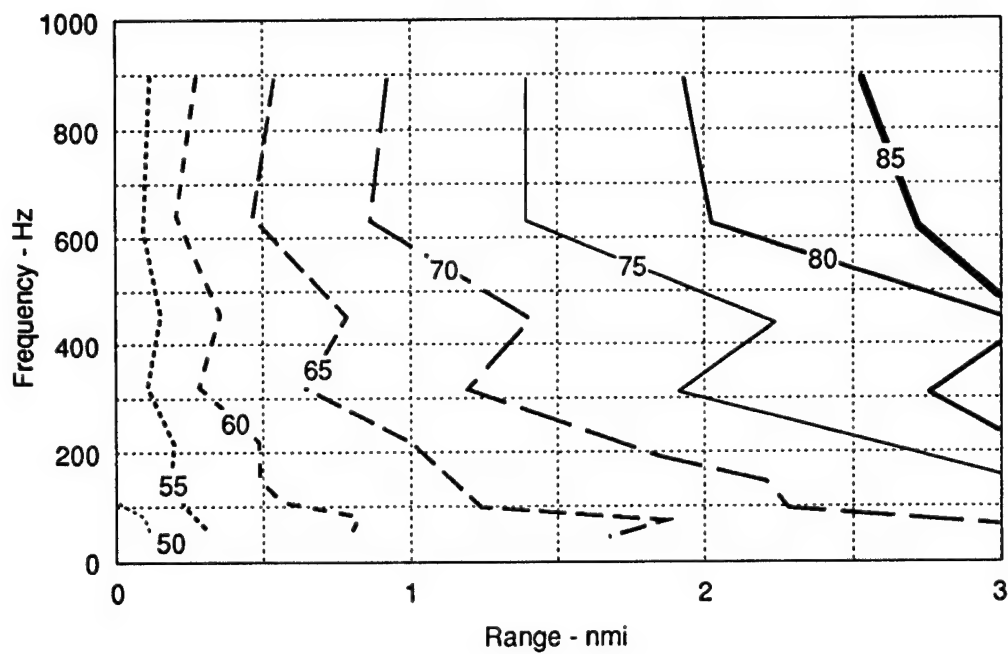
Figure 2.6
88 m receiver transmission loss versus range and frequency.

2.2 PROPAGATION MODELING

Normal mode theory was used to calculate acoustic propagation in the exercise area. These calculations assumed a range invariant environment. Calculations presented below were based on a water depth of 186 m, the depth at the array, the sound speed profile measured at the array location (Fig. 1.3 and Table 1.1), and the geoacoustic model presented in Table 1.2. In the model-data comparisons, the data were from the upslope portion of Track 2. At 2.5 nmi, the water depth along this track was 142 m, a 22% change in depth and a bottom slope of 0.5°. Although this track was not range-invariant, the bottom slope was small and has been ignored in the following discussions.

The geoacoustic model was the result of modifications to improve model-data comparisons. The modifications implemented to improve the comparisons eliminated a sound speed discontinuity at the water-sediment interface and redefined the sound speeds in the sedimentary rock. The initial geoacoustic model from the GEMINI project had a low sound speed duct at the sediment surface that caused a dramatic increase in modeled TL at higher frequencies which was not observed in the data. Elimination of this duct greatly improved the model-data comparisons. The sound speed in the sedimentary rock determined the number of propagating normal modes and the attenuation experienced by the higher order modes. For this study, the sound speeds in the sedimentary rock have the highest level of uncertainty. If further analysis warrants, the values for these parameters can be modified while maintaining a coherent and realistic description of the sediment within the exercise area.

Normal modes were calculated at 57, 226, and 452 Hz for the environment described above using the NEMESIS model [14]. The environment supports 12 modes at 57 Hz, 46 modes at 226 Hz, and 91 modes at 452 Hz. At each frequency, mode 1 represents a Scholte interface wave which does not contribute significantly to the propagation when both the source and receiver are in the water column. The remaining modes each contribute to the propagation, at least to 1 nmi. Beyond 1 nmi sediment attenuation begins to eliminate the higher order modes.

Figures 2.7–2.9 present model-data comparisons for a receiver at 88 m depth. The model-data comparisons at 57 Hz, Fig. 2.7, are within 1 dB at the peaks in TL. The interference nulls in the two curves occur within 0.1 nmi of each other. At this receiver depth, the 57 Hz modeled TL is dominated by two interfering modes. Slight changes in
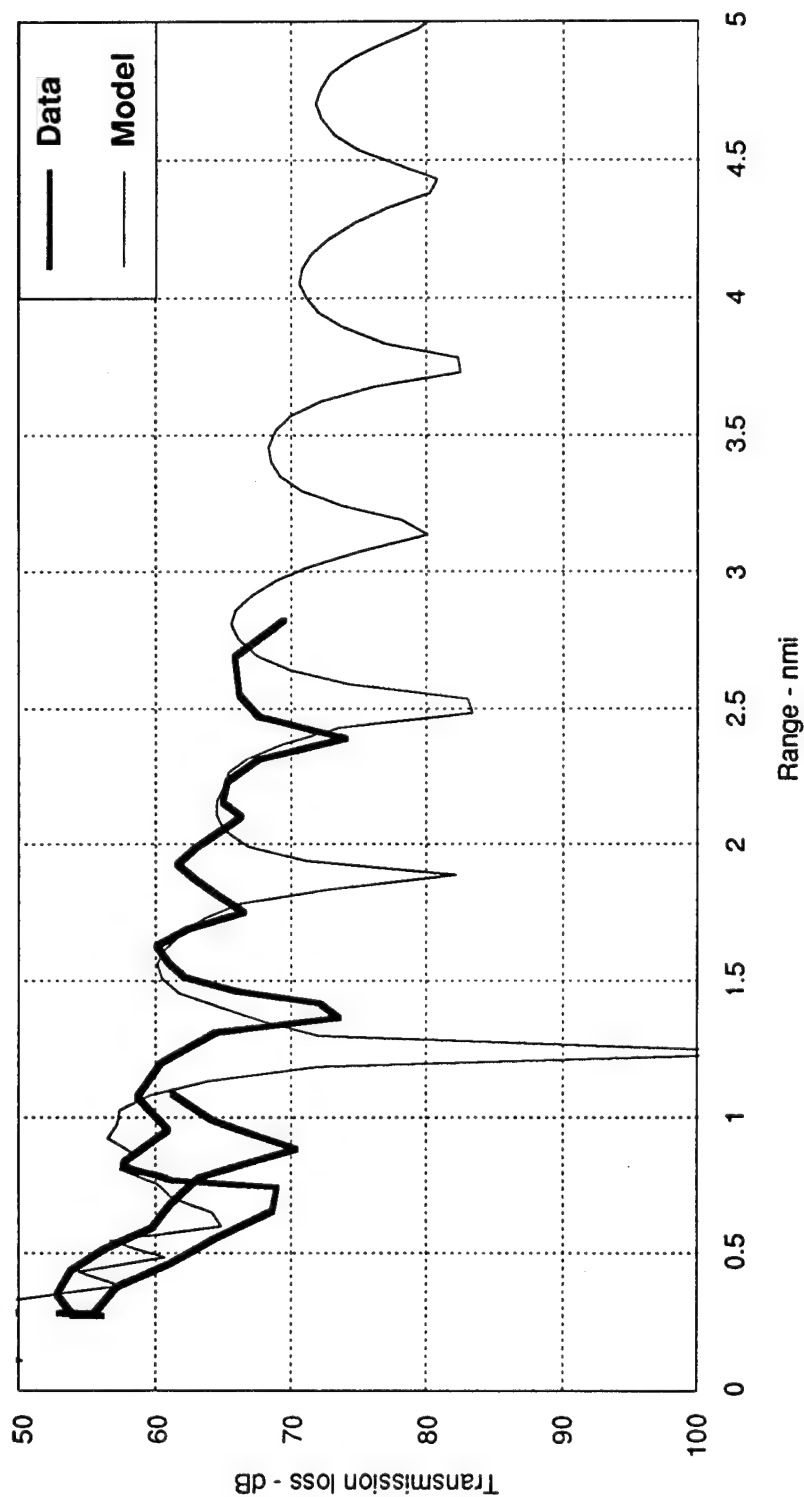
Figure 2.7
Model-data comparison of transmission loss for the 90 m receiver.
Frequency, 57 Hz

27
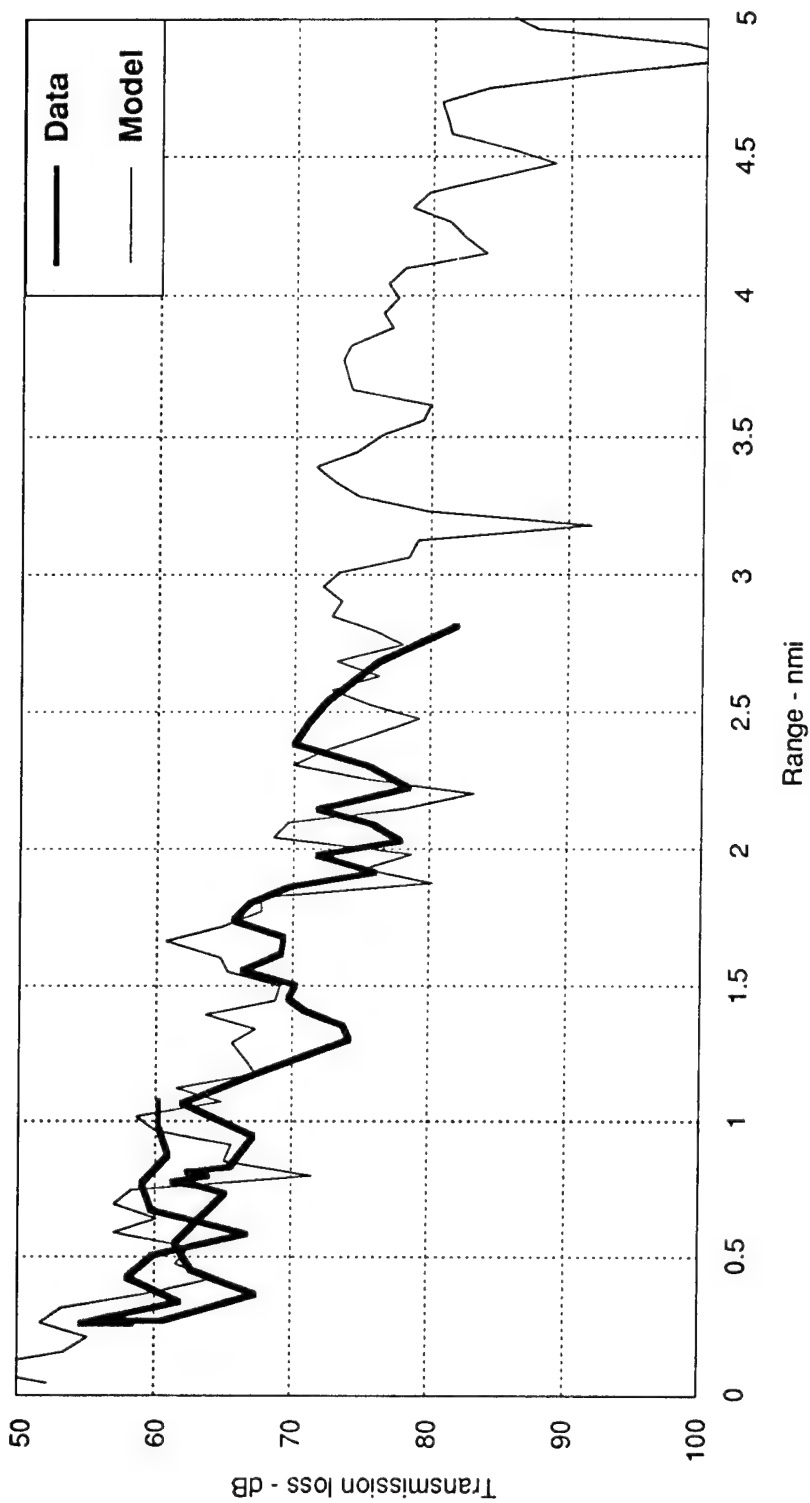
Figure 2.8
Model-data comparison of transmission loss for the 90 m receiver.
Frequency, 226 Hz

28
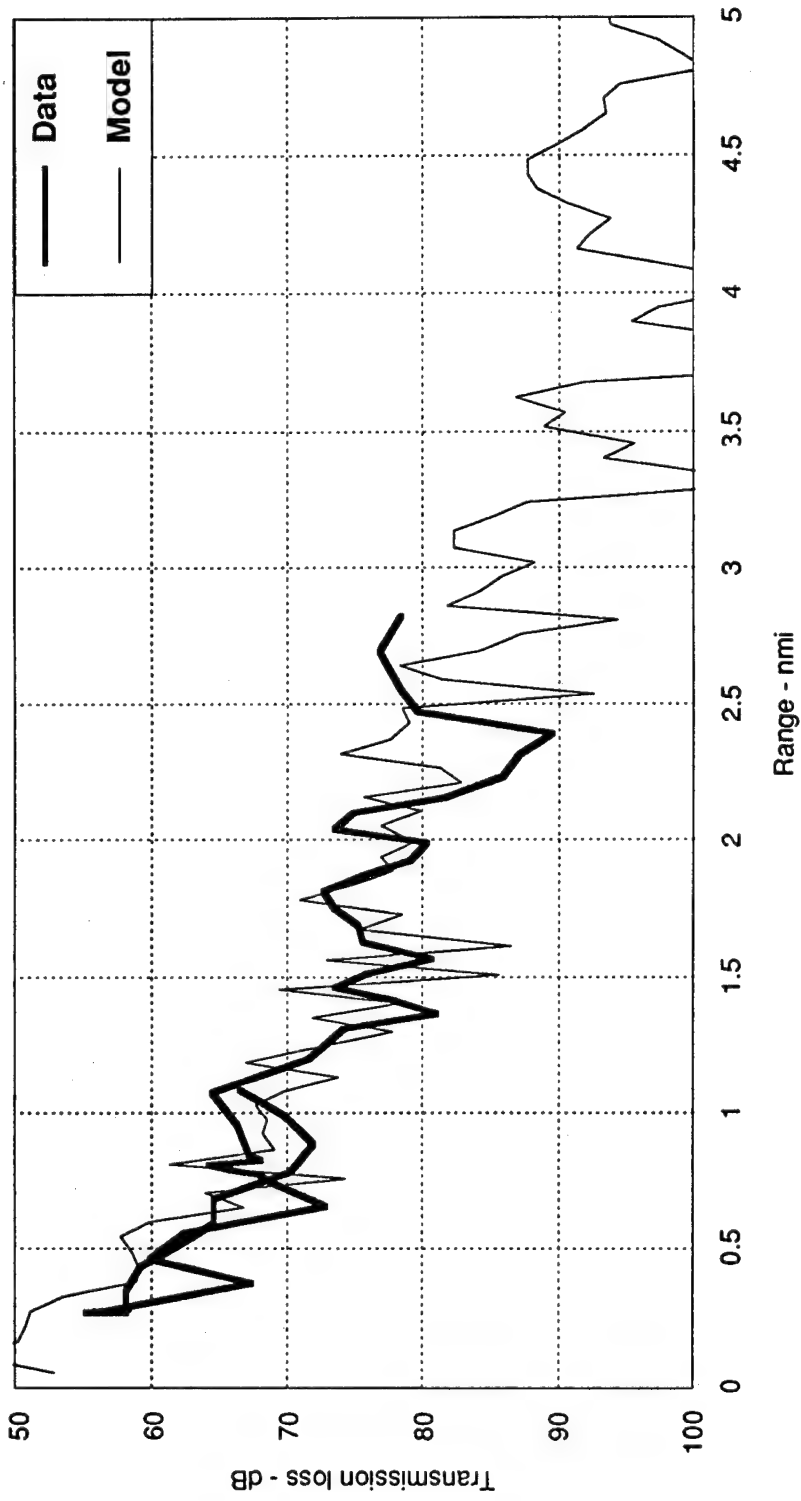
Figure 2.9
Model-data comparison of transmission loss for the 90 m receiver.
Frequency, 452 Hz

29

the receiver depth, source depth, or sound speed profile could introduce the additional interference patterns seen in the data. The 226 Hz comparisons in Fig. 2.8 are also in close agreement beyond 0.4 nmi. The peak values in these two curves are often within 1 dB of each other with the modeled results showing slightly less loss. The 452 Hz comparisons in Fig. 2.9 are similar to those seen in Fig. 2.8, with the peak values within 1–2 dB at ranges greater than 0.6 nmi. Under-sampling in range, especially in the data, prevents adequate definition of the interference nulls at these higher frequencies, and comparisons between null locations is inappropriate. Comparisons such as those presented in Figs. 2.7–2.9 are subject to some uncertainty. For the data presented here, variations of 0.1 nmi in range, accompanied by an increase of up to +4 dB in the modeled TL, will still maintain the level of agreement just presented.

The TL characteristics and model-data comparisons at 226 and 452 Hz noted above are also seen at other receiver depths. However, the 57 Hz TL characteristics seen at 88 m differ from those seen at deeper depths. The 57 Hz propagation to the deeper receivers involves a larger number of modes. Figure 2.10 presents the model-data comparison at 57 Hz for the 180 m receiver. The periodic interference pattern in both the data and the calculations has disappeared and is replaced by an interference pattern characteristic of a larger number of contributing modes.

Based on the agreement between the measured and modeled TL results, the model was used to extend TL to longer ranges and to introduce additional source depths. Figures 2.11 and 2.12 present calculated incoherent TL for source depths of 6 and 100 m and a receiver depth of 88 m. The 6 m calculations are representative of TL for surface ship noise and the 100 m calculations, of a submerged target. The 6 m TLs increase rapidly with range; at 20 nmi, TL at 57 Hz is 110 dB, and at 226 Hz and 452 Hz TL exceeds 120 dB at ranges of 16 and 9.9 nmi, respectively. With the source at 100 m, propagation has improved slightly relative to a 35 m source (data). At 5 nmi, TL is 68.5 dB at 57 Hz, 80.5 dB at 226 Hz, and 85.8 dB at 452 Hz. Based on these calculations, contributions to the noise field should be limited to short range sources, while at the same time signals from a submerged target can propagate over longer distances without rapidly losing significant amounts of energy. However, calculations based on a range dependent adiabatic normal mode model, presented in the next section, indicate that noise from sources upslope can contribute significantly to the noise field.

30
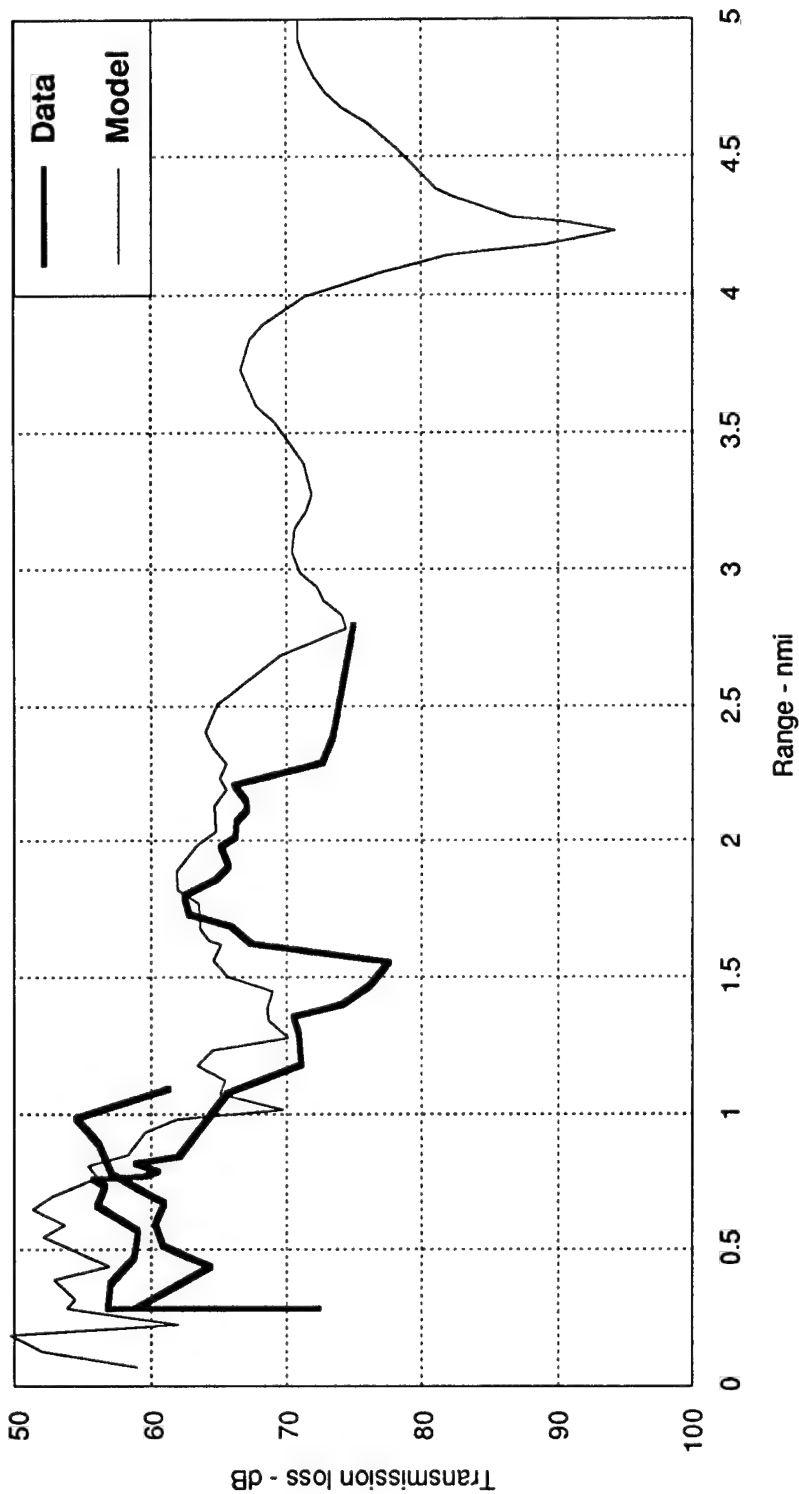
Figure 2.10
Model-data comparison of transmission loss for the 180 m receiver.
Frequency, 57 Hz

31
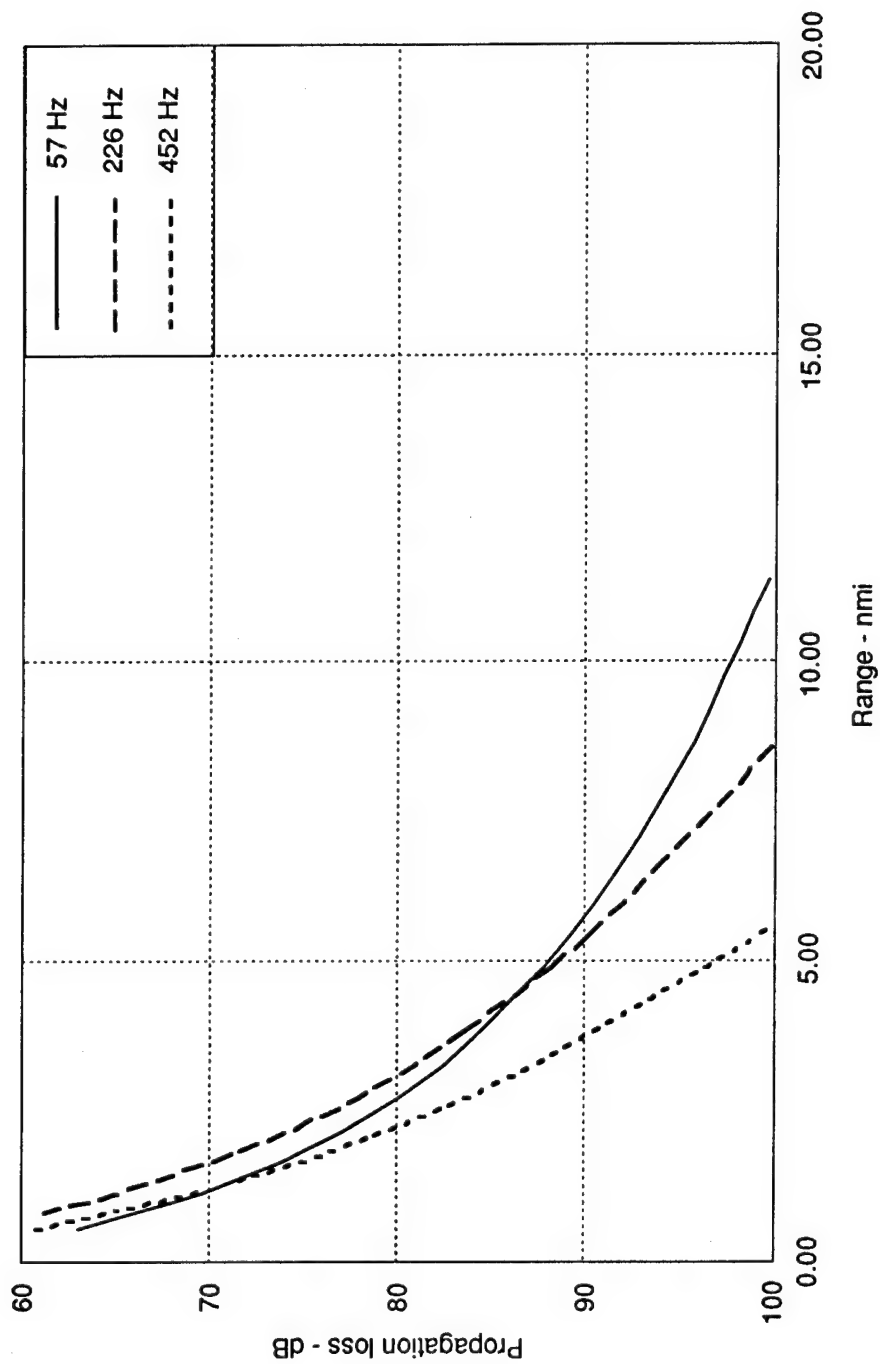
Figure 2.11

Incoherently calculated transmission loss to an 88 m receiver, 6 m source depth.

32
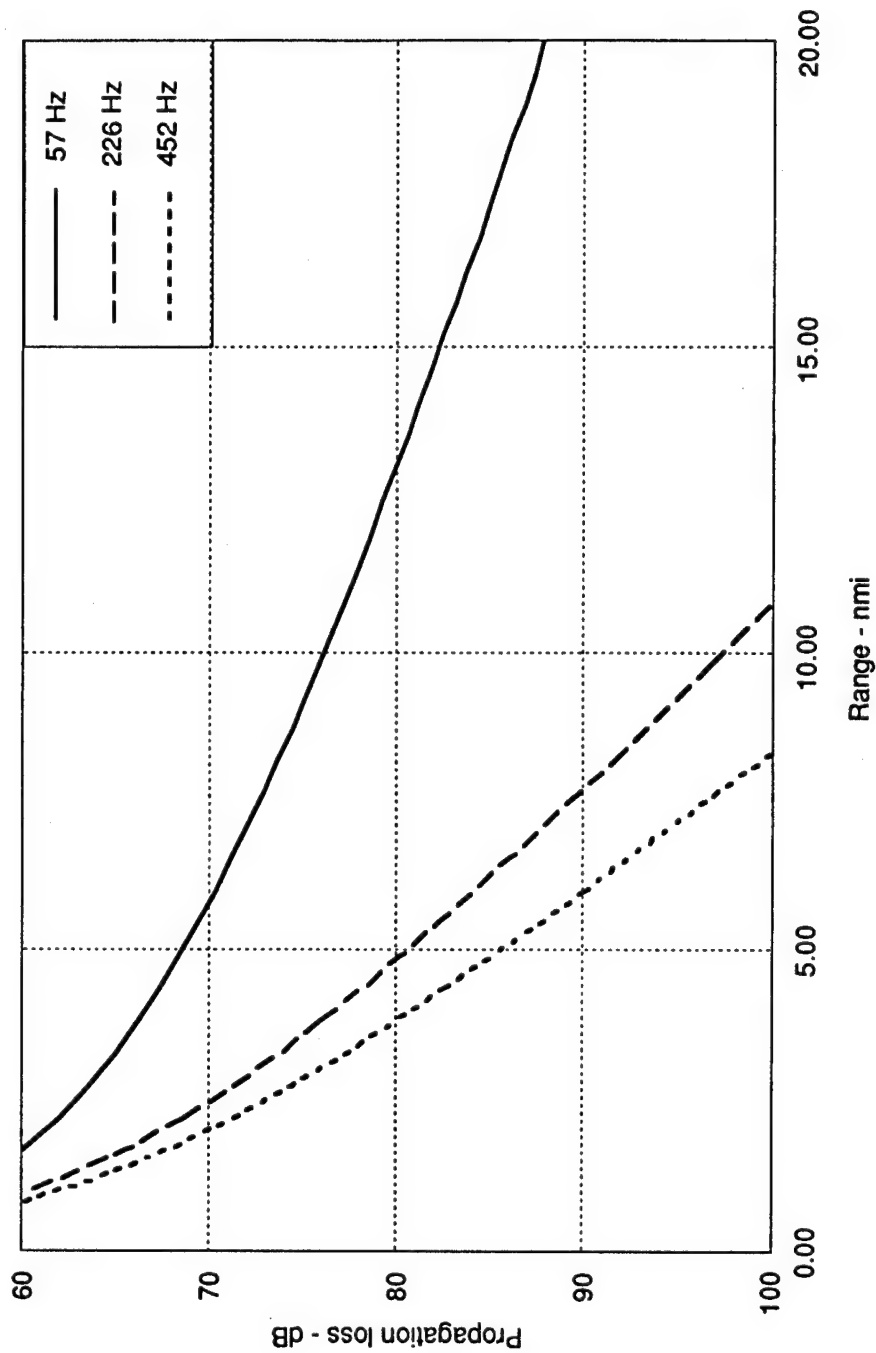
Figure 2.12
Incoherently calculated transmission loss to an 88 m receiver, 100 m source depth.

Legend:
- 57 Hz
- 226 Hz
- 452 Hz

Range - nmi

Propagation loss - dB

33

2.3   ARRAY SIGNAL PERFORMANCE

In the discussions that follow, signal gain (SG) will be used as a measure of array signal performance. Two beamformers were used to investigate SG: a conventional beamformer (CBF) and a modal beamformer (MBF). CBF assumes plane wave propagation and computes the array response in terms of the energy distribution in the vertical angles. MBF assumes normal mode propagation and computes the energy distribution in normal modes calculated for specific environments. MBF requires a priori knowledge of the acoustic environment and is subject to degradation due to environmental mismatch. For both beamformers, SG was normalized to an ideal maximum of 0 dB: all the signal energy arrives on a single beam axis for CBF, and all energy arrives in a single mode for MBF. Shallow water propagation often involves numerous multiple arrivals, splitting the energy between a number of beams or modes, so that the ideal maximum is rarely obtained, even for model calculations.

In the discussions that follow, subarray apertures were used to estimate SG. For the CBF results, a minimum element spacing of a half wavelength was used. Figure 2.13 presents the broadside beam patterns for the subarray apertures selected. The directivity index (DI) and the beamwidth (BW) presented in Fig. 2.13 reflect the number of elements used in each subarray: five elements at 57 Hz and six elements at 226 and 452 Hz.

Figures 2.14–2.16 present the SG for CBF at 57, 226, and 452 Hz. In these figures and those that follow, plot (a) presents the direction of the loudest one or two beams while plot (b) presents the highest SG for each time interval. The source begins at a range of 3 nmi and approaches the array. At 1655, the source is at a CPA range of 0.25 nmi, and the range then increases to 2 nmi. At 57 Hz (Fig. 2.14), the signal energy is split between two beams with the maximum SG varying between -20° and +30°. As the range decreases to less than 0.5 nmi (between 1646 and 1700), energy on the upper beam sweeps from 10° to 30°. In this same time period, the lower beam disappears, possibly a result of high bottom loss at higher grazing angles.

The peak response angles in Fig. 2.14 exhibit a slight anomaly. Theoretically, the positive and negative peak response angles should be symmetric about the horizontal, and the angles should exhibit symmetry about CPA, but Fig. 2.14 does not exhibit this symmetry. Array tilt would account for the lack of symmetry. Differences in the positive and negative response peak angles and the differences in response angle before and after

34
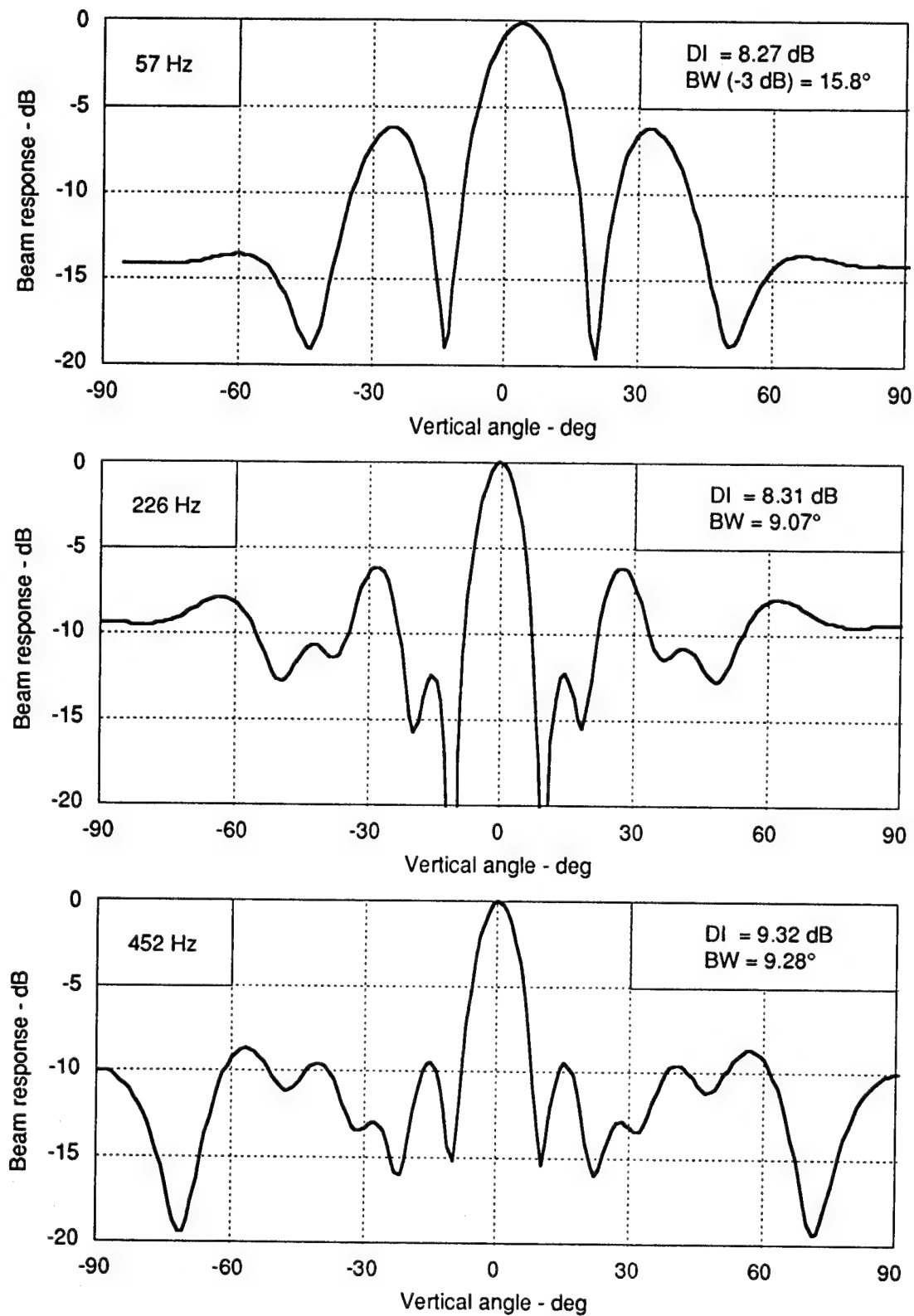
Figure 2.13
Vertical beam pattern for the horizontal beam.

(a) Peak direction

(b) Peak level
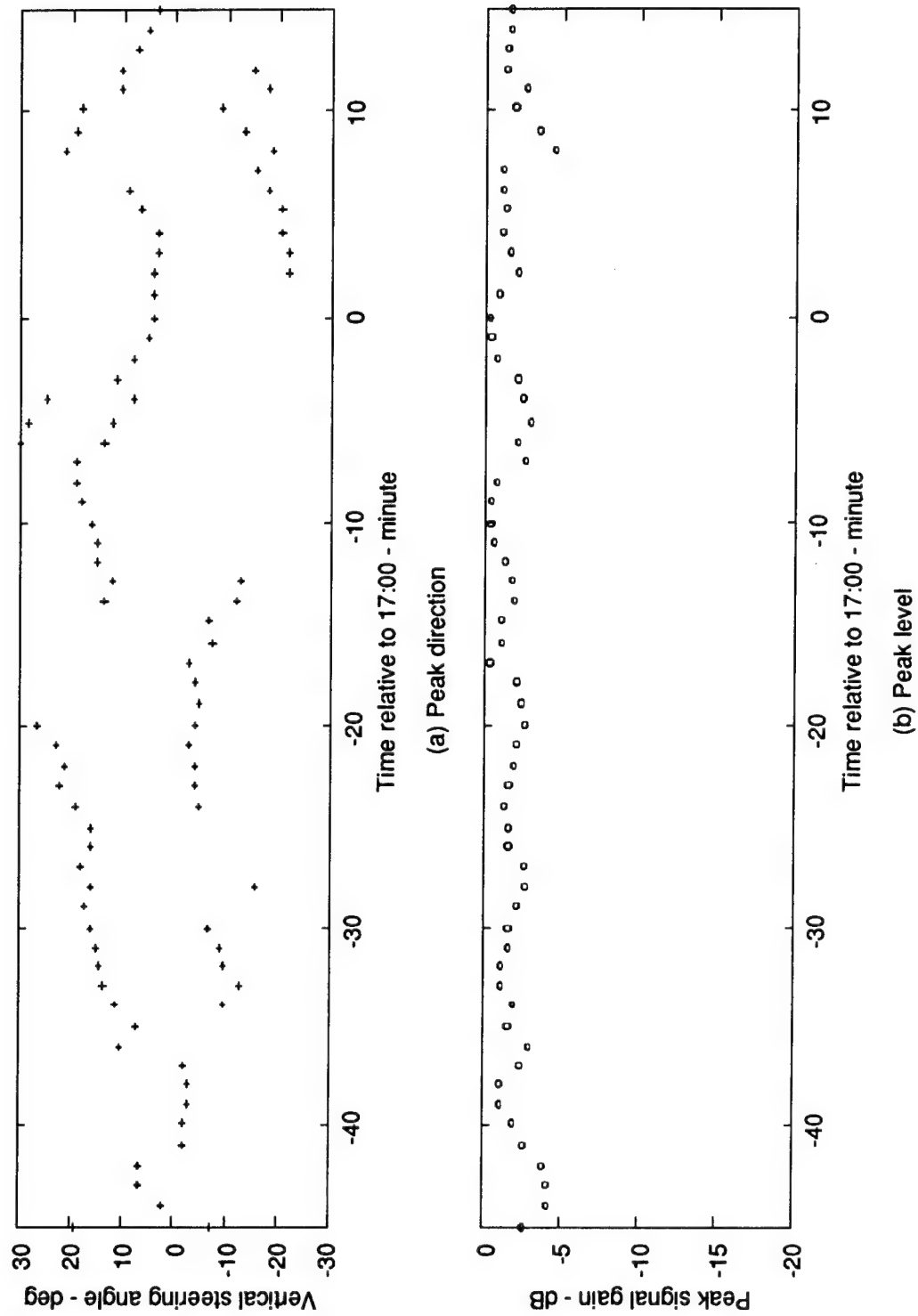
Figure 2.14

Measured peak signal gain from a conventional beamformer, 57 Hz.
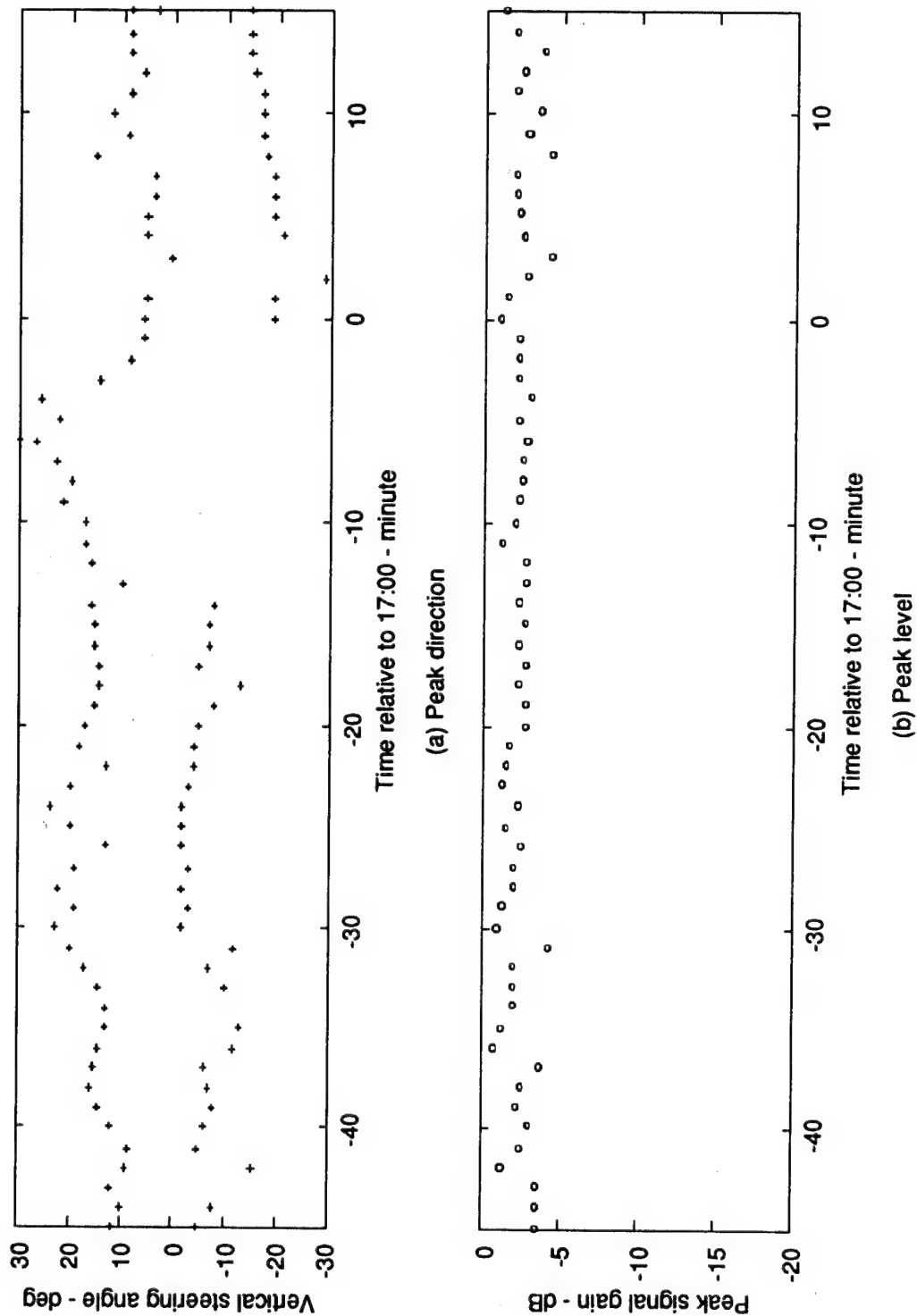
Figure 2.15

Measured peak signal gain from a conventional beamformer, 226 Hz.

Figure 2.16

Measured peak signal gain from a conventional beamformer, 452 Hz.

(a) Peak direction

(b) Peak level

38

CPA, were used to estimate vertical array tilt with respect to the source track. Observed differences of 4.5°–10° suggest the array tilt across the 57 Hz aperture was 3.8° ±1.2° upslope (toward shore).

At 226 Hz (Fig. 2.15), the energy is also split between two beams with peak arrival angles between -20° and +30° for ranges greater than 1 nmi. The average peak response angle for these beams are -7° and +13°. At ranges less than 1 nmi, the positive peak response angle increases as range decreases. In this same interval the downward beam disappears at ranges less than 0.5 nmi, as was seen at 57 Hz. The asymmetry about the horizontal and about CPA were again used to estimate array tilt. Based on the differences in peak response angles the estimated tilt across the 226 Hz subaperture was 3° ±0.2° upslope.

In Fig. 2.16, the 452 Hz energy arrives on two beams with steering angles of -3° to -5° and +12° to +14°. As was seen at the other frequencies, the peak response angle increases as range decreases below 1 nmi while the downward pointing beam disappeared inside of 0.5 nmi. The asymmetry in the peak response angles yielded an estimated array tilt of 5.0° ±0.5° upslope in the 452 Hz subaperture.

The estimates of the array tilt agree across frequency and are between 2.5° and 5.5° upslope. The subarrays used in CBF increased in length with decreasing frequency, and therefore the measurements imply a relatively straight array. A catenary array would exhibit more tilt in the higher frequency apertures. It should be noted that the measured tilt is actually the projection of array tilt into the plane of the source track, and represents a minimum tilt in the array. Tidal currents in the exercise area were expected to be less than 0.5 kt in a north-northeast direction. In a 0.5 kt current, the array tilt was designed to be 5° or less. Since the measured tilt is close to the expected value, it has been assumed that the measured tilt closely represented the total tilt of the array which was in a north-northwest direction. The major impact of an array tilt of this magnitude is to change the direction of the beams. SG degradation in the new beam directions should be much less than 1 dB.

The average maximum SGs at 57, 226, and 452 Hz were -1.7, -1.9, and -1.5 dB, respectively. The largest SG achieved at any one time was -0.2 dB at 57 Hz. For all frequencies, the maximum SG at all ranges always exceeded -4.1 dB. SG degradation of this magnitude can result from numerous factors, including non-planar wavefronts due to

39

varying sound speed across the array or multipath propagation. Even without considering these environmental factors, CBF performance is within 2 dB of the ideal performance.

Now let us examine the MBF output. Ideally, a modal beamformer requires the array to cover the entire wave guide with hydrophones spaced at a half wavelength or less. If the entire water column is not covered, the beamformer cannot always resolve adjacent modes, and the response is smeared across mode number. Although hydrophones throughout the entire array were used in the beamformer to increase the modal resolution, the array only covered 90 m of the 186 m water column, and therefore the modal beamformer smeared energy across several modes, and placed energy in the Scholte modes.

Figures 2.17–2.19 present SG for MBF. In these figures, plot (a) differs from those presented for the CBF results. The mode of maximum response has been highlighted. This helps identify trends in the response and counters some of the effects of the mode smearing.

In Fig. 2.17, the 57 Hz response peak sweeps from mode 2 to mode 9 during two time intervals: 1625–1640 and 1645–1655. Based on the mode phase velocities, this is equivalent to ray angles sweeping through angles of 0°–27°. These angles are the same as those observed using CBF during this same time period (Fig. 2.14).

At 226 Hz, Fig. 2.18, the peak response is scattered across modes 2–30 at ranges of 1–2 nmi (1625–1645), characteristic of multipath arrivals. Mode 2 dominates the propagation with an average maximum response of -3.0 dB. At ranges less than 1 nmi (1645–1700), the response is more characteristic of a direct path arrival with the energy moving into the higher modes as the range decreases.

The MBF output at 452 Hz, Fig. 2.19, exhibits a low order mode contribution and a high order mode contribution. An average maximum response of -2.6 dB occurs at the lower order modes for ranges between 1 and 2 nmi. At ranges less than 1 nmi, the response again is representative of a direct arrival.

The average maximum SGs for all ranges were -2.7 dB at 57 Hz, -3.2 dB at 226 Hz, and -3.5 dB at 452 Hz. The maximum gain at all frequencies and all ranges always exceeded -6 dB. Figures 2.17–2.19 showed the propagating energy to be

40

(a) Peak mode
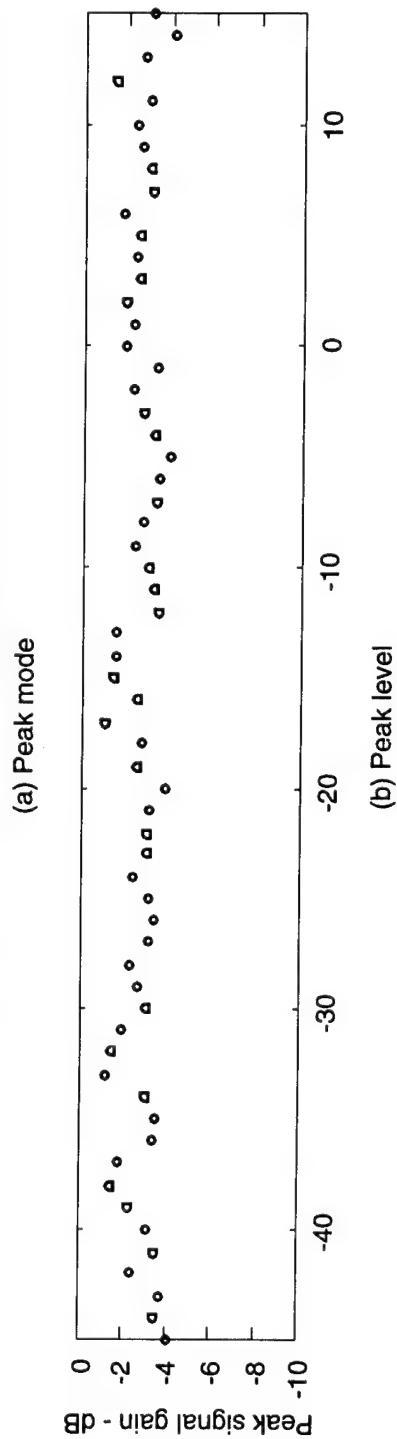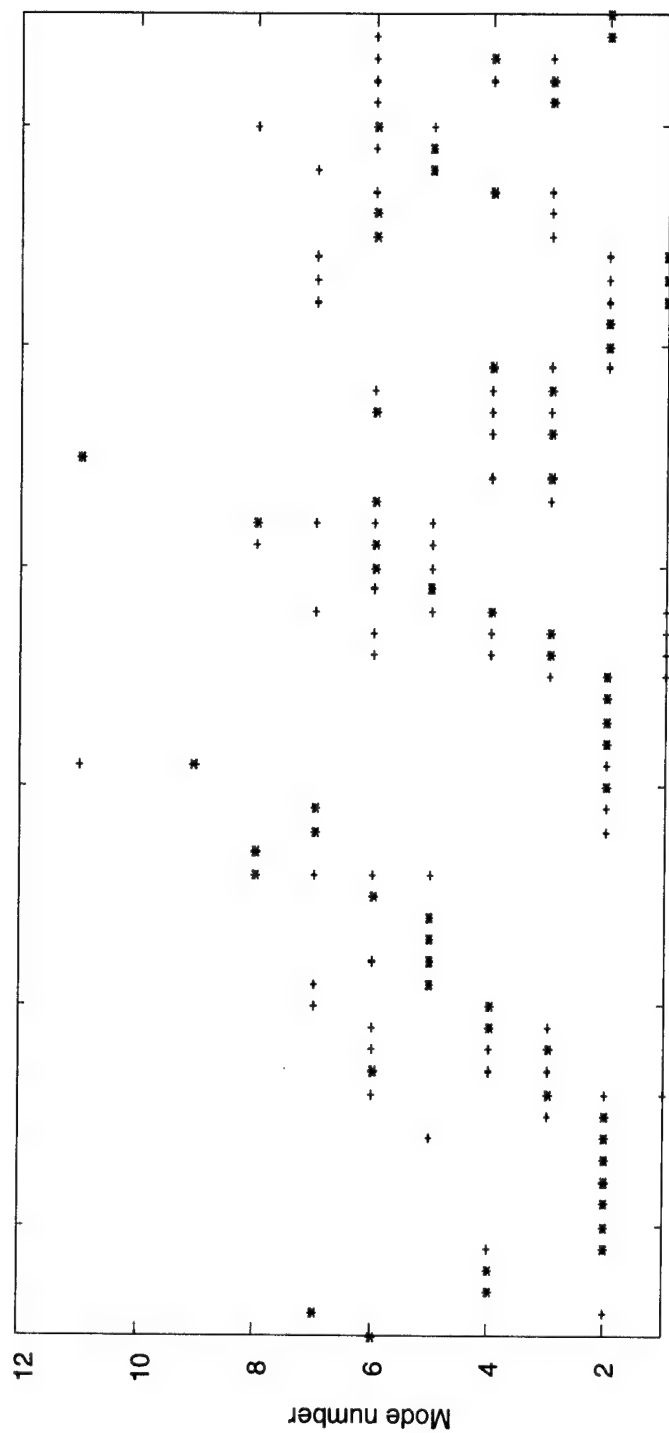
(b) Peak level

Figure 2.17

Measured peak signal gain from a modal beamformer, 57 Hz.

41
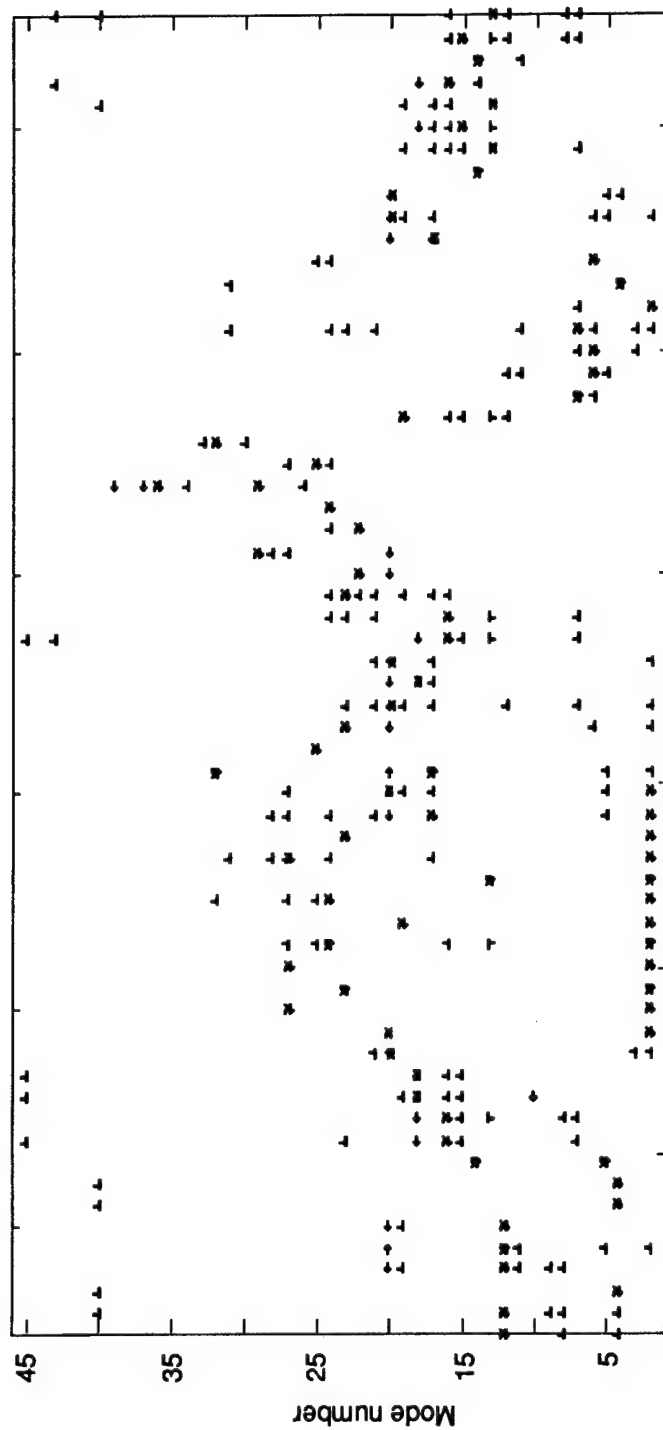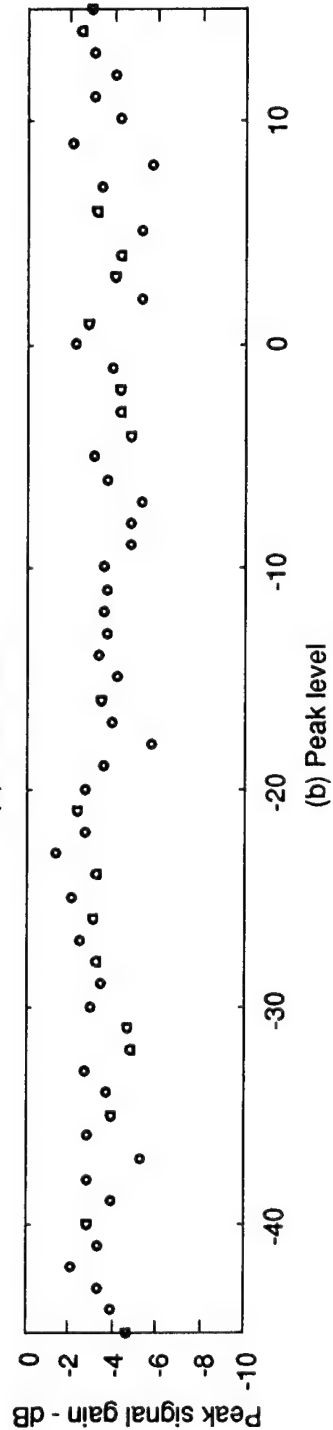
Figure 2.18

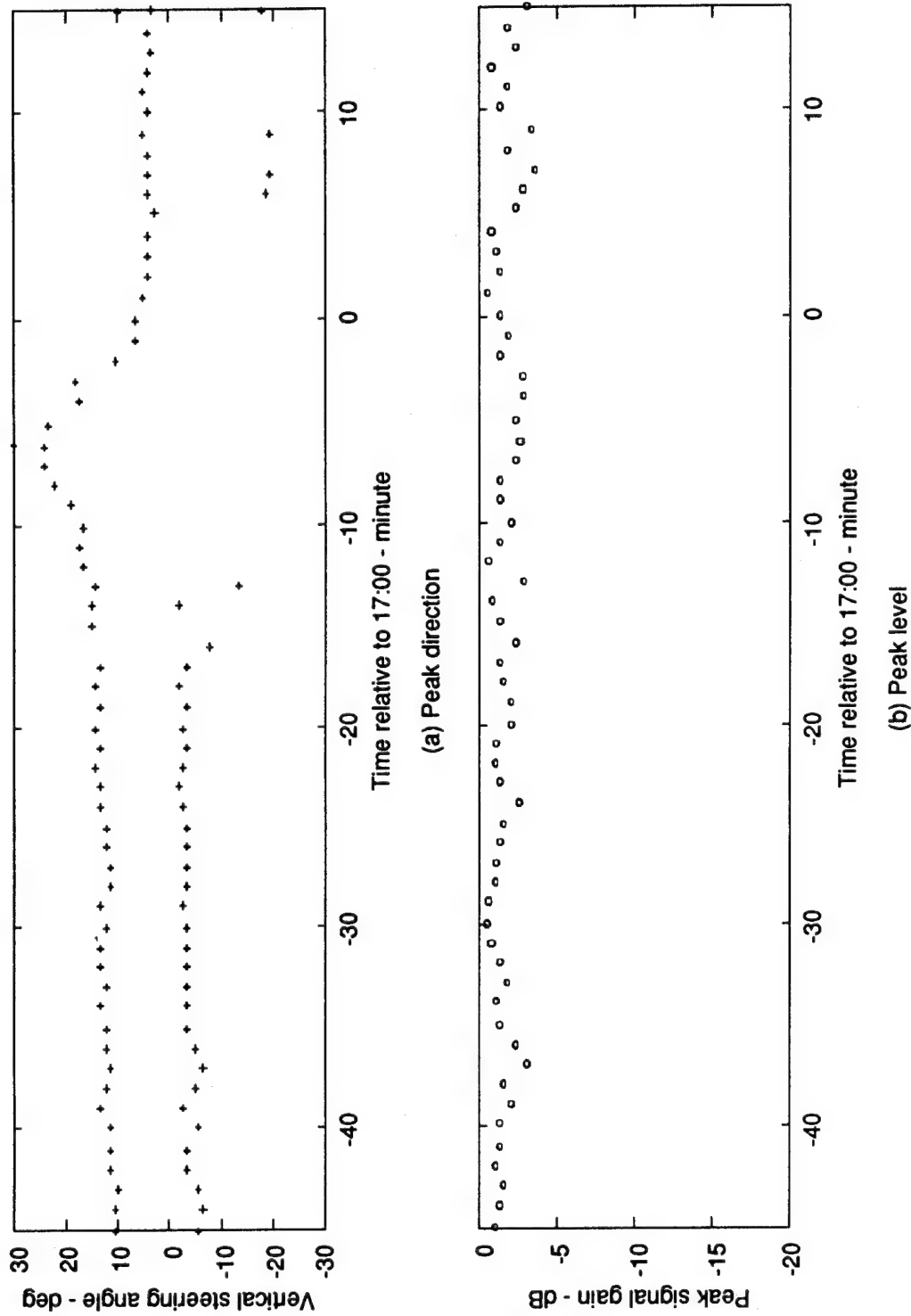**Measured peak signal gain from a modal beamformer, 226 Hz.**

(a) Peak mode

(b) Peak level

42
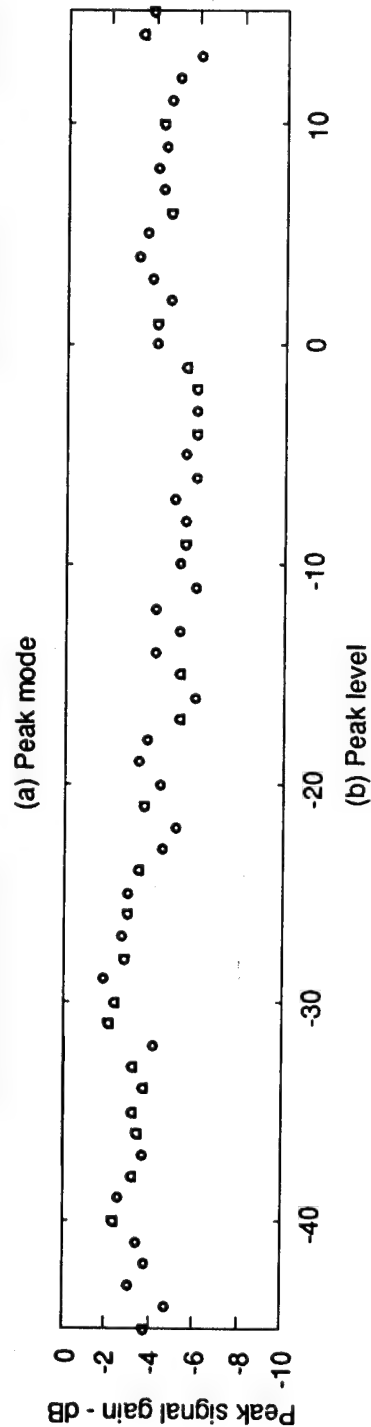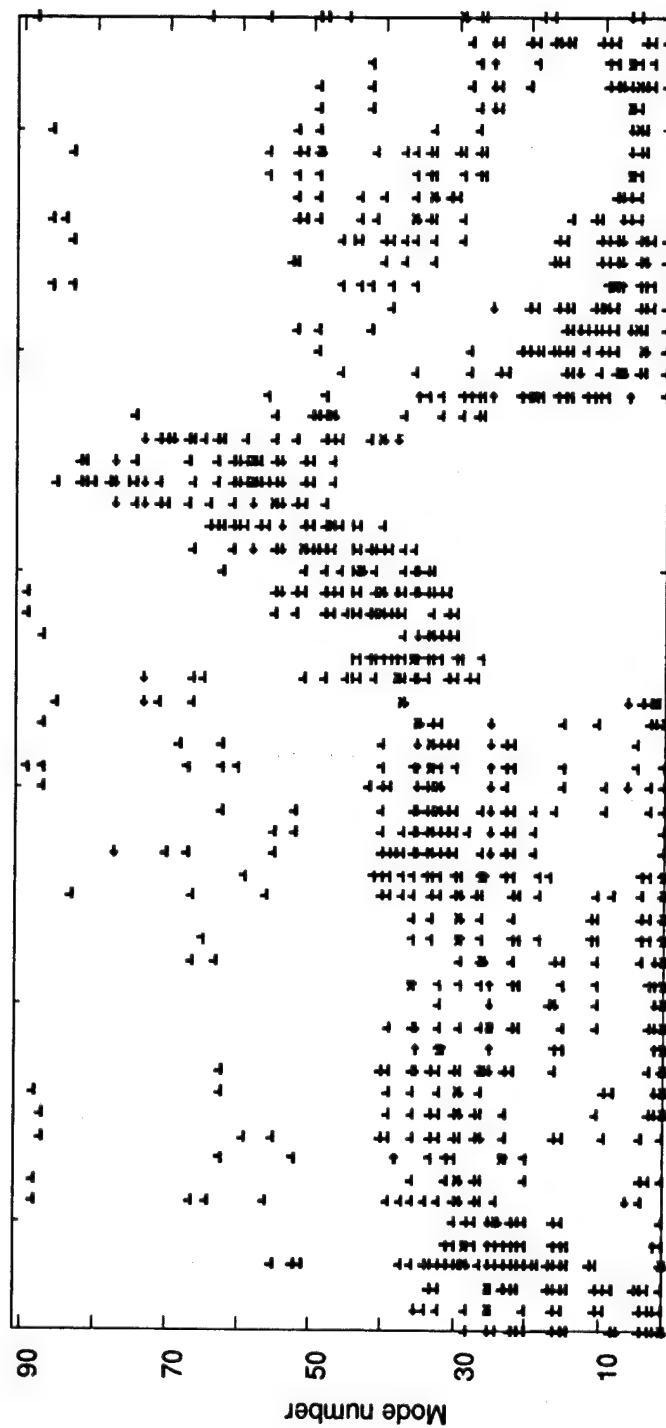
Figure 2.19

Measured peak signal gain from a modal beamformer, 452 Hz.

(a) Peak mode

(b) Peak level

43

distributed in several modes, directly resulting in the 3.5 to 4.0 dB degradation in MBF performance with respect to an ideal case.

Comparisons between the two beamformers indicate that for this array, CBF performed slightly better than MBF. Over the entire propagation event, CBF achieved SGs of -2.0 to -1.5 dB while MBF achieved SGs of -3.5 to -2.7 dB. At these short ranges, multipath propagation and wavefront curvature can contribute 2–3 dB degradation to the SG of both beamformers, so model calculations are needed to determine the exact amount of degradation that is attributable to the environment.

The environmental model, derived earlier, was used to address the question of the theoretical (not ideal) array performance in the exercise area and the actual amount of SG degradation seen in the measurements. Results from the theoretical SG calculations for the CBF are presented in Figs. 2.20 and 2.21 for 226 and 452 Hz, respectively. In these calculations the source depth was 35 m and the range varied from 0 to 7 km (3.75 nmi). These calculations were compared to the measured CBF results.

The model-data comparison of both the angle and SG were made for the loudest beams. Figures 2.20 and 2.21 exhibit a slight frequency dependence in the directions of the hot beams. At 226 Hz, the maximum response at ranges greater than 1 km (0.5 nmi) occurred at ±11° from the horizontal, while at 452 Hz, the maximum response occurred at ±9°. On these beams the average modeled SGs were -1.6 dB at 226 Hz and -0.9 dB at 452 Hz. In the data after the array tilt was removed, the loudest 226 Hz beams were at ±10° with an average SG of -1.9 dB and at 452 Hz, the beams were at ±8° with an average SG of -1.5 dB. The modeled beams pointed 1° higher and exhibited 0.5 dB more SG than actually achieved by the array.

A comparison of the overall structure of SG versus range shows the modeled results display energy arriving at slightly higher angles to the array. This may indicate that the geoacoustic model should have higher attenuations at deeper depths or that the acoustic basement was actually deeper than that used in the geoacoustic model.

The model-data comparisons show that the actual SG degradation is 0.5 dB or less. The geoacoustic model derived for the exercise area accounted for 0.9–1.6 dB SG degradation with respect to an ideal beamformer.

44

(a) Peak direction

Source-to-receiver range - km

(b) Peak level
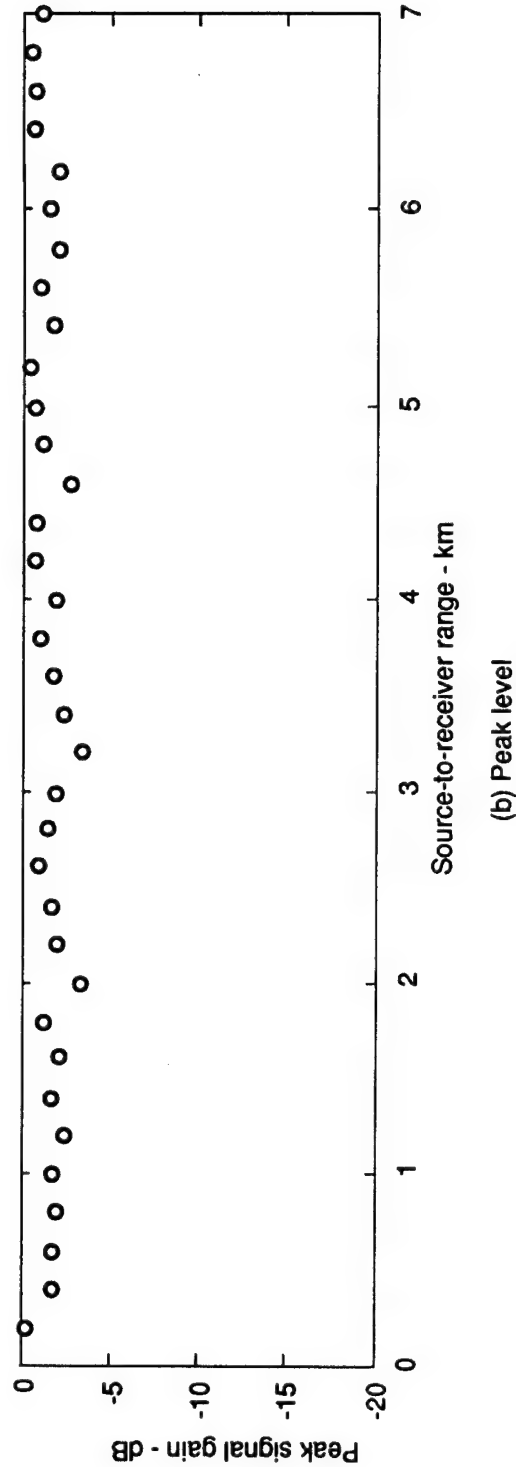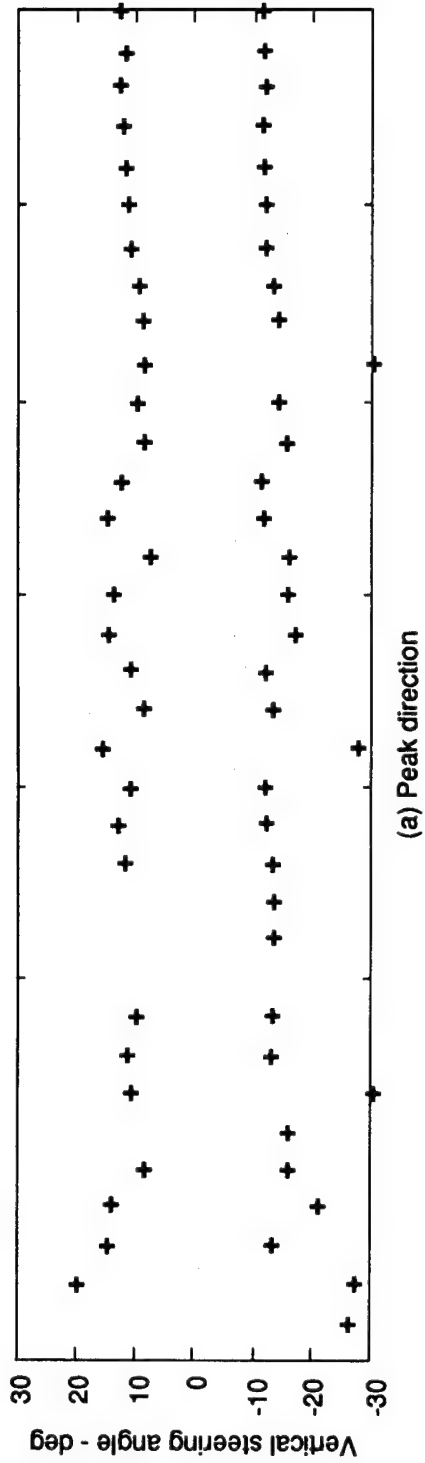
Figure 2.20

Theoretical signal gain from a conventional beamformer, 226 Hz.

45

(a) Peak direction

(b) Peak level
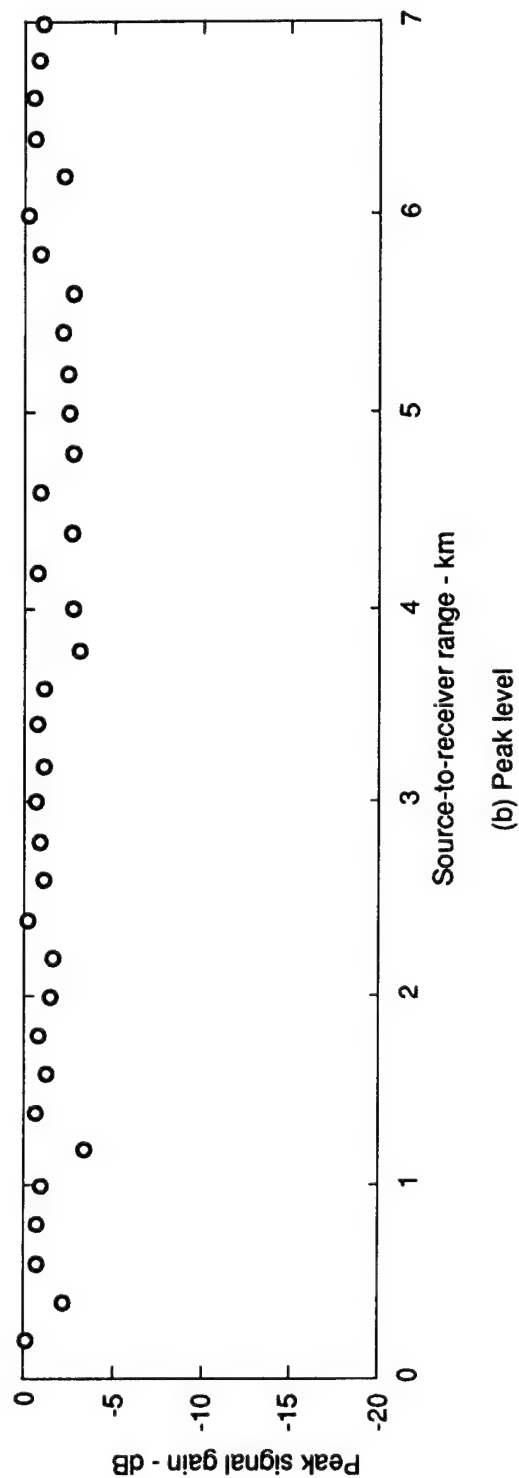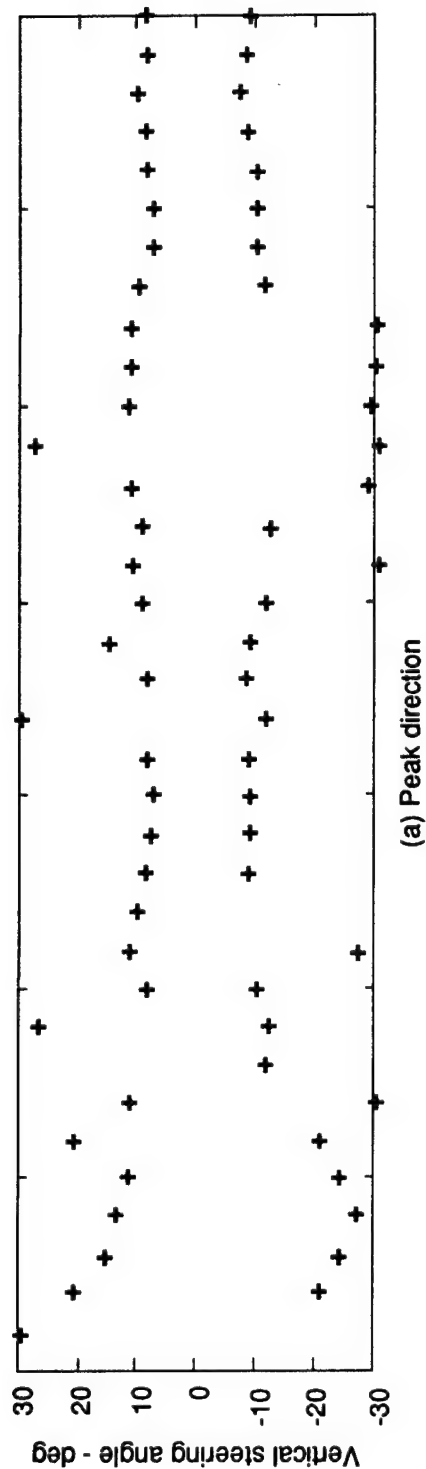
Figure 2.21

Theoretical signal gain from a conventional beamformer, 452 Hz.

3. AMBIENT NOISE

3.1 AMBIENT NOISE MEASUREMENTS

The April 1989 exercise included a dedicated ambient noise recording event. During this event, the RV Longhorn transited approximately 4.5 nmi north of the array site and shut down the main propulsion engines and non-essential equipment. From 1930 to 2130 the ship drifted approximately 1.4 nmi west (Fig. 1.6); the range varied between 4.15 and 4.65 nmi. The recorded wind for this time period was constant out of the southeast at 20 kt.

Problems with the measurements collected during the noise event were discovered after conventional beamforming was performed on this data set. A strong similarity to the broadside beam pattern was observed in the measured array response (Fig. 3.1), a result indicative of radio interference on the data link. Unlike the results from the cw event, array tilt is not evident. If the array response was the result of a spatially distributed acoustic process, array tilt would broaden the response by as much as twice the tilt angle. If the array response was for a directional acoustic source, array tilt would introduce a bias in the response. Although the measured response in Fig. 3.1 is broader than the plane wave beam pattern, it is suspected that the efforts to maintain proper rf SNRs were not adequate, and that RFI contaminated these noise measurements.

The ambient noise results presented below are for noise recorded during the 1615–1715, 26 April 1989 cw event. Efforts to eliminate RFI during the cw event were effective, as indicated by the observed array tilt and the agreement between the modeled and measured SG results. During this time period, the RV Longhorn began at a range of 3 nmi and transited towards the array at 5 kt. Between 1650 and 1704, the RV Longhorn was within 1 nmi of the array, and the data appear to be dominated by the tow ship noise. The Longhorn continued transiting away from the array to a range of 2 nmi. The wind during this time was steady at 17 kt out of the southeast.

Figure 3.2 presents AN time series during the cw event for a hydrophone depth of 134 m. The curves present data in 1/10 octave bands centered at 68, 191, and 380 Hz. These frequency bands lie between the projector lines transmitted for cw propagation analysis. At 1650, AN levels begin to increase as the RV Longhorn approaches within 1 nmi of the array site, introducing significant tow ship noise. The incoherent TL in

47
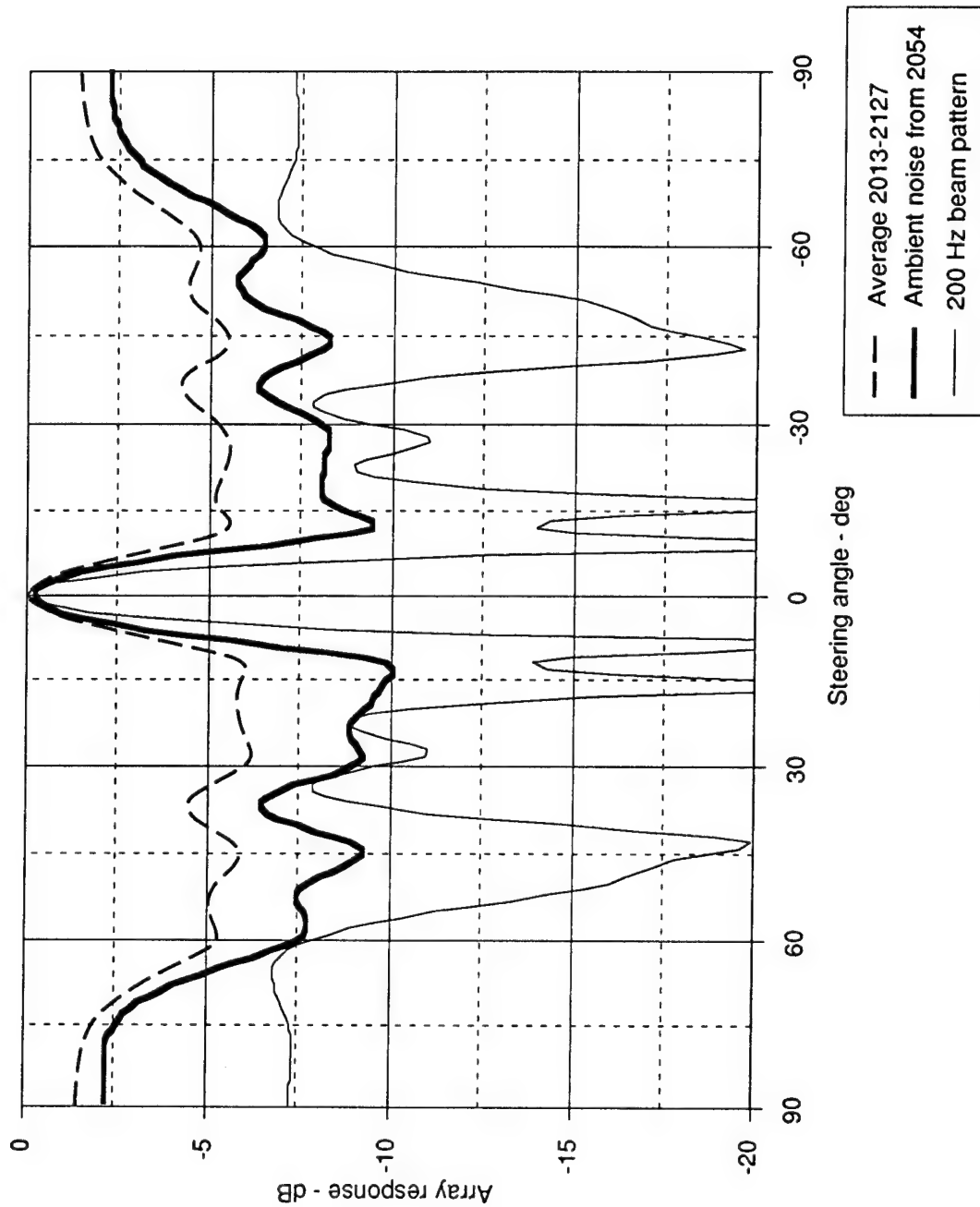
Figure 3.1

Comparison between beam pattern and measured array response, 200 Hz.

Legend:
- Average 2013-2127
- Ambient noise from 2054
- 200 Hz beam pattern

48
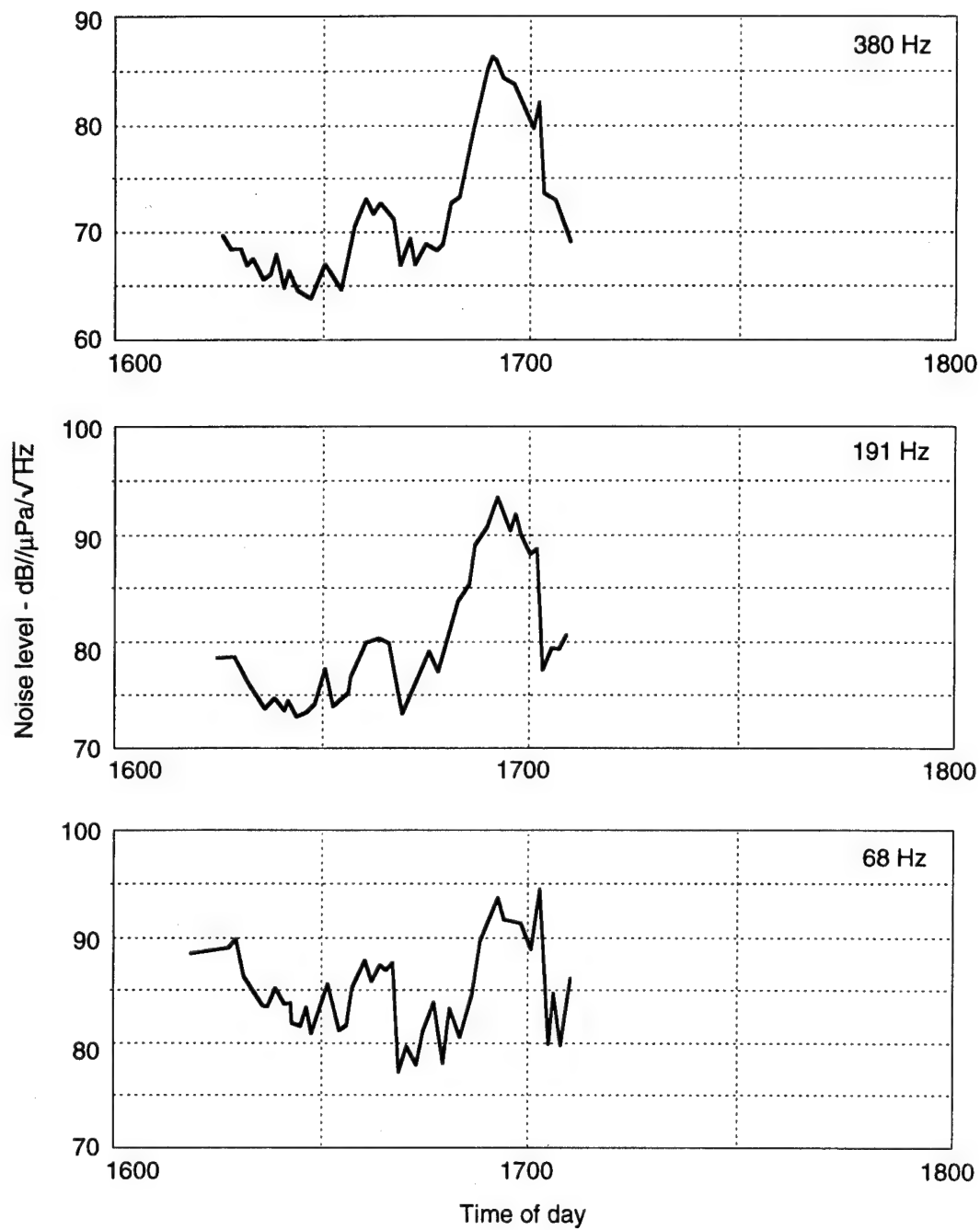
Figure 3.2
Ambient noise time series on day 116.

Fig. 2.11 shows that TL for a shallow source should increase rapidly as a function of range: increasing by at least 10 dB as range increases from 0.3 to 1 nmi. Similar changes are seen in noise level between 1650 and 1655, and therefore this increase is assumed to be associated with the tow ship. TL should continue to increase as the range increases beyond 1 nmi, but no similar change in AN is seen in the data prior to 1650. Therefore, prior to 1650, the measured noise data are relatively free of tow ship noise. The same conclusion is reached for the noise measured after 1704; that is, after 1704, the measurements are not biased by the tow ship.

3.2 AMBIENT NOISE SPECTRA

Figure 3.3 presents percentile plots of the measured spectra from the 178 m hydrophone for the time period 1615–1640, 26 April 1989. Ambient noise decreased with increasing frequency. At 10 Hz the median level was 93 dB//1μPa/$\sqrt{\text{Hz}}$, and decreased to 87.5 dB at 50 Hz, 82.5 dB at 100 Hz, and 67.5 dB at 400 Hz. These levels and the shape of the spectra were characteristic of noise dominated by shipping. Although shipping was not observed in the vicinity of the array, there are shipping lanes in this coastal region (Fig. 1.5), which could have contributed to the ambient noise.

Figure 3.4 presents a comparison between the measured median spectral levels and noise levels measured in other shallow water areas [15–18]. Water depths for these data sets were 160 m for curve b, 120 m for curves c and e, and 183 m for curve d. The lowest frequency in the Elba measurements, curve e, was 400 Hz, but modeled wind noise calculations extending down to 50 Hz were reported with the data. The 20–25 kt wind speed calculations reported with the Elba measurements were used to extend curve e in Fig. 3.4 to 50 Hz.

Shipping is present in the shallow water areas represented by curves b, c, and d in Fig. 3.4. The Elba results, curve e, are believed to be wind noise only. At frequencies below 350 Hz, the results from the present analysis are well above the Elba wind noise levels and exhibit levels and a frequency dependence similar to those seen in the regions with shipping. Therefore, noise in this area is assumed to have been dominated by shipping, in spite of the lack of radar contacts. Distant shipping, outside radar coverage, is assumed to have been the dominant source of noise.
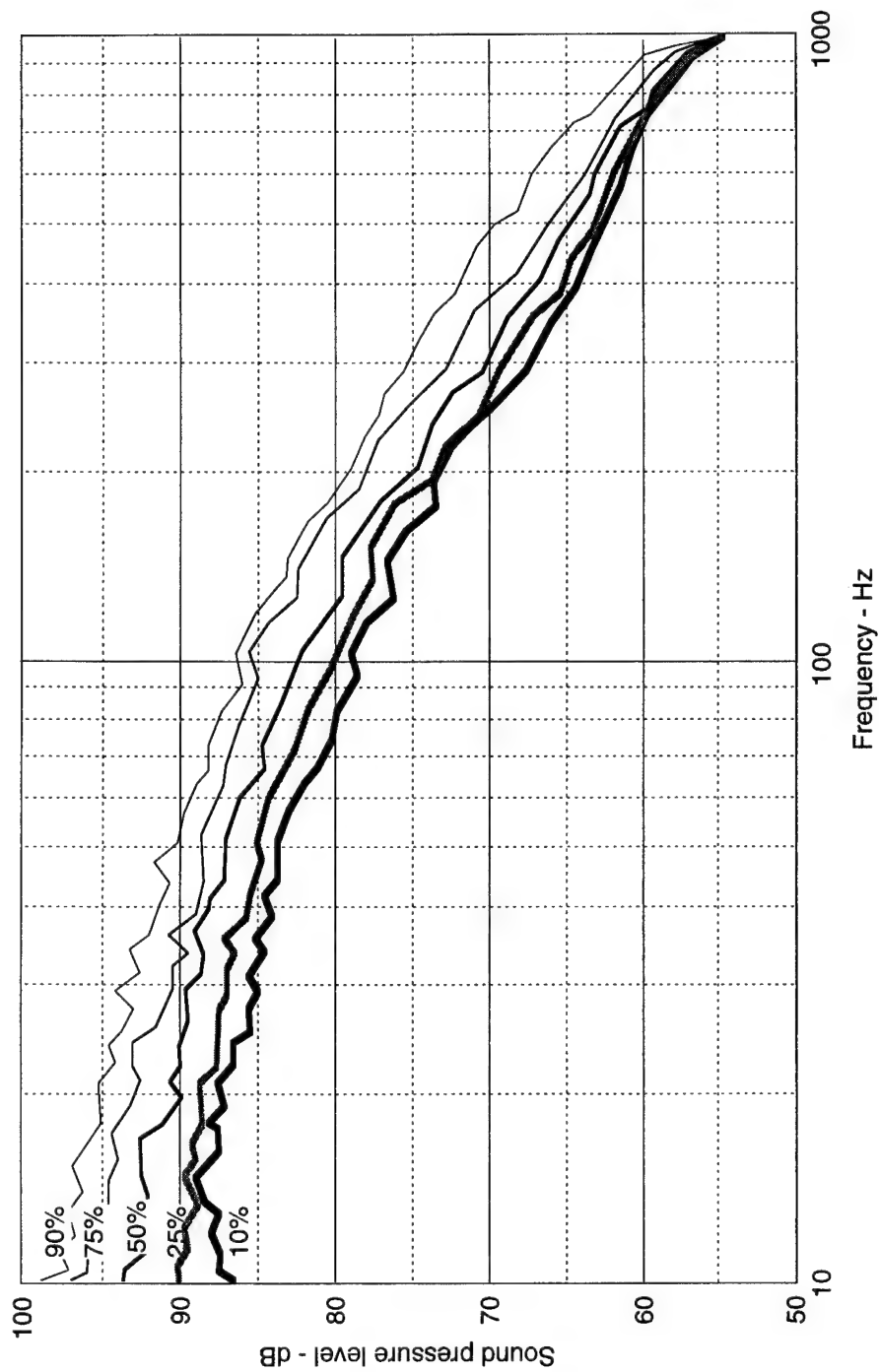
Figure 3.3
Ambient noise percentile spectra.
Receiver depth 178 m, day 116, 1615-1640
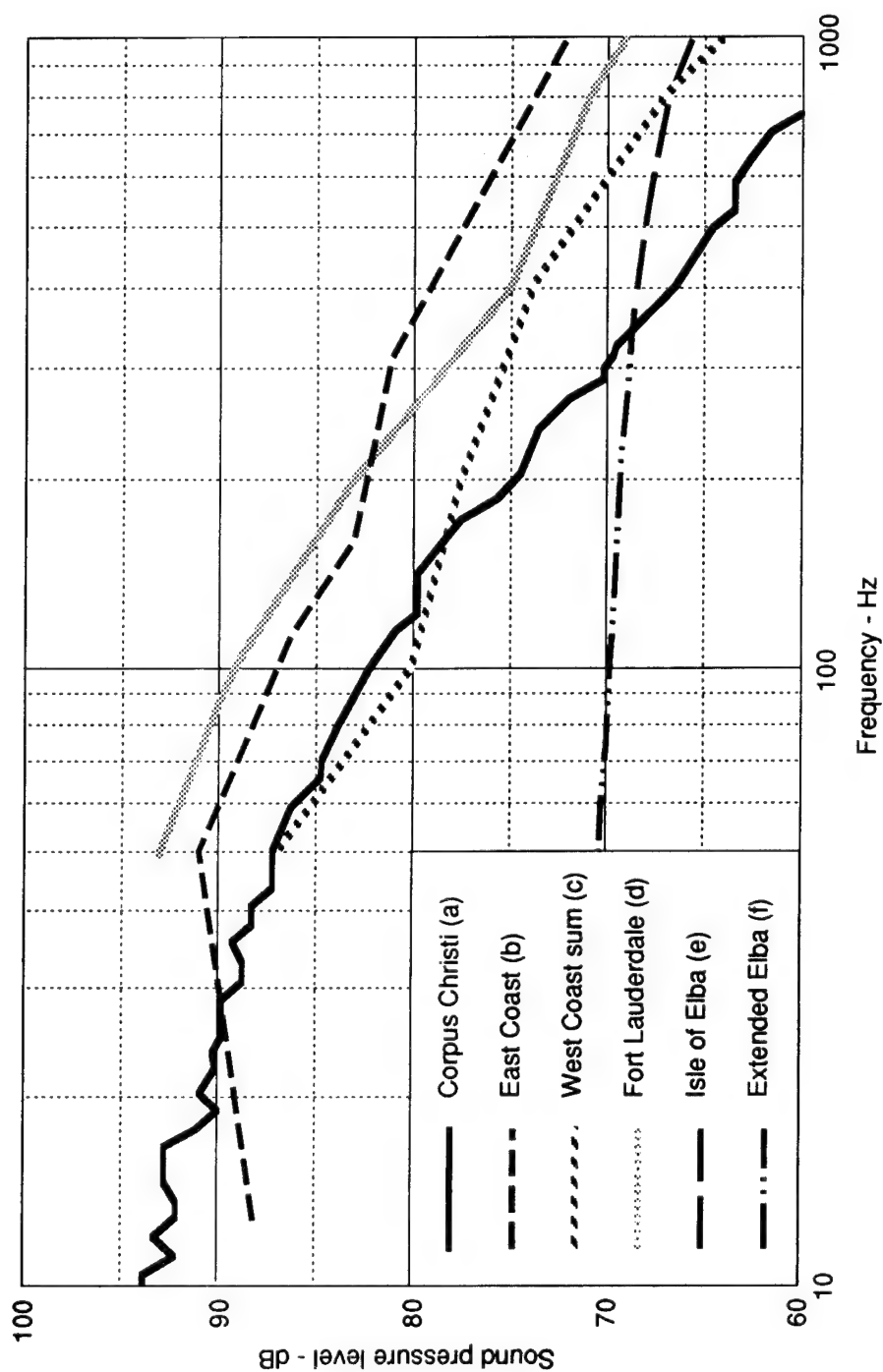
Figure 3.4

Measured ambient noise levels from five shallow water regions.

3.3   VERTICAL ARRAY NOISE GAIN

Analysis of the noise gain (NG) was performed on noise recorded during the cw event. Tenth octave bands centered at frequencies of 50, 200, and 400 Hz were selected for analysis. These bands are between the cw projector lines used in the propagation measurements, thus avoiding contamination by the projector.

Figure 3.5 presents the measured NG at 200 Hz during the cw event. Like the figures of SG, NG is presented with plot (**a**) showing the directions for the one or two loudest beams, and plot (**b**) showing the maximum NG. The same normalization scheme discussed in the SG section was applied to the noise data, so that NG = 0 dB indicates that all the noise arrives on one beam. Prior to 1640, NG had peaks between ±10° and peak values of ~-4 dB, compared to the -10 log(N) = -9 dB that one would expect in isotropic noise fields. As the RV Longhorn approaches within 1 nmi (after 1645) the peak moves to steeper angles until the ship reaches CPA at 1655. At the same time, it appears that the peak response for the downward looking beam also sweeps up toward the surface, which is the opposite of what should happen. As the arrival angles become steeper with the approach of the Longhorn, the attenuation in the sediment reduces the negative-angle energy of the noise to levels below the sidelobe contributions from the direct path components, and sidelobe contributions dominate the response at negative angles. This gives the appearance of negative-angle energy sweeping up toward the surface. After the Longhorn passes the array, the whole process reverses, with the peak response angles sweeping back down towards horizontal.

Similar results are seen at 400 Hz (Fig. 3.6). Noise arrives between ±10° at the longer ranges, and as the Longhorn approaches the array, the peak response shifts toward the surface. The effects of the sidelobes are also seen in the short range data. While the Longhorn is at the longer ranges, NG is -5 to -6 dB, 3 to 4 dB above the nominal -10 log(N) = -9 dB for isotropic noise.

The noise at 50 Hz, Fig. 3.7, was more omnidirectional than the higher frequencies, but horizontal peaks are still evident. The arrival angles were scattered between ±15° while the Longhorn was at longer ranges, and then spread to ±20° as the Longhorn approached the array. Throughout most of the time period, NG was -4 to -6 dB, just slightly higher than the nominal -10 log(N) = -7 dB expected for isotropic noise.

(a) Peak direction

(b) Peak level
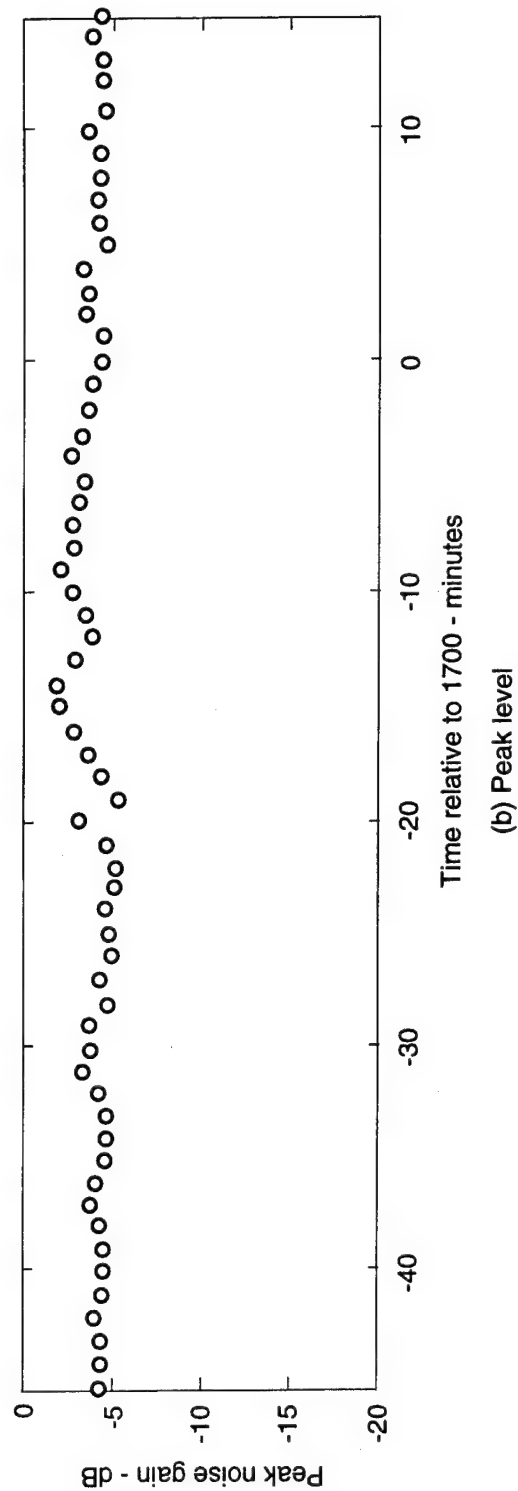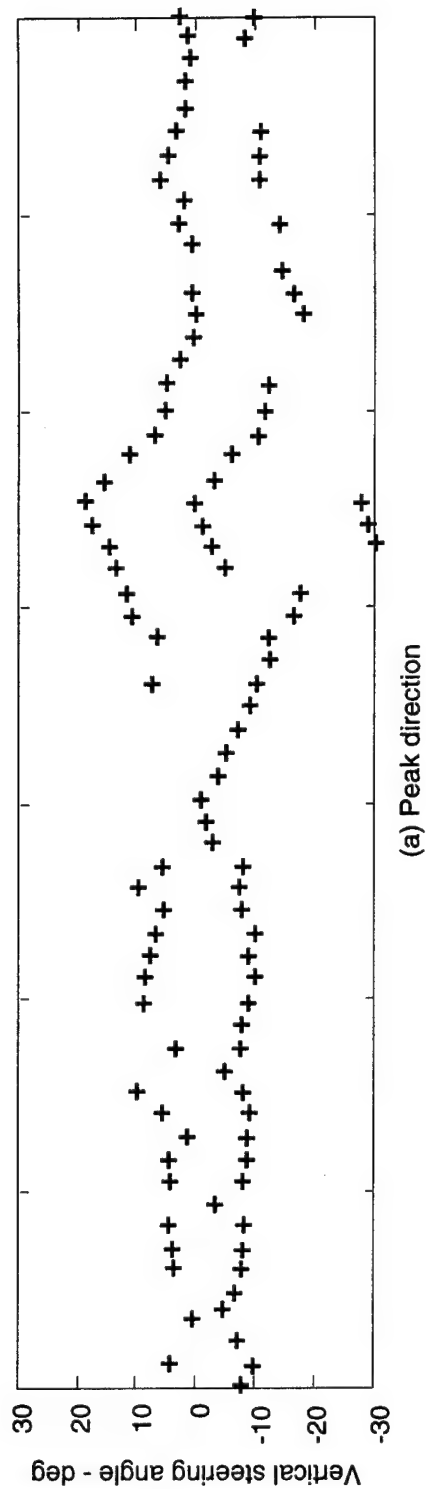
Figure 3.5
Measured noise gain, 200 Hz.

54

(a) Peak direction

(b) Peak level

Time relative to 1700 - minutes
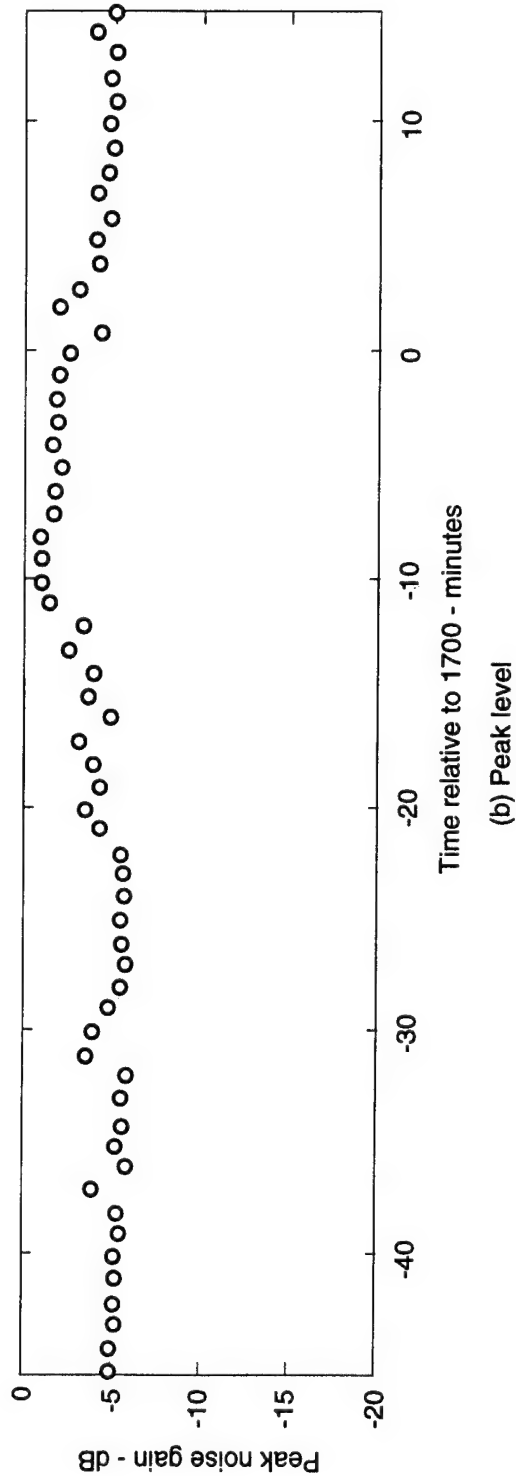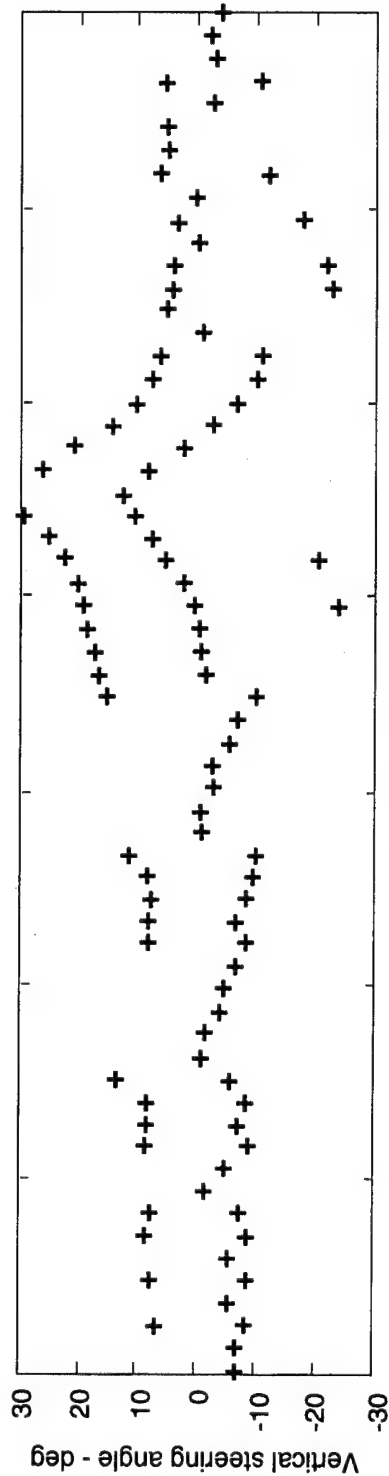
**Figure 3.6
Measured noise gain, 400 Hz.**

55

(a) Peak direction

(b) Peak level
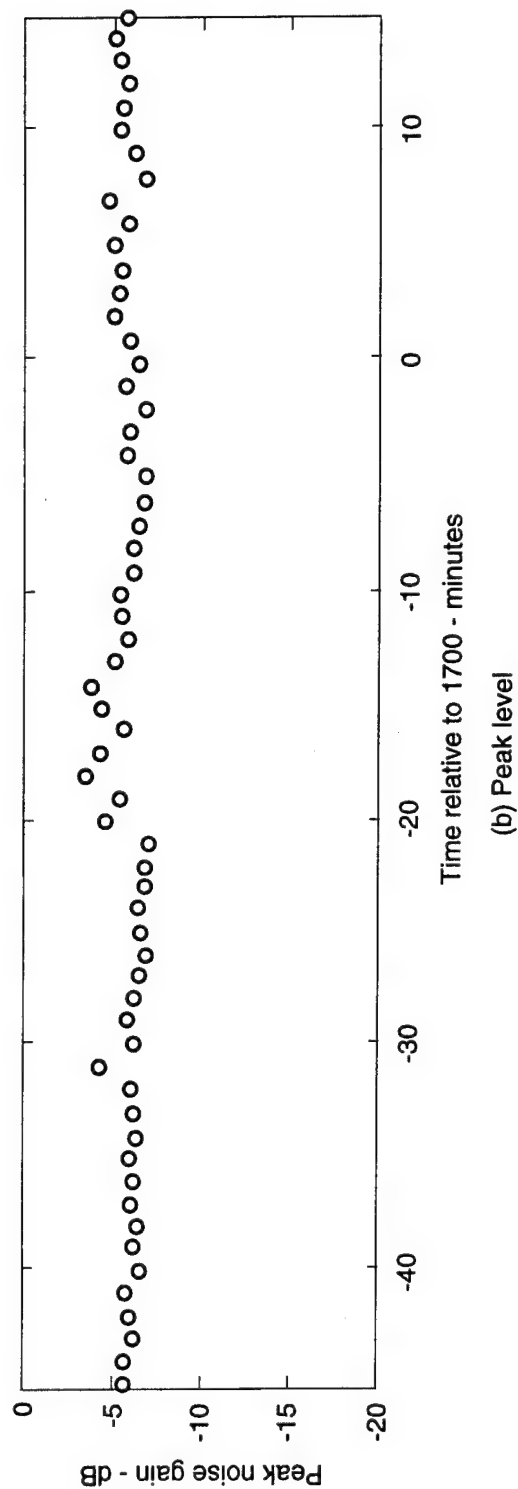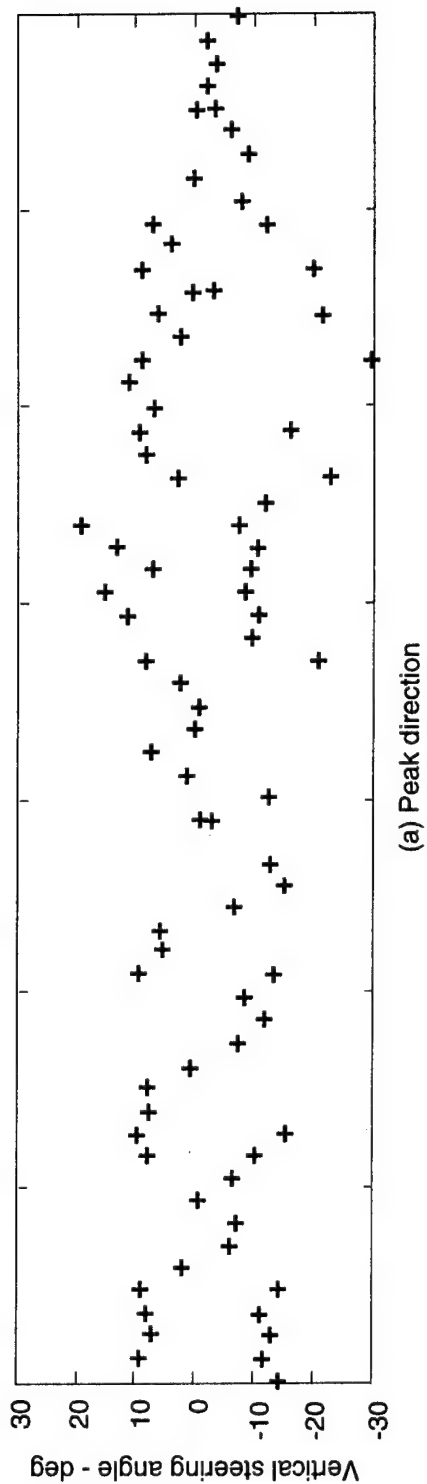
Figure 3.7
Measured noise gain, 50 Hz.

Although there are similarities between NG (Figs. 3.5–3.7) and SG (Figs. 2.14–2.16), the differences are important and indicate that these peaks at longer ranges are not the result of the presence of the exercise ship. The peaks in NG are symmetric about the horizontal and are separated by less than 20°. At the same time, peaks in SG are asymmetric about the horizontal, and are separated by more than 20°. Array tilt can yield this type of asymmetry. Energy arriving from the direction of the tilt will appear on higher angle beams, while energy from the opposite direction will appear on lower angle beams. Since the source is in a single direction, array tilt will tend to create asymmetry in SG plots. Noise is azimuthally distributed, and any asymmetry due to noise in one direction tends to offset the asymmetry for noise in the opposite direction. The most dramatic similarity between NGs and SGs occurs when the Longhorn is within 1 nmi of the array. During these time intervals the Longhorn dominated the noise, and therefore one should expect the SG and NG to be similar, since the sources are physically connected together.

An average 200 Hz NG (Fig. 3.8) was computed for the time period 1615–1640 to display the angular characteristics of NG while the Longhorn was away from the array. The 200 Hz NG at 1632 is also presented in Fig. 3.8, selected because two peaks are quite evident at this time. The average NG has peaks at -6° and +5° without a significant null in between, while at 1632, peaks occurred at -10.5° and +6.5° with a 1 dB null at -2°. The maximum NG for these two curves was -4.5 dB, and the -3 dB beamwidth was 30°. Secondary peaks occurred at ±30° and ±60° and were only 2.5–3.0 dB down from the main peaks.

3.4   MODELED NOISE GAIN

Theoretical NG was calculated for the exercise area based on the K&I noise model. Calculations for omnidirectional noise sources at 1 m depth are presented in Fig. 3.9. The results exhibit peaks at ±29°, which differ significantly from the ±5°–10° seen in the data.

The K&I model was developed to model wind noise characteristics. Spectral analysis of the measurements, however, indicated that the noise was probably dominated by distant shipping. The K&I model assumes an infinite sheet of noise sources, and therefore does not accurately describe the existing noise field during the exercise. NG for distant shipping noise could be more accurately modeled by SG for a distant source.

57
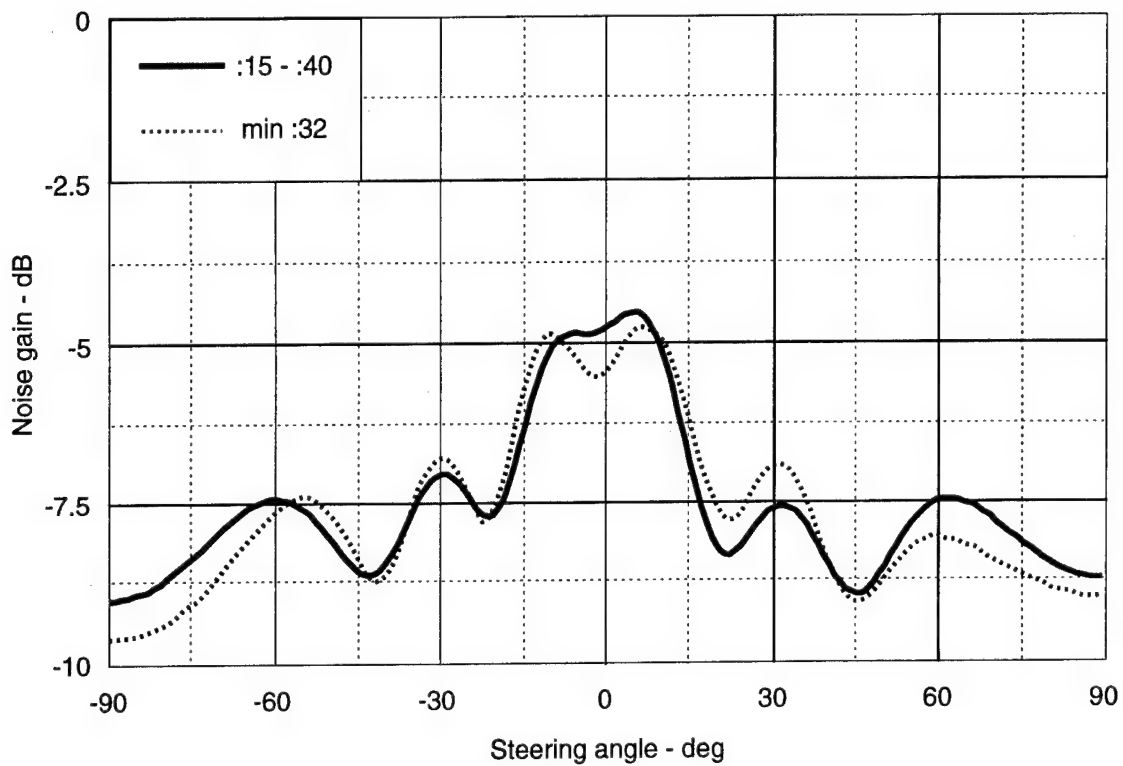
Figure 3.8
Average array response to measured ambient noise, 200 Hz.

58
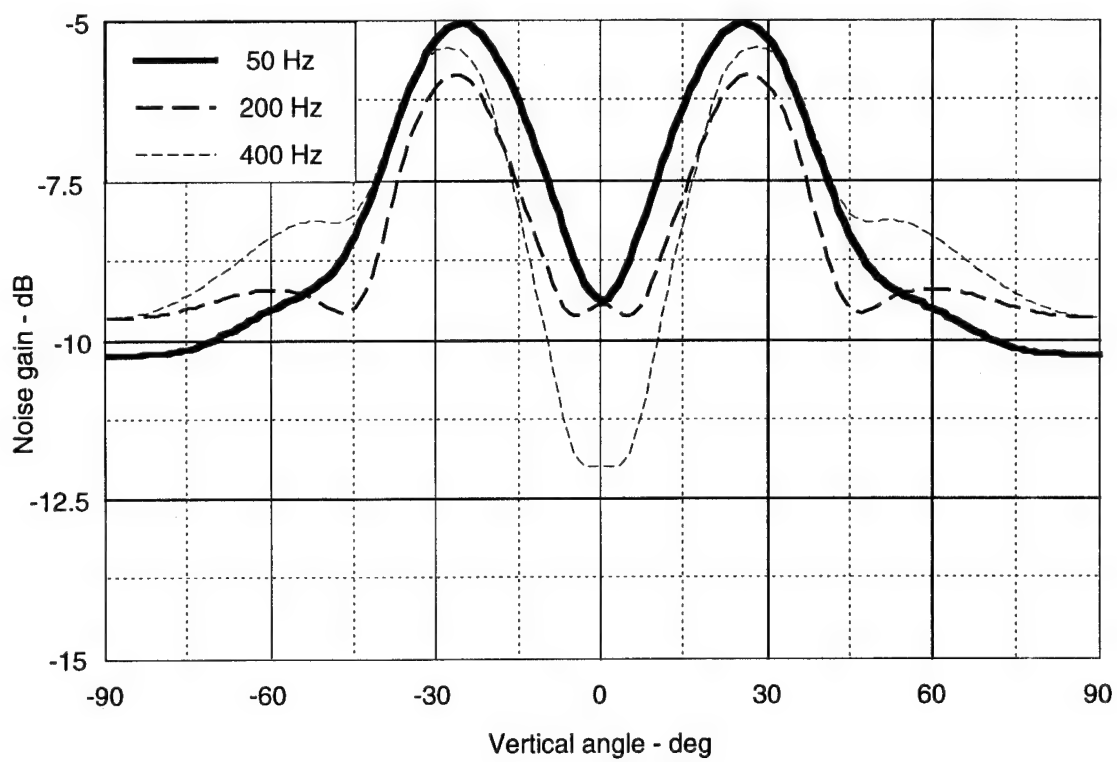
Figure 3.9
Modeled array response.
Noise source depth = 1 m

Figure 3.10 presents average SG calculated at 200 Hz for a 5 m source at ranges of 10–60 km (5.5–32 nmi). Maximum SG occurs at ±10°–13°, slightly greater angles than seen in the data. For the calculations to peak at shallower angles, the lowest order modes need more excitation. Figure 3.11 presents the first three modes for the exercise environment. These modes correspond to arrival angles between ±7°. The amplitude of these modes is approximately zero at depths less than 5 m, and therefore it would be very difficult for shallow noise sources to couple any energy directly into these modes.

The combination of the downward refracting profile and the water depth prevents shallow sources from exciting the lowest order modes. One mechanism which would increase low order mode excitation is range variability of the environment. Although the slope of the bottom in the exercise area is only 0.3°, the bottom depth changes by 100 m over a range of just 10 nmi.

Figures 3.12 and 3.13 present the first three mode functions at 200 Hz for the archival profile in Fig. 1.3, and water depths of 140 and 100 m, respectively. As the water depth decreases, the mode amplitudes near the surface becomes appreciable. Shallow sources in 100 m of water excite the lowest order modes, and these modes can propagate down slope.

The bathymetry along the 270° radial at the array site (Fig. 3.14) was used to address the issue of a range dependent environment. An adiabatic normal mode model computed the acoustic propagation using mode sets centered at the ranges indicated in Fig. 3.14. The water depth was 186 m for mode set 1, 140 m for mode set 2, and 100 m for mode set 3. In the calculations that follow, the array was located in the deep water, and a 5 m source transited into shallower water. TL for a 143 m deep receiver (middle of the array) is presented in Fig. 3.15. The shallow source depth and the bottom characteristics cause TL to increase rapidly with range. TL increases from 60 dB at 0.1 nmi to 80 dB at 5 nmi and 110 dB at 20 nmi.

Figures 3.16–3.18 present peak beam angle and maximum SG calculated at 200 Hz for a source located in range intervals centered about the source positions indicated in Fig. 3.14. In Fig. 3.16, a source in 140 m of water excites mode set 2, which convert into mode set 1. Gain peaks of -3 to -1 dB occur at ±7°–15°. In Figs 3.17 and 3.18 a source in 100 m of water excites mode set 3, which couples into mode set 2 and
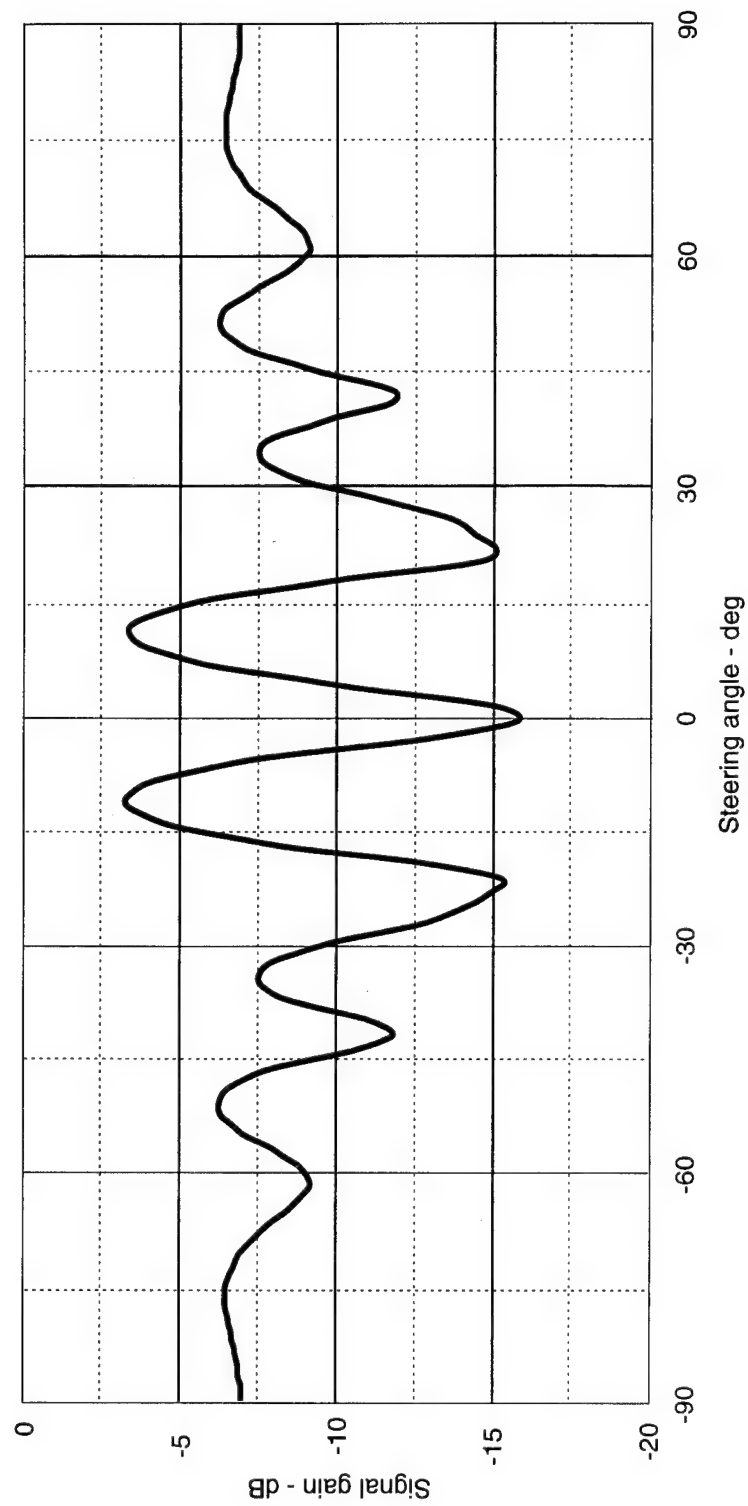
Figure 3.10

Averaged modeled array response for a 5 m source in a 10-60 km range interval, 200 Hz.

61
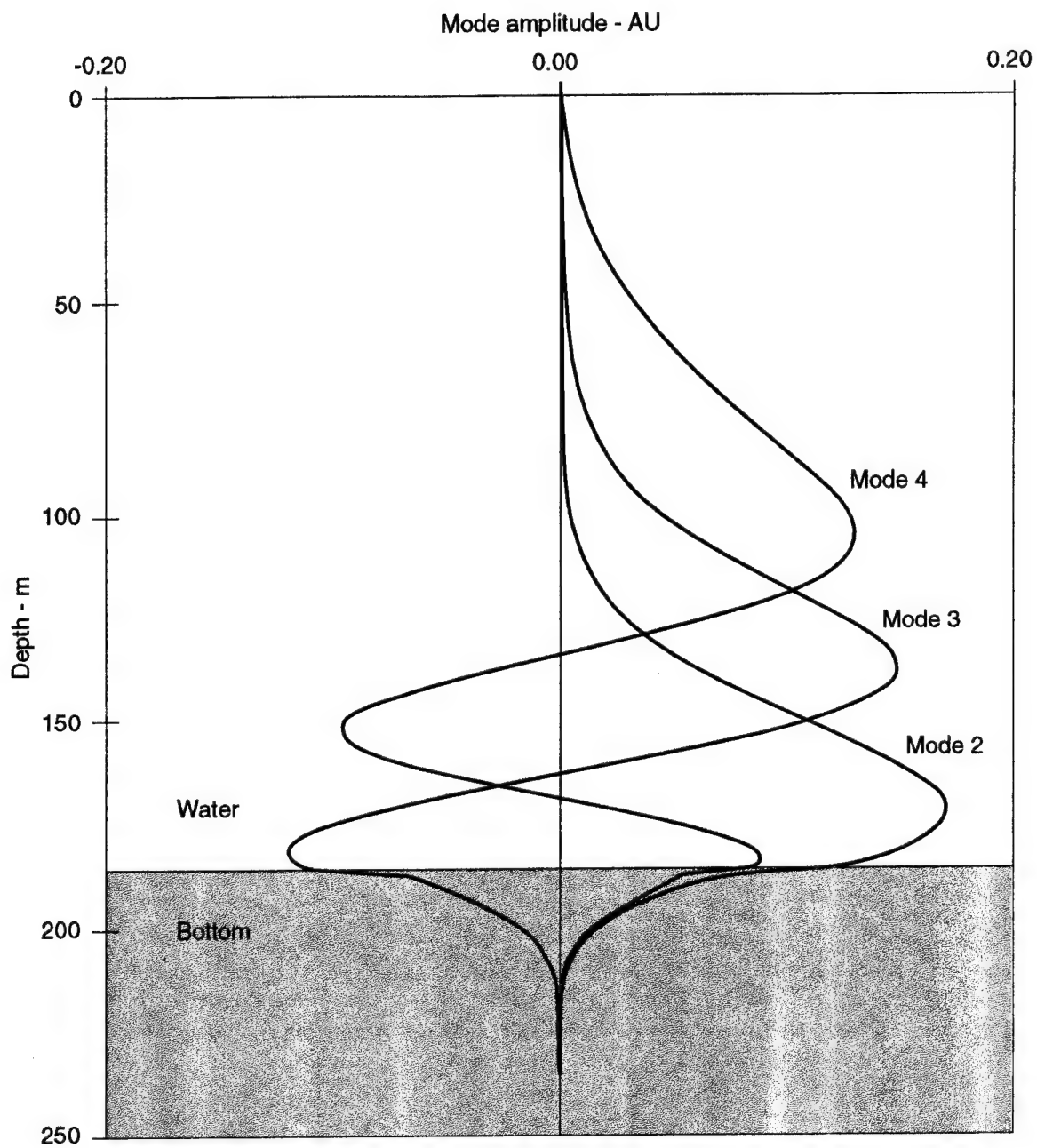
Figure 3.11
Normal modes for 186 m water depth in the exercise area, 200 Hz.
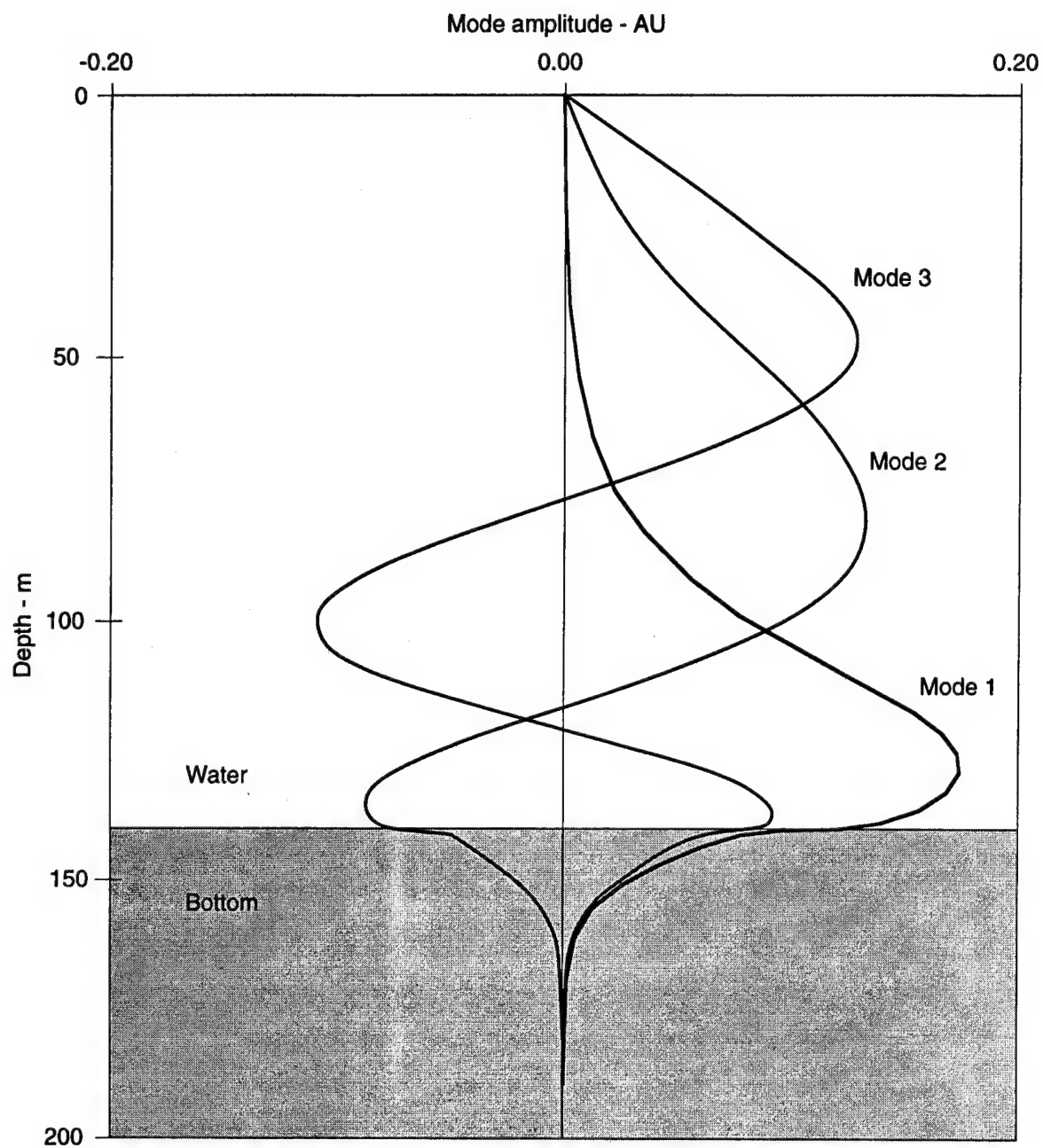
Figure 3.12
Normal modes for 140 m water depth in the exercise area, 200 Hz.

63
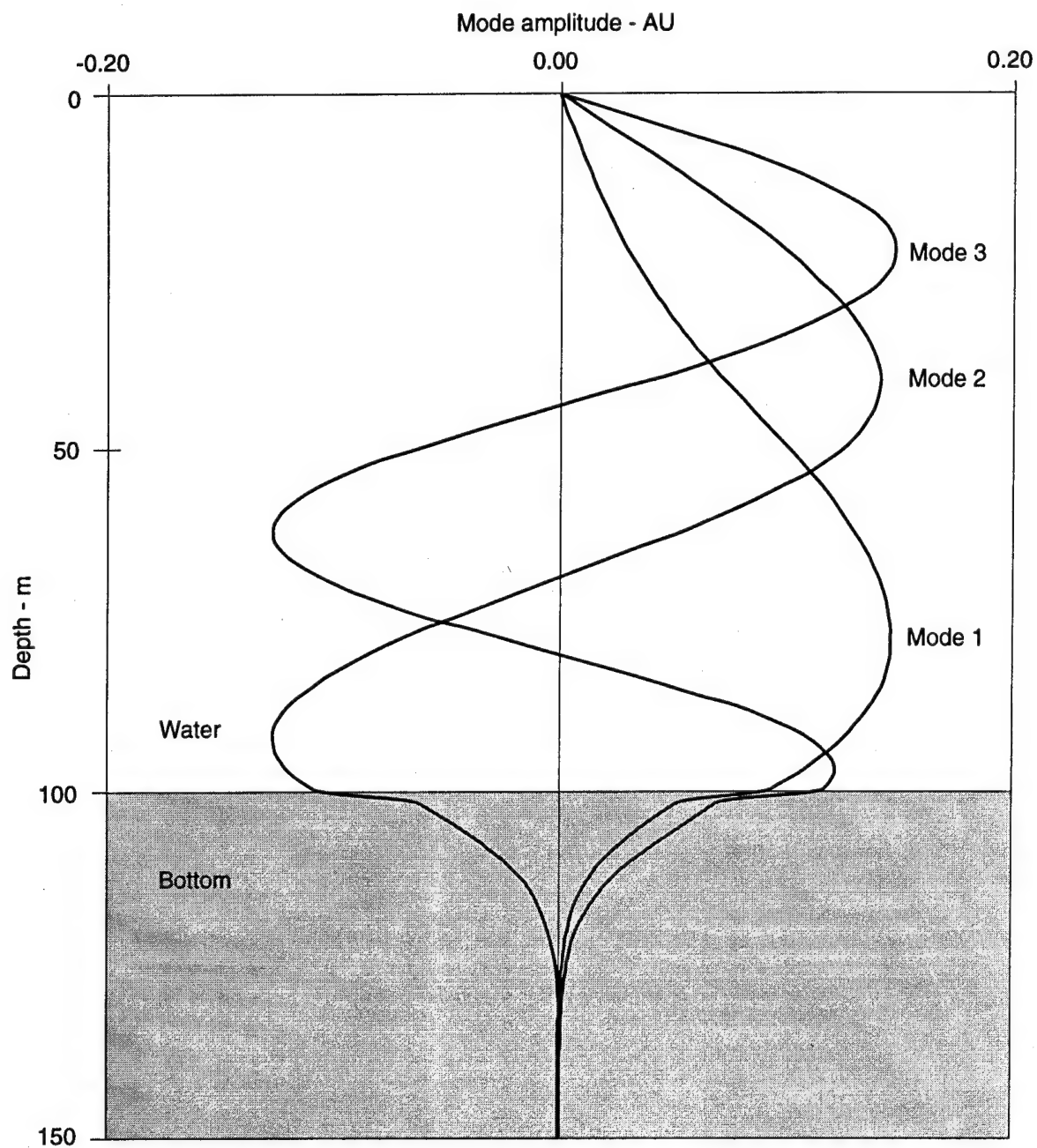
Figure 3.13
Normal modes for 100 m water depth in the exercise area, 200 Hz.
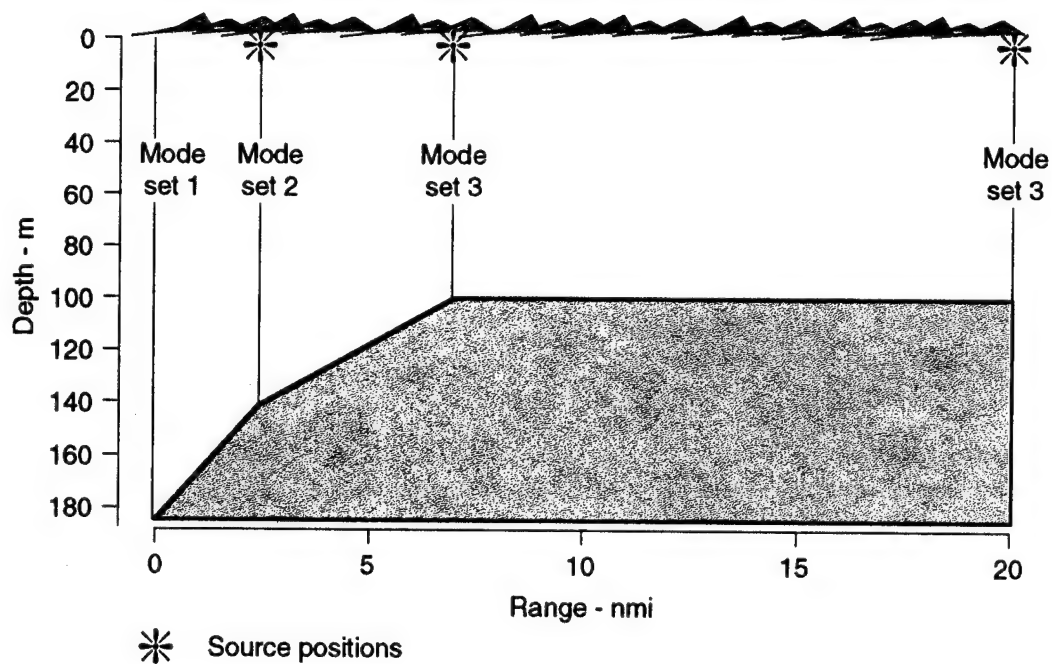
Figure 3.14
Modeled bathymetry west of the exercise site.

ARL - UT
AS-94-1121
KCF/RFO
8-95/as3
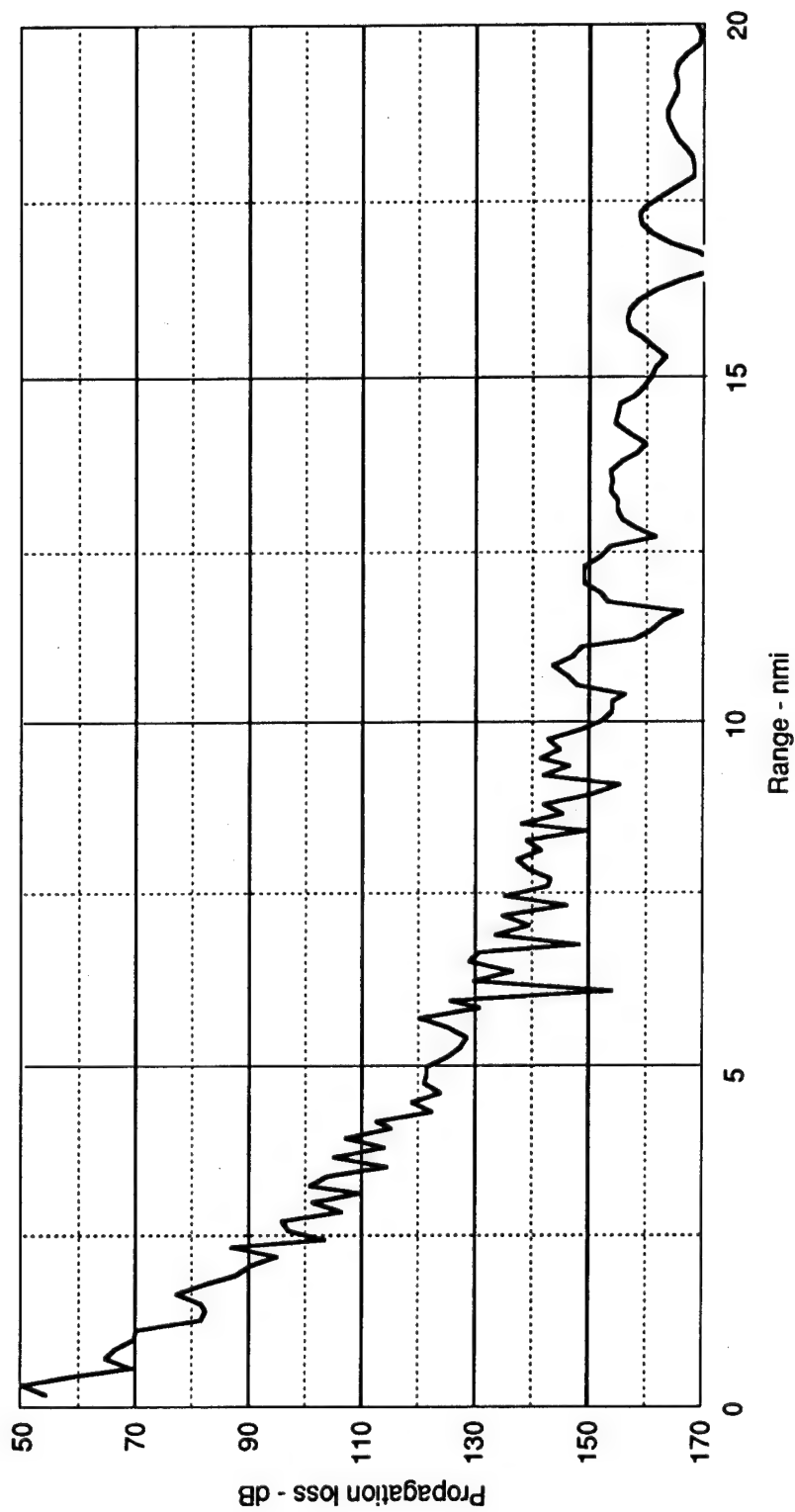
Figure 3.15
Transmission loss at 200 Hz in a range variable environment.
5 m source depth, 143 m receiver depth

66
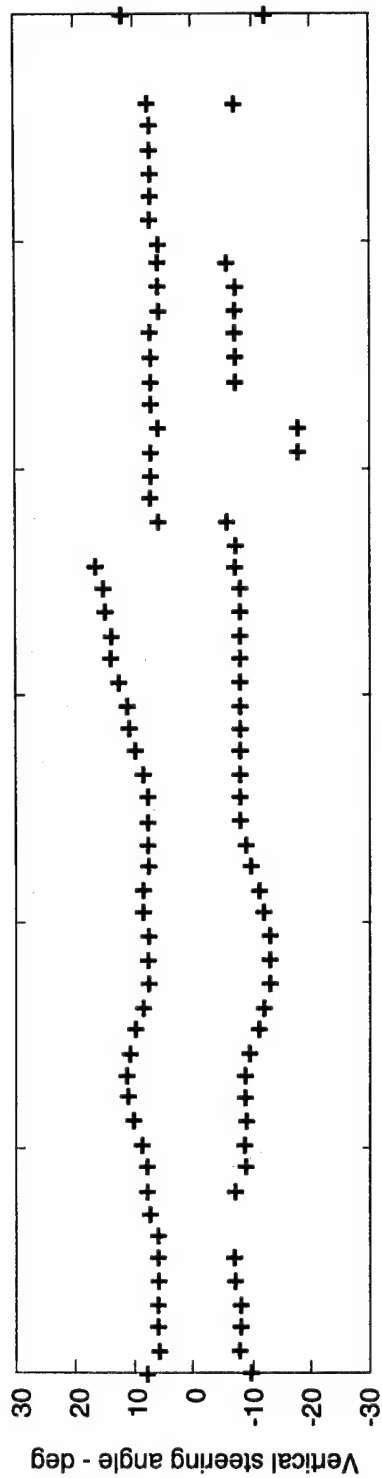
(a) Peak direction

(b) Peak response
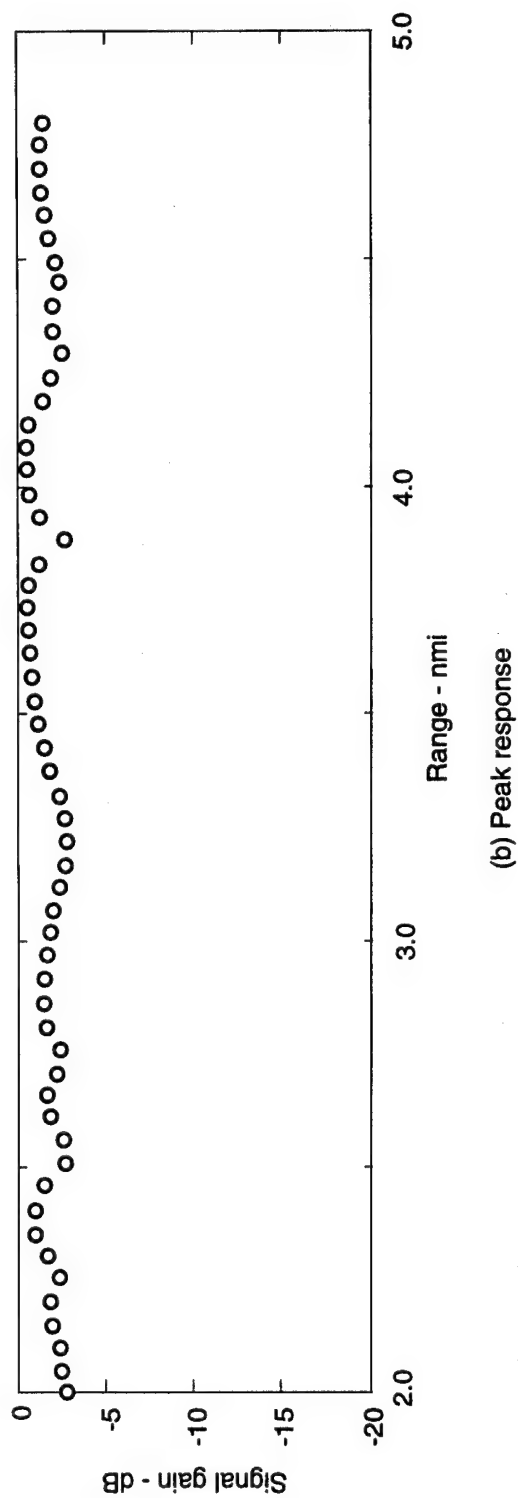
Figure 3.16
Maximum array response calculated for the bathymetry
in Fig 3.14 with the source in the 2-5 km range interval, 200 Hz.

(a) Peak direction
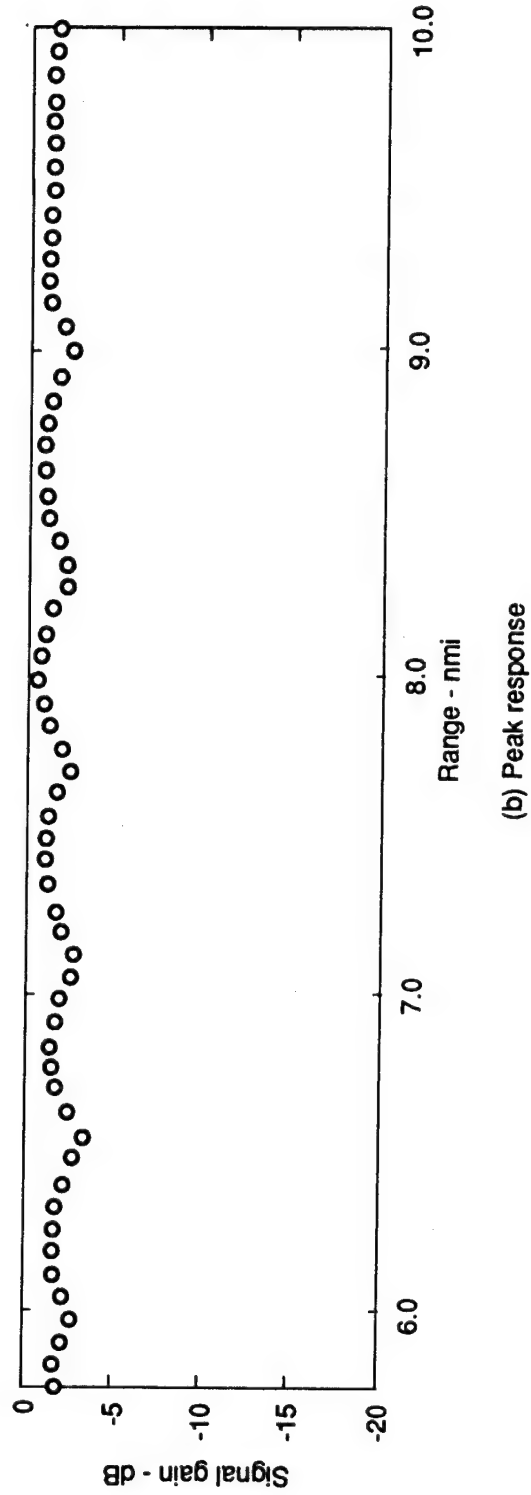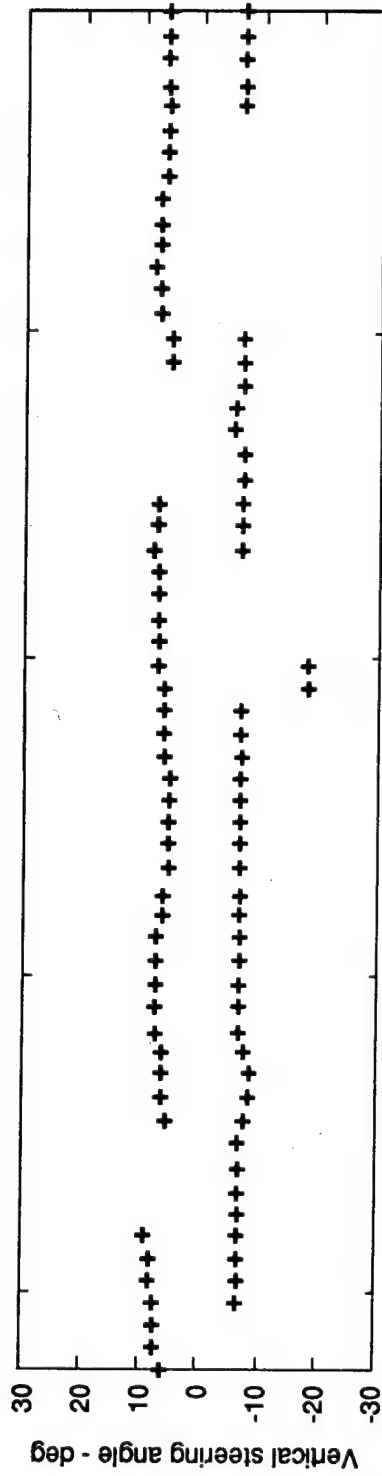
(b) Peak response

Figure 3.17
Maximum array response calculated for the bathymetry
in Fig 3.14 with the source in the 5-10 km range interval, 200 Hz.

68
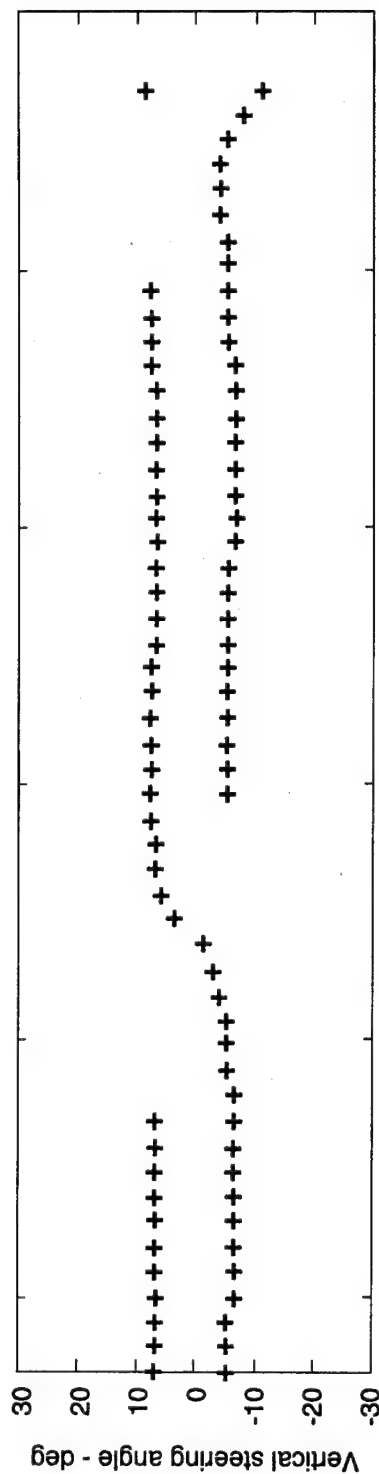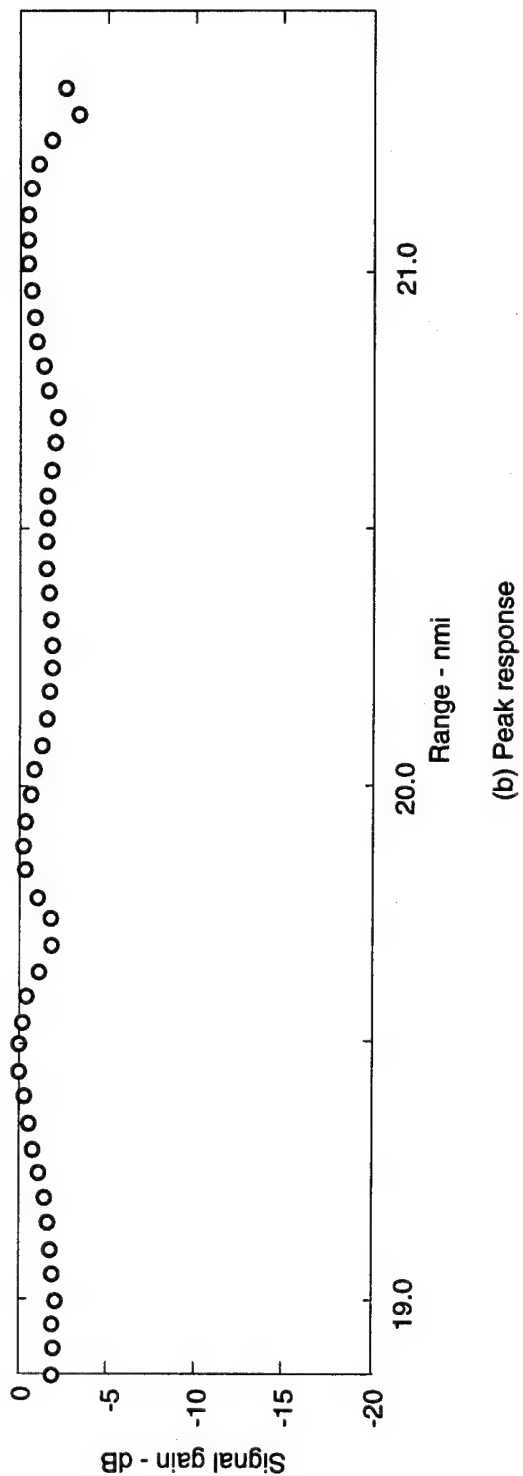
Figure 3.18

Maximum array response calculated for the bathymetry
in Fig. 3.14 with the source in the 18.8-21.4 km range interval, 200 Hz.

then mode set 1. In these range intervals the peak gains of -3 to -1 dB occur at ±5°–10° in Figs. 3.17 and Fig. 3.18.

A range averaged gain was computed for the three range intervals discussed above (Fig. 3.19). In these averages there is a persistent null at 0° with major peaks at ±6°–7°, and secondary peaks at ±40° and ±60°. There is also a very deep null at ±25°. The secondary peak at ±30° seen in the data is not present in these calculations. However, ±30° is very close to the peak angles predicted by the K&I model. A combination of local wind noise and distant shipping noise propagating down slope could explain the observed directionality characteristics of the noise. A proper combination of source levels and ranges to distant shipping could generate the measured results. As an example, the NGs in Fig. 3.9 were added to the 10 nmi signal gains in Fig. 3.19, 2 dB were subtracted from the total (just for the sake of the comparison with the data), and the results were compared to the measurements (Fig. 3.20). To identify where the mode arrivals actually occur, mode arrival angles were grouped into 1° bins and the bin counts were also presented in Fig. 3.20. With the modes restricted to ±40°, any calculated array response at steeper angles results from sidelobes. The combined gain has peaks at ±6°–7° with a broad plateau at ±15°–40° and secondary peaks at ±62°. The most obvious difference between the curves in Fig. 3.20 is the depth of the null at 0°; the calculations have a 3 dB null, while there is no significant null in the measured data. The array tilt noted in the propagation analysis would tend to fill in the null and broaden the peaks. The calculated levels in the ±15°–40° region are aproximately the same level as the ±30° peak in the data. Since the modes are restricted to ±40°, the secondary peak at ±60° is a sidelobe of the main peaks. This example illustrates that a combination of the two model results can be used to explain the measurements. However, to properly model NG, locations of the distant shipping and source levels for those ships and the local wind are needed.

3.5   CONCLUSIONS

The primary objective of the experiment was to collect data to support analysis of the vertical structure of the ambient noise field in shallow water. A major issue to be addressed by the analysis was the validity of the K&I noise model in predicting noise vertical directionality in a region dominated by shipping noise. Much of the noise measurements was contaminated by radio interference. However, noise recorded during the cw propagation events could support vertical noise analysis, and analysis was
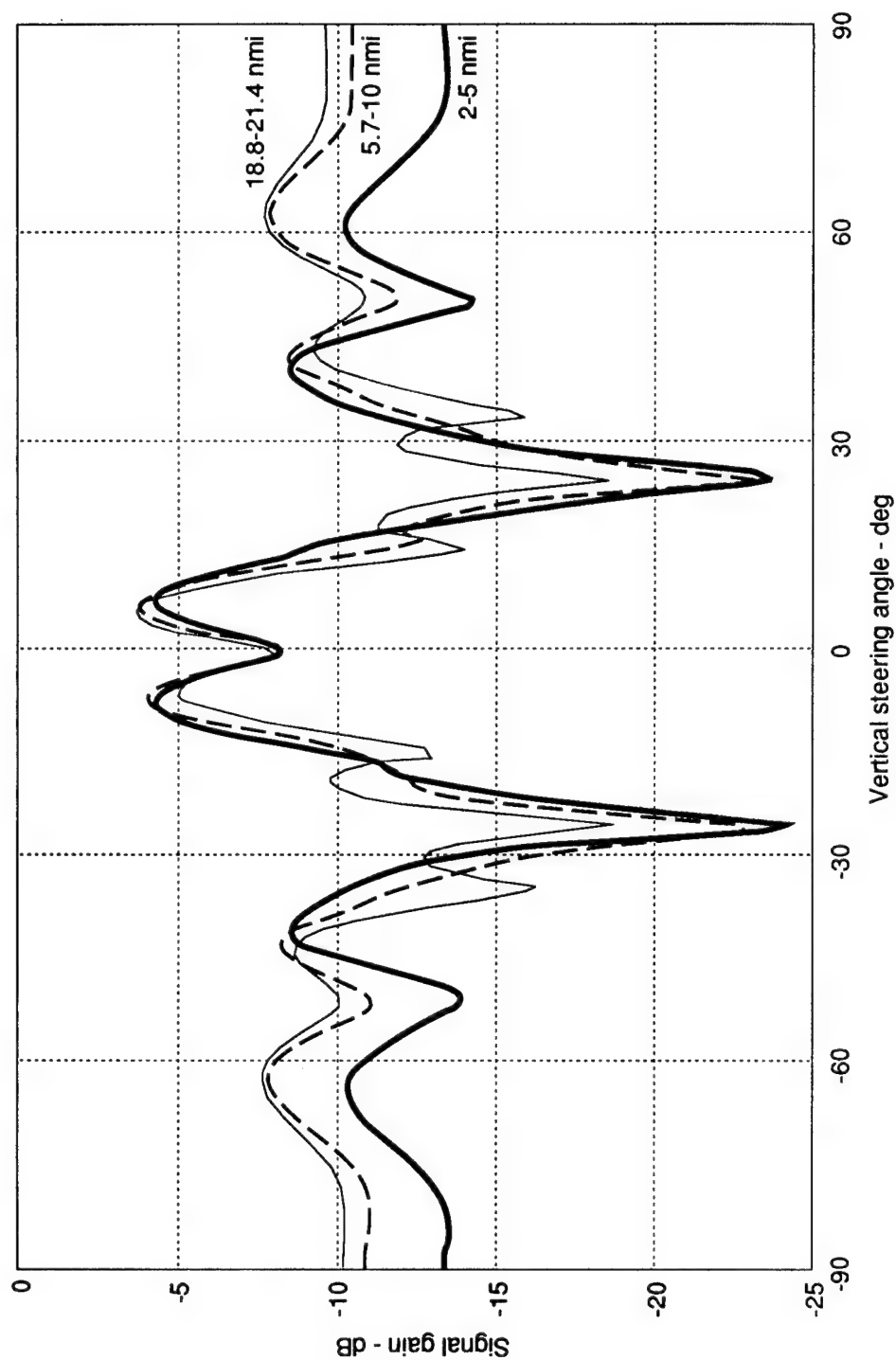
Figure 3.19

Range averaged array response in the range dependent environment of Fig. 3.14, 200 Hz.

71
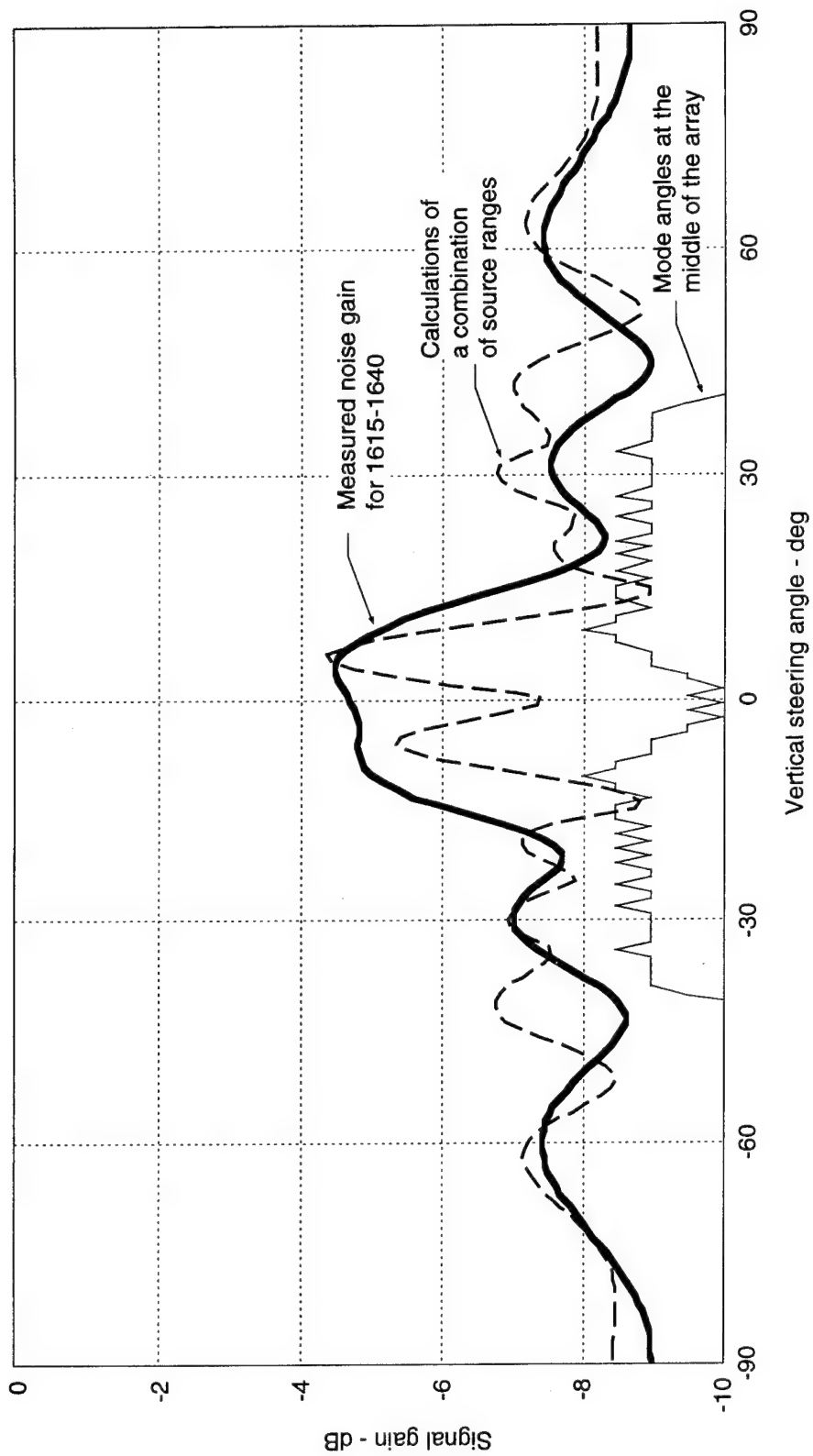
Figure 3.20
Comparison between noise gain and calculated array response for sources in a range variable environment, 200 Hz.

performed on these data. The noise was found to be dominated by shipping-like noise, although no shipping (except for the exercise ship) was in the immediate vicinity of the array site. It was concluded that distant shipping contributed to the measured noise levels. The noise directionality from the K&I model did not match the measured results. NG peaks occurred at ±5°–10° in the data compared to ±28°–30° in the model. A range variable environment and an adiabatic normal mode model were required in order to match peaks in the calculated NG to peaks in the measurements. To produce a calculated peak in the NG at ±7°, energy has to propagate down slope to the array. A combination of the K&I model calculations and distant source calculations can mimic the features found in the measured noise directionality.

This page intentionally left blank.

APPENDIX A
SHALLOW WATER ACOUSTIC MEASUREMENTS EXERCISE PLAN

This page intentionally left blank.

OBJECTIVES

The objectives of this experiment are designed to address the issues pertinent to passive surveillance in shallow water. The experiment is designed to measure the acoustic parameters necessary for estimating maximum achievable array gain (AG) and for determining broadband detection capabilities.

Achievable Array Gain

The maximum achievable AG is a function of the achievable noise gain (NG) and the achievable signal gain (SG). NG will be dependent upon two related properties of the noise field: (1) the vertical noise directionality and (2) the decorrelation of the noise between hydrophones.

A vertical line array of 25 hydrophones will be used to measure the vertical directionality of the noise in the frequency band 40-3000 Hz. The same hydrophones and data will be used to measure noise decorrelation as a function of hydrophone separation.

SG is also needed when determining maximum achievable AG. There will be CW projector lines, broadcast along a source track, to provide a measure of SG. SG will be measured across the frequency band 40-3000 Hz.

Broadband Detection

This experiment will consider broadband detection based on correlation techniques. There will be three techniques considered: autocorrelation, vertical crosscorrelation, and horizontal crosscorrelation. Broadband signals will be broadcast along a source track. The signals will cover the frequency band 40-1000 Hz. Broadband signals will be recorded on the vertical line array and simultaneously on a sonobuoy, moored a few hundred meters away from the VLA.

77

EXERCISE PLAN

Location

The shallow water measurement exercise will be held in April 1988, approximately 75 nmi south-southeast of Port Aransas, Texas (Corpus Christi, Texas), Figure A.1. The bottom in this area is composed of homogeneous sand, free of sand ripple. At this time of year, the sound speed profile will be slightly downward refracting. Bottom slopes in the area range from $0°$ up to $3°$. This area has a minimum number of oil rigs, all of which are in production and thus are not considered to be loud noise sources.

Site location is limited to an area with nominal bottom depths of 200 m and with bottom slopes less than $1.5°$. The nominal site location is:

26° 55.20' N	96° 27.00' W

Modifications will be made to this location to provide a site with a water depth of 200 m.

Source Tracks

There will be four source events: continuous wave tones (CW), hyperbolic frequency modulated (HFM) sweeps, and two broadband (BB) signals. Source tracks for all projector tows will be bow-tie patterns along the track presented in Table A.1, and Figure A.2. Table A.1 gives approximate latitudes and longitudes for this track. The track begins at point 1, continues to point 2, and on through the remaining points in ascending order. Source speed along the track will be 5 kt. The times, based on this speed, are relative to the beginning of each event (Table A.1). Total duration for each source run will be approximately 10 h.
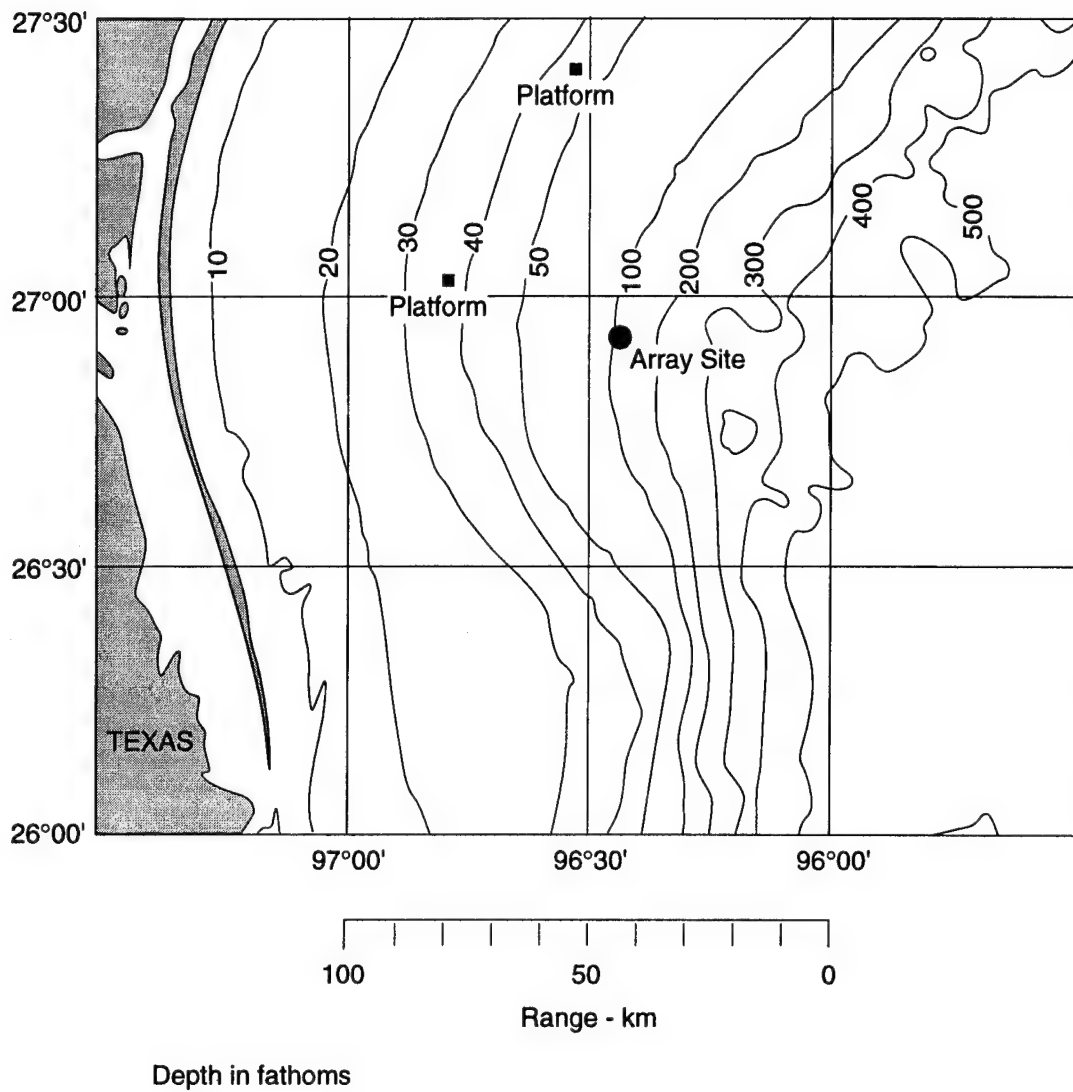
Figure A.1
Shallow water exercise area.

79

Table A.1
Approximate locations defining source track.

	Latitude	Longitude	Range (nmi)	Bearing (°E of N)	Time
1	26° 55.20' N	96° 27.00' W	---	---	0:00
2	26° 56.43' N	96° 34.75' W	7.02	280.1°	1:24
3	27° 02.12' N	96° 25.62' W	9.93	55.0°	3:23
4	26° 55.20' N	96° 27.00' W	7.02	190.5°	4:47
5	26° 48.29' N	96° 28.38' W	7.02	190.1°	6:11
6	26° 54.00' N	96° 19.25' W	9.93	54.9°	8:11
7	26° 55.20' N	96° 27.00' W	7.02	279.9°	9:35

Acoustic Events

There will be five events during this exercise: one ambient noise event, one CW event, one HFM event, and two broadband events. During the projector events, the source depth will be 60 m. Table A.2 gives the frequencies for each event. The CW frequencies are spaced one half octave apart, and range from 40 Hz to 905 Hz. The HFM signals will be 100 Hz sweeps with the low frequency for each sweep given in Table A.2. Sweep duration will be 5 s. The sequence is to cycle through the five frequency bands once a minute with the start of a new frequency every 10 s. The broadband signal will be from 40 Hz up to 250 Hz (higher if possible).

Table A.2
Source characteristics.

Event	Frequencies (Hz)	Levels (dB//1 µPa/$\sqrt{\text{Hz}}$))
cw	57, 80, 113, 160, 226, 320, 452, 640, 905	165 dB or maximum level
BB	40 - 250	140
HFM	100, 300, 500, 700, 1000	175
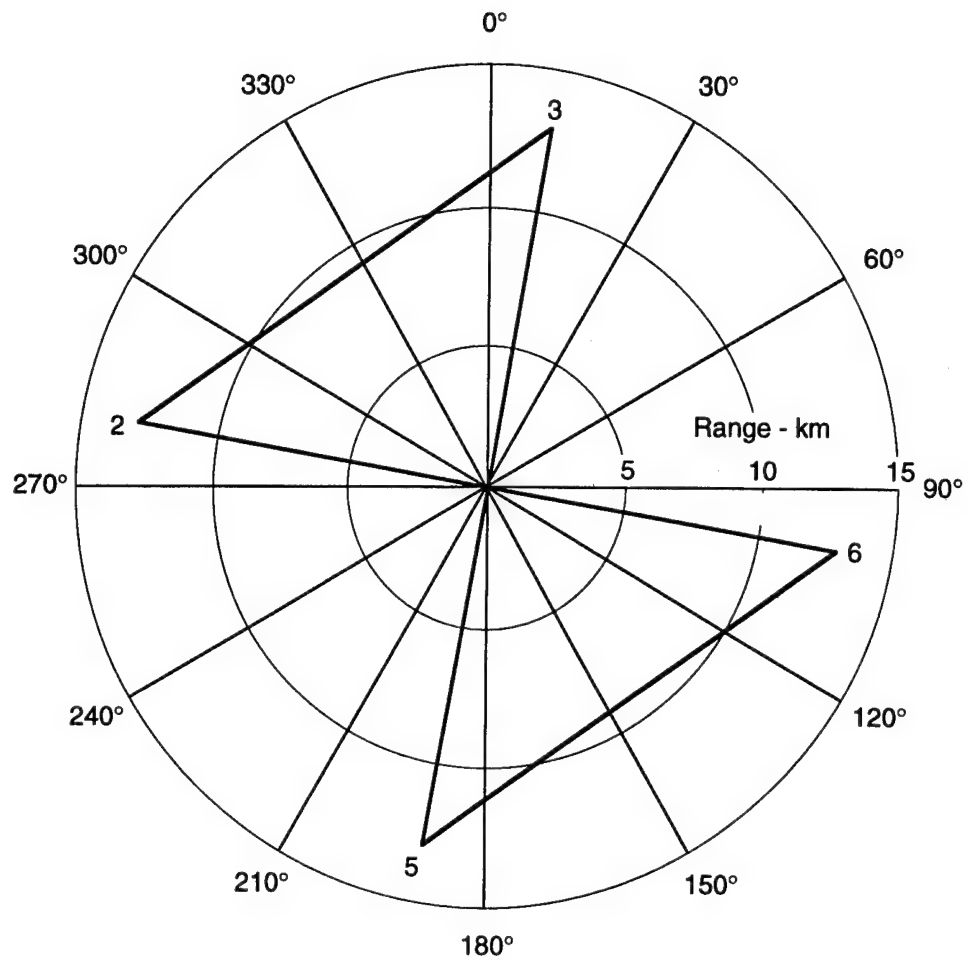
Figure A.2
Source track for all propagation source events;
numbers indicate track positions
(positions 1, 4, and 7 are at the center).

81

In addition to the propagation signals, 100 ms ranging pulses are to be broadcast every 5 min, on the 5 min-multiples past the hour (:00, :05, :10, :15, ⋯). These pulses will be triggered automatically by the time code generator.

During the acoustic events, the received signal level will be monitored. If these acoustic signals drop below the ambient noise levels, the radial legs of the bow ties will be shortened.

If time permits, a fixed source event will be conducted. With the array redeployed, the ship will go to point 2 and lower the source to the bottom. The frequency lines used in event CW 1 will then be broadcast for four hours while the ship holds position.

Acoustic Recording

During the acoustic events, received acoustic signals will be recorded on an analog recording system. Data will be recorded using a 28-channel RACAL Storehorse recorder, set up for FM wideband group II recording. The recording tape speed will be $3\,^3/_4$ ips.

Information recorded during the acoustic events, except for the broadband event, will include the following:

(1) 22 hydrophone channels from the vertical array,
(2) one sonobuoy channel, SSQ-36 during the AXBT events,
(3) tape recorder servo signal, and
(4) time code signal.

Channel assignments for these events are given in Table A.3. During the broadband event array elements 17, 19, and 23 will be disconnected and the SSQ-53B sonobuoy channels will be recorded on the Storehorse channels 10, 14, and 20.

Table A.3
Recorder channel assignments.

Rcdr Chan	Input	Rcdr Chan	Input	Rcdr Chan	Input
1	array # 1	11	array # 6	21	array # 9
2	sonobuoy	12	array #21	22	array #16
3	array # 2	13	array #7	23	array #10
4	demux tone	14	*array #19*	24	array #15
5	array # 3	15	array #13	25	array #11
6	FM	16	OTS	26	array #14
7	array # 4	17	timecode	27	array #12
8	array #25	18	array #18	28	Timecode
9	array # 5	19	array # 8		
10	*array #23*	20	*array #17*		

Receiver/Recorder Calibration

The calibration sequences given in Table A.4 will be used to calibrate the receiver/recorder system. These sequences will be injected into the receiver amplifiers and recorded on the tape recorder prior to the first event and after the last event. The receiving system configuration, including amplifier gain settings, will be as close to the expected configuration as possible. If significant changes occur in the recording system during the exercise, the final calibration signals will be recorded with those settings. If possible, the calibration signals should be recorded on all recorder channels simultaneously. This will provide a channel-to-channel phase calibration.

Table A.4
Calibration sequence.

Time	Signal	Level
0 - 5 min	True White Noise	0 dBV
10 - 15 min	500 Hz	0 dBV
15 - 20 min	500 Hz	-20 dBV
20 - 25 min	1000 Hz	0 dBV

All amplifier settings during the calibration and the data recording will be recorded in the exercise log.

Ship Location

The ship location will be recorded every 5 minutes during each acoustic event. The Loran C receiver, set to automatic print mode, will be connected to a printer terminal through an RS 232 port. The print cycle time will be set to 5 minutes during source events and 15 minutes during the ambient noise event.

Weather

During the acoustic events, wind speed will be recorded once every hour, on the hour, and as warranted by changing weather conditions. The RV Longhorn has two anemometers that can provide wind speed measurements. The readings will be logged in the exercise log.

Schedule

Before departure, Loran C propagation errors will be removed by setting the Loran C position to the latitude and longitude position of the RV Longhorn pier. The position of the pier is

27° 50.23' N 97° 03.17' W.

Commence exercise in Port Aransas, Texas, and proceed to the receiver site. Verify calibration of recording system, and readjust if necessary. Arrive at site and begin deployment of the array. Test source receiver and transmitter. Deploy SSQ-36 sonobuoy and record AXBT output.

Transit to Point 2. Record ambient noise for 8 h. While on station, scientific crew will collect a sound velocity profile (SVP) and, if time and weather permit, a bottom grab sample.

Return to array site. Refurbish the array--replace batteries, perform any necessary repairs, and conduct tests. Recheck the recording system calibration. Change source characteristics to those required for CW event.

Deploy array. Test source, receiver, and transmitter. Deploy SSQ-36 sonobuoy and record AXBT output.

Commence CW tow along the source track. The source shall be at a depth of 60 m. At points 4 and 7 deploy SSQ-36 sonobuoys for temperature profile measurements.

Refurbish the array: replace batteries, perform any necessary repairs, and conduct tests. Recheck the recording system calibration. Change source characteristics to those required for first BB event.

Deploy array. Deploy sonobuoy moor. Test source, receiver, and transmitter. Deploy SSQ-57A sonobuoy. Deploy SSQ-36 sonobuoy and record AXBT output.

Commence first BB event (BB1). At points 4 and 7 deploy SSQ-36 sonobuoys for measurements of temperature profile. At the end of BB 1, recover the array, and scuttle the SSQ-57A, if it is still afloat.

Refurbish the array: replace batteries, perform any necessary repairs, and conduct tests. Recheck the recording system calibration and source characteristics.

Deploy array. Deploy sonobuoy anchoring buoy. Test source, receiver, and transmitter. Deploy SSQ-57A sonobuoy. Deploy SSQ-36 sonobuoy and record AXBT output.

Commence second BB event (BB2). At points 4 and 7 deploy SSQ-36 sonobuoys for measurements of temperature profile. If time and weather permit, additional ambient noise measurements will be collected at the end of the broadband event. The RV Longhorn will hold station and operate in quiet mode. Measurements will continue until the batteries in the array are depleted.

At the end of event BB2, recover the array, and scuttle the SSQ-57A, if it is still afloat. Recover the sonobuoy moor.

Refurbish the array: replace batteries, perform any necessary repairs, and conduct tests. Recheck the recording system calibration. Change source characteristics to those required for HFM event.

Deploy array. Test source receiver and transmitter. Deploy SSQ-36 sonobuoy and record AXBT output.

Commence HFM event. At points 4 and 7 deploy SSQ-36 sonobuoys for measurements of temperature profile. At the end of this HFM event, recover the array, collect SVP, and sediment grab sample.

Transit to Port Aransas, Texas. FINEX.

Table A.5 presents the exercise schedule, giving event, position, approximate event duration, and approximate total elapsed time. The last column provides a convenient place to record when the event occurred. In this table, the term "steaming" indicates a speed of 5 kt, while the term "transit" indicates a speed of 8-10 kt.

Table A.5
Exercise schedule.

No.	Event	Location	Duration hh:min	Elapsed time h
1	Depart Port Aransas and transit to site	26° 55.20' N 96° 27.00' W	8:00	8.0
2	Deploy array	26° 55.20' N 96° 27.00' W	4:00	12.0
3	Transit to Point 2 SVP, sed. samp.	26° 56.43' N 96° 34.75' W	1:00	13.0
4	Record ambient noise	26° 56.43' N 96° 34.75' W	8:00	21.0
5	Transit to array site	26° 55.20' N 96° 27.00' W	1:00	22.0
6	Redeploy array	26° 55.20' N 96° 27.00' W	4:00	25.0
7	Collect SVP, sed. samp.	26° 55.20' N 96° 27.00' W	1:00	26.0
8	Begin cw tow steam Point 2, XBT	26° 56.43' N 96° 34.75' W	1:24	27.5
9	Steam to Point 3	27° 02.12' N 96° 25.62' W	1:24	29.0
10	Steam to Point 4	26° 55.20' N 96° 27.00' W	2:00	31.0
11	Steam to Point 5 XBT	26° 48.29' N 96° 28.38' W	1:24	32.5
12	Steam to Point 6	26° 54.00' N 96° 19.25' W	2:00	34.5
13	Steam to Point 7	26° 55.20' N 96° 27.00' W	1:24	36.0
14	Redeploy array	26° 55.20' N 96° 27.00' W	4:00	40.0
15	Deploy SSQ-53B	26° 55.20' N 96° 27.00' W	2:00	42.0

Table A.5
(cont'd)

No.	Event	Location	Duration hh:min	Elapsed time h
16	Begin BB1 event steam Point 2, XBT	26° 56.43' N 96° 34.75' W	1:24	43.5
17	Steam to Point 3	27° 02.12' N 96° 25.62' W	2:00	45.5
18	Steam to Point 4	26° 55.20' N 96° 27.00' W	1:24	47.0
19	Steam Point 5 XBT	26° 48.29' N 96° 28.38' W	1:24	48.5
20	Steam to Point 6	26° 54.00' N 96° 19.25' W	2:00	50.5
21	Steam to Point 7	26° 55.20' N 96° 27.00' W	1:24	52.0
22	Redeploy array	26° 55.20' N 96° 27.00' W	4:00	56.0
23	Deploy SSQ-53B	26° 53.20' N 96° 28.20' W	2:00	58.0
24	Begin BB2 event steam to Point 2	26° 56.43' N 96° 34.75' W	1:24	59.5
25	Steam to Point 3	27° 02.12' N 96° 25.62' W	2:00	61.5
26	Steam to Point 4	26° 55.20' N 96° 27.00' W	1:24	63.0
27	Steam to Point 5	26° 48.29' N 96° 28.38' W	1:24	64.5
28	Steam to Point 6	26° 54.00' N 96° 19.25' W	2:00	66.5
29	Steam to Point 7	26° 55.20' N 96° 27.00' W	1:24	68.0
30	Redeploy array	26° 55.20' N 96° 27.00' W	4:00	72.0

No.	Event	Location	Duration hh:min	Elapsed time h
31	Begin HFM event steam to Point 2	26° 56.43' N 96° 34.75' W	1:24	73.5
32	Steam to Point 3	27° 02.12' N 96° 25.62' W	2:00	75.5
33	Steam to Point 4	26° 55.20' N 96° 27.00' W	1:24	77.0
34	Steam to Point 5	26° 48.29' N 96° 28.38' W	1:24	78.5
35	Steam to Point 6	26° 54.00' N 96° 19.25' W	2:00	80.5
36	Steam to Point 7	26° 55.20' N 96° 27.00' W	1:24	82.0
37	Retrieve array SVP, sed. samp.	26° 55.20' N 96° 27.00' W	2:00	84.0
38	Transit to Port Aransas	27° 50.23' N 97° 03.17' W	8:00	96.0

This page intentionally left blank.

APPENDIX B
GULF OF MEXICO SEDIMENT ANALYSIS

This page intentionally left blank.

Introduction

Mechanical measurements were performed on two grab samples taken from the Gulf of Mexico's continental shelf at latitude 26°56.6' N, longitude 96°27.27' W. Water depth at this site is approximately 200 m.

Method

Analysis was performed by first drying a portion of each sample, weighing it, and then preparing the sample so it could be sieved through a stack of U. S. standard sieves (2 - 4.25 ϕ). The sample was then weighed again after sieving to determine grain size and distribution.

A portion of each sample was also prepared to look at the biogenic material associated with the sediment. This was performed by washing the sample to remove most of the detrital material until only the large (~3 ϕ) sand grains and the biogenic material remained. This material was then placed on a glass slide and observed in a stereo microscope at 10X.

Results

The material from this site is a "benthic foram bearing detrital silty-clay." The sediments are olive green in color and dry to a light gray. Approximately 90% of the analyzed material was less than 4 ϕ. The larger grains appear to be quartzose and were well rounded to sub-rounded. The biogenic material (~2%) consisted of mostly outer shelf benthic foraminifera tests with a small amount of ostracod tests. An occasional gastropod shell and sponge spicule were observed along with other unidentifiable shell fragments.

Conclusions

The samples studied are representative of typical middle to outer shelf sediments in the Gulf of Mexico. The predominant detrital makeup is due to the active transport by suspension and gravity flows outward from the Texas and Louisiana coast. The biogenic material associated with these samples is also representative of the middle to outer neuritic (shelf) zone.

This page intentionally left blank.

REFERENCES

1. E. Axelrod, B. Schoomer, and W. Von Winkle, "The Vertical Directionality of Ambient Noise in the Deep Ocean at a Site near Bermuda," J. Acoust. Soc. Am. **37**, 77-83 (1965).

2. W. Hodgkiss and F. Fisher, "Vertical Directionality of Ambient Noise at 32°N as a Function of Longitude," MPL Technical Memorandum 387, Marine Physical Laboratory, Scripps Institution of Oceanography, La Jolla, California (revised 1987).

3. R. Hamson, "The Theoretical Responses of Vertical and Horizontal Line Arrays to Wind-Induced Noise in Shallow Water," J. Acoust. Soc. Am. **78**, 1702-1712 (1985).

4. M. Buckingham and S. Jones, "A New Shallow-Ocean Technique for Determining the Critical Angle of the Seabed from the Vertical Directionality of the Ambient Noise in the Water Column," J. Acoust. Soc. Am. **81**, 938-946 (1987).

5. W. Kuperman and F. Ingenito, "Spatial Correlation of Surface Generated Noise in a Stratified Ocean," J. Acoust. Soc. Am. **67**, 1888-1996 (1980).

6. R. Gragg and C. Penrod, "Shallow Water Performance of Omnidirectional Sensors and Vertical Arrays (U)," Applied Research Laboratories Technical Report No. 83-1 (ARL-TR-83-1), Applied Research Laboratories, The University of Texas at Austin, 1983. (CONFIDENTIAL)

7. R. Temple, D. Harrington, and J. Martin, "Monthly Temperature and Salinity Measurements of Continental Shelf Waters of the Northwestern Gulf of Mexico, 1963-65," NOAA Technical Report NMFS SSRF-707, National Oceanographic and Atmospheric Administration, Washington, DC, 1977.

8. H. McLellan and W. Nowlin, "The Waters of the Gulf of Mexico as Observed in February and March 1962," A&M Project 286, Agricultural and Mechanical University of Texas, College Station, Texas, Reference 62-16D, 1962.

9.   J. Mathews, P. Bucca, and J. Geddes, "Preliminary Environmental Assessment of the PROJECT GEMINI Site--Corpus Christi, Texas," NORDA Report No. 120, Naval Ocean Research and Development Activity, NSTL Station, Mississippi, June 1985.

10.   Berryhill (Ed.), "Environmental Studies: South Texas Outer Continental Shelf, 1975, An Atlas and Integrated Summary," USGS Report No. BLM/YM/ES-77/2, U.S. Geological Survey, Reston, Virginia, for Bureau of Land Management, Washington, DC, April 1977.

11.   H. Berryhill et al., "Environmental Studies, South Texas Outer Continental Shelf, 1975: Geology, Part I, Geologic Description and Interpretation," U.S. Geological Survey, Reston, Virginia, for Bureau of Land Management, Washington, DC (1977).

12.   United States, Ocean Assessments Division, Strategic Assessment Branch, *Gulf of Mexico : Coastal and Ocean Zones Strategic Assessment: Data Atlas*, National Oceanographic and Atmospheric Administration, U.S. Department of Commerce (1985).

13.   F. Jensen, "Sound Propagation in Shallow Water: A Detailed Description of the Acoustic Field Close to Surface and Bottom," J. Acoust. Soc. Am. **70**, 1397-1406 (1981).

14.   R. Koch, C. Penland, P. Vidmar, and K. Hawker, "On the Calculation of Normal Mode Group Velocity and Attenuation," J. Acoust. Soc. Am. **73**, 820-825 (1983).

15.   K. Focke, L. Thompson, and T. Scoggins, "Measurement of the Ocean Acoustic Environment in Shallow Water off the Coast of Fort Lauderdale," Applied Research Laboratories Technical Report No. 87-54 (ARL-TR-87-54), Applied Research Laboratories, The University of Texas at Austin, 1987.

16.   S. Mitchell, N. Bedford, and C. Penrod, "OUTPOST ENCORE Environmental Acoustic Measurements (U)," Applied Research Laboratories Technical Letter No. 84-14 (ARL-TL-EV-84-14), Applied Research Laboratories, The University of Texas at Austin, 1984. (SECRET)

17. T. Tulko, W. Gregory, and D. Bradley, "Acoustic Survey for Four Selected Shallow Water Sites on the East Coast of the United States (U)," NSWC/WOL Technical Report No. 76-64, Naval Surface Weapons Center, White Oak, Silver Springs, Maryland, 1976. (CONFIDENTIAL)

18. R. Hamson, "The Effect of Propagation Conditions on Wind-Generated Noise at Real Shallow Water Sites," in *Sea Surface Sound*, edited by B. Kreman (Kluwer Academic, Amsterdam, Netherlands, 1988), pp. 281-293.

This page intentionally left blank.

DISTRIBUTION LIST
ARL-TR-94-20
Technical Report under Contract N00039-88-C-0043
TD No. 01A021, Acoustic Support for Shallow Water Distributed Systems (Part 2)

Copy No.

Director
Naval Research Laboratory
4555 Overlook Avenue SW
Washington, DC 20375-5000

1	Attn: E. Franchi (Code 7100)
2	S. Wolf (Code 7127)
3	B. Palmer (Code 7160)
4	B. Pasewark (Code 7127)
5	M. Czarnecki (Code 7110)
6	M. Orr (Code 7120)

Office of Naval Research
Department of the Navy
Arlington, VA 22217-5660

7	Attn: J. DeCorpo (Code 32)
8	S. Ramberg (Code 321)
9	J. Simmen (Code 321OA)
10	K. Dial (Code 321SS)
11	T. Goldsberry (Code 321W)
12	R. Doolittle (Code 321US)
13	J. Andrews (Code 321LS)
14	R. Peloquin (Code 3220M)

Commanding Officer
Naval Research Laboratory
Stennis Space Center, MS 39529-5004

15	Attn: D. Ramsdale (Code 242)
16	R. Wagstaff (Code 245)
17	P. Bucca (Code 222)

Commanding Officer
Office of Naval Research
Stennis Space Center, MS 39529-7050

18	Attn: E. Chaika (Code 322)

Office of the Deputy Assistant Secretary of the Navy
Mine and Undersea Warfare Programs
Department of the Navy
Washington, DC 20350-1000

19	Attn: E. Zdankiewicz
20	M. Kijeski

Copy No.

Office of the Chief of Naval Operations
Department of the Navy
Washington, DC 20350-2000
21   Attn: J. Schuster (N87T)

Office of the Chief of Naval Operations
Naval Observatory
34th and Massachusetts Ave. NW
Washington, DC 20390-1800
22   Attn: R. Winokur (N096T)

Commander
Space and Naval Warfare Systems Command
Department of the Navy
Arlington, VA 22245-5200
23   Attn: C. Andriani (PD80A)
24   CAPT W. Hatcher (PMW182-1)
25   R. Snuggs (PMW182T)
26   R. Cockerill (PMW182-15)
27   G. Gotthardt (PMW182-21)
28   L. Fabian (PMW182-3)
29   J. Feuillet (PMW182-52)
30   LCDR J. Flayharty (PMW184D)

Commanding Officer
Naval Command Control and Ocean Surveillance Center
RDT&E Division
53560 Hull St.
San Diego, CA 92152-5001
31   Attn: M. Morrison (Code 705)
32   J. McCarthy (Code 714)
33   T. Kaye (Code 7402)
34   J. Lockwood (Code 734)
35   N. Booth
36   C. Persons (Code 732)
37   D. Barbour (Code 733)
38   H. Bucker (Code 541)

Commanding Officer
Office of Naval Intelligence
4301 Suitland Rd.
Washington, DC 20395-5020
39   Attn: E. McWethy (Code 256)
40   B. Kalny (Code 256)

Distribution List for ARL-TR-94-20 under Contract N00039-88-C-0043, TD No. 01A021 (cont'd)

<u>Copy No.</u>

	Commander Naval Air Systems Command 1411 Jefferson Davis Hwy. Washington, DC 20361-7121
41	Attn: E. Benson (PMA264B)

	Commanding Officer Naval Air Warfare Center Aircraft Division, Warminster Street and Jacksonville Roads Warminster, PA 18974-5000
42	Attn: J. McCandless
43	J. McEachern (Code 4.5C)
44	J. Savage
45	B. Steinberg

	Officer in Charge Naval Underwater Warfare Center New London Detachment New London, CT 06320-5594
46	Attn: B. Cole (Code 31)
47	P. Herstein (Code 3112)
48	N. Owsley

	Commanding Officer Naval Oceanographic Office Stennis Space Center, MS 29522-5001
49	Attn: W. Jobst (Code O)

	Advanced Research Projects Agency 3701 N. Fairfax Dr. Arlington, VA 22203-1714
50	Attn: C. Stuart (MSTO)

	Commanding Officer Coastal Systems Station, Dahlgren Division Naval Surface Warfare Center Panama City, FL 32407-5000
51	Attn: G. McLeroy

	Superintendent Naval Postgraduate School Monterey, CA 93940
52	Attn: Library

Distribution List for ARL-TR-94-20 under Contract N00039-88-C-0043, TD No. 01A021 (cont'd)

<u>Copy No.</u>

53 - 64	DTIC-OCC Defense Technical Information Center 8725 John J. Kingman Road, Suite 0944 Fort Belvoir, VA 22060-6218

The Johns Hopkins University
Applied Physics Laboratory
Johns Hopkins Road
Laurel, MD 20723-6099

65	Attn: K. McCann
66	R. Mitnick
67	S. Magruder
68	B. Newhall
69	R. Seesholtz

Applied Research Laboratory
The Pennsylvania State University
P.O. Box 30
State College, PA 16801

70	Attn: S. McDaniel
71	D. McCammon

Marine Physical Laboratory
Scripps Institution of Oceanography
The University of California, San Diego
San Diego, CA 92132

72	Attn: W. Kuperman
73	G. deSpain
74	W. Hodgkiss

Woods Hole Oceanographic Institution
86-95 Water Street
Woods Hole, MA 02543

75	Attn: J. Lynch
76	G. Frisk

Director
North Atlantic Treaty Organization
SACLANT ASW Research Centre
APO New York 09019

77	Attn: D. Bradley
78	F. Jensen
79	T. Akal
80	F. Ingenito
81	D. Gingras

Distribution List for ARL-TR-94-20 under Contract N00039-88-C-0043, TD No. 01A021 (cont'd)

<u>Copy No.</u>

	AMRON Corporation 2001 Jefferson Davis Hwy. #610 Arlington, VA 22202-3603
82	Attn: C. Christenson
	AT&T Bell Laboratories Room 15C304 Whippany Road Whippany, NJ 07981
83	Attn: J. Eickmeyer
84	R. Patton
	Bolt, Beranek, and Newman 1300 N. 17th St. Suite 1200 Arlington, VA 22209
85	Attn: J. O'Conner
	The Mitre Corporation 7525 Colshire Drive McLean, VA 22102
86	Attn: K. Hawker
87	J. Hagy
	ORINCON Corporation 4350 North Fairfax Drive, Suite 470 Arlington, VA 22203
88	Attn: H. Cox
	Science Applications International Corporation P.O. Box 1303 McLean, VA 22102
89	Attn: J. Hanna
90	R. Cavanaugh
	TRW, Inc. Systems Integration Group P.O. Box 10400 Fairfax, VA 22031
91	Attn: M. Flicker
92	C. Dabney
93	L. Wood
94	Library, ARL:UT
95	Environmental Sciences Group, ARL:UT
96	Reserve, ARL:UT